

EFFECTS OF FUNCTIONAL GROUPS ON THE SOLUBILITIES OF
POLYHEDRAL OLIGOMERIC SILSESQUIOXANES (POSS) IN
SUPERCRITICAL CARBON DIOXIDE

A THESIS SUBMITTED TO
THE GRADUATE SCHOOL OF NATURAL AND APPLIED SCIENCES
OF
MIDDLE EAST TECHNICAL UNIVERSITY

BY

BAŞAK KANYA

IN PARTIAL FULFILLMENT OF THE REQUIREMENTS
FOR
THE DEGREE OF MASTER OF SCIENCE
IN
CHEMICAL ENGINEERING

AUGUST 2015

Approval of thesis:

**EFFECTS OF FUNCTIONAL GROUPS ON THE SOLUBILITIES OF
POLYHEDRALOLIGOMERIC SILSESQUIOXANES (POSS) IN
SUPERCRITICAL CARBON DIOXIDE**

submitted by **BAŞAK KANYA** in partial fulfillment of the requirements for the degree of **Master of Science in Chemical Engineering Department, Middle East Technical University** by,

Prof. Dr. Gülbin Dural Ünver
Dean, Graduate School of **Natural and Applied Sciences**

Prof. Dr. Halil Kalıpçılar
Head of Department, **Chemical Engineering**

Assoc. Prof. Dr. Çerağ Dilek Hacıhabiboğlu
Supervisor, **Chemical Engineering Dept., METU**

Examining Committee Members:

Prof. Dr. Halil Kalıpçılar
Chemical Engineering Dept., METU

Assoc. Prof. Dr. Çerağ Dilek Hacıhabiboğlu
Chemical Engineering Dept., METU

Prof. Dr. Nesrin Hasırcı
Chemistry Dept., METU

Prof. Dr. Levent Yılmaz
Chemical Engineering Dept., METU

Prof. Dr. Can Erkey
Chemical and Biological Engineering Dept., Koç Uni.

Date: 18.08.2015

I hereby declare that all information in this document has been obtained and presented in accordance with academic rules and ethical conduct. I also declare that, as required by these rules and conduct, I have fully cited and referenced all material and results that are not original to this work.

Name, Last name : Başak KANYA

Signature :

ABSTRACT

EFFECTS OF FUNCTIONAL GROUPS ON THE SOLUBILITIES OF POLYHEDRALOLIGOMERIC SILSESQUIOXANES (POSS) IN SUPERCRITICAL CARBON DIOXIDE

Kanya, Başak

M.S., Department of Chemical Engineering

Supervisor : Assoc. Prof. Dr. Çerağ Dilek Hacıhabiboğlu

August 2015, 88 pages

In this study, the phase behavior of the binary systems containing CO₂ and various hybrid polyhedral oligomeric silsesquioxanes (POSS) with different functional groups were investigated. A high-pressure view cell was used to measure the dew-points or cloud-points at temperatures between 308K and 323K, up to 30 MPa. Among the studied POSS structures, methacryl, isooctyl and octaisobutyl POSS were observed to form homogenous solutions with CO₂, while octamethyl POSS was found to be insoluble in the supercritical fluid. The solubilities of both methacryl and isooctyl POSS in supercritical carbon dioxide (scCO₂) decrease with increasing temperature, while isooctyl POSS exhibits nearly an order of magnitude higher solubility than methacryl POSS at both temperatures. The octaisobutyl POSS-CO₂ binary system exhibits a crossover pressure, below which the solubility of the component decreases with increasing temperature. Above this pressure, as the temperature is increased, the solubility of POSS in scCO₂ increases. These results show that the functional groups of POSS affect its solubility in scCO₂ and the phase behavior of the POSS-CO₂ binary system significantly.

After the solubility experiments the obtained phase behavior data of methacryl POSS, isooctyl POSS, and octaisobutyl POSS were correlated using density based models. The models used are; Mendez-Santiago and Teja (MST) model, Chrastil model, Bartle model, del Valle and Aguilera (del Valle) model, and Kumar and Johnston (K-J) model. All of these models gave good fit to the solubility data.

In the last part of this study the obtained phase equilibrium data of POSS-CO₂ binary system was used to design an environmentally benign material processing application using scCO₂. In this application scCO₂-soluble solid POSS, which were trifluoropropyl POSS and octaisobutyl POSS, were impregnated into a CO₂-philic, biodegradable and biocompatible polymer, poly (lactic acid) (PLA) with scCO₂. The morphological analysis by scanning electron microscopy (SEM) analysis and thermal characterization of the impregnated PLA films and neat PLA film by differential scanning calorimetry (DSC) and thermogravimetric analysis (TGA) instruments were performed. The effect of POSS addition on glass transition temperature, melting temperature, and thermal stability were investigated. It was observed that POSS could be loaded into PLA with the supercritical fluid impregnation technique. The resulted polymer composites had an increase in their T_g with respect to neat PLA showing that the intermolecular interactions within the polymer matrix were enhanced. However, sufficient loading could not be obtained with current process conditions and POSS types loaded to obtain significant improvement in the thermal stability of the films.

Keywords: Silica cage, CO₂-philic, organic–inorganic hybrid materials, binary system, crossover pressure.

ÖZ

POLİHEDRAL OLİGOMERİK SİLSESKUIOKSANLARIN (POSS) SÜPERKRİTİK KARBONDİOKSİT İÇİNDEKİ ÇÖZÜNÜRLÜKLERİNE FONKSİYONEL GRUPLARIN ETKİLERİ

Kanya, Başak

Yüksek Lisans, Kimya Mühendisliği Bölümü

Tez Yöneticisi: Doç. Dr. Çerağ Dilek Hacıhabiboğlu

Ağustos 2015, 88 sayfa

Bu çalışmada, farklı fonksiyonel gruplara sahip hibrit yapıdaki çeşitli polihedral oligomerik silseskuioksan (POSS) ve CO₂ içeren ikili sistemlerin faz davranışları incelenmiştir. Çiğlenme ve bulutlanma noktası ölçümleri yüksek basınç hücresi kullanılarak 308 ve 323K sıcaklıklarında en yüksek 30 MPa basınca çıkılarak belirlenmiştir.

Çalışılan POSS yapıları arasından metakril, izooktil and oktaizbütil gruplarını içeren POSS'lar CO₂ ile homojen çözeltiler oluştururken oktametil POSS'un süperkritik akışkan içinde çözünür olmadığı tespit edilmiştir. Metakril ve izooktil POSS süperkritik karbon dioksit içindeki çözünürlükleri artan sıcaklıkla azalırken izooktil POSS metakril POSS' a göre her iki sıcaklıkta da 10 kat daha yüksek çözünürlük sergilemiştir. Oktaizobütil POSS-CO₂ ikili sisteminde bir geçiş basıncı gözlenmiştir. Geçiş basıncının altındaki basınçlarda oktaizobütil POSS'un süperkritik karbondioksit içindeki çözünürlüğü artan sıcaklıkla azalmaktadır. Bu basıncın üzerindeki basınçlarda ise artan sıcaklık, oktaizobütil POSS'un scCO₂ içindeki çözünürlüğünü arttırmaktadır. Elde edilen bu sonuçlar POSS'ların sahip oldukları

fonksiyonel grupların onların scCO₂ içindeki çözünürlüklerini ve POSS-CO₂ ikili sistemlerinin faz davranışlarını önemli ölçüde etkilediğini göstermektedir.

Çözünürlük çalışmaları devamında, POSS-CO₂ sistemlerinin faz denge verileri özkütleyle dayanan korelasyonlarla modellenmiştir. Kullanılan modeller; Mendez-Santiago ve Teja modeli, Chrastil modeli, Bartle modeli, del Valle ve Aguilera modeli ve Kumar and Johnston modelidir. Bu modellerin hepsi ile çözünürlük verilerine oldukça uyan sonuçlar elde edilmiştir.

Bu çalışmanın son bölümünde POSS-CO₂ ikili sistemlerinin çözünürlük ve faz dengesi bilgileri kullanılarak, polimerlerin scCO₂ ile çevreye duyarlı malzeme işleme uygulamalarının geliştirilmesi üzerine çalışılmıştır. Bu uygulamada scCO₂'de çözünebilen katı trifloropropil POSS ve oktaizobütil POSS, CO₂ ile etkileşime girebilen, biyobozunur ve biyoyumlu Poli(laktik asit) (PLA)'ya süperkritik karbon dioksit ile yüklenmiştir. Yükleme yapılmış PLA filmleri ve saf PLA filmlerinin taramalı elektron mikroskobu (SEM) ile morfolojik analizi ve diferansiyel taramalı kalorimetre (DSC) ve termogravimetrik analiz (TGA) ile ısıl analizleri yapılmıştır. Elde edilen DSC ve TGA sonuçlarıyla yüklenen POSS'un camsı geçiş sıcaklığına, erime sıcaklığına ve termal kararlılığına olan etkisi incelenmiştir. Yapılan analizlerle süperkritik emprenye tekniği kullanılarak POSS'un PLA içine yüklenebildiği gözlenmiştir. Elde edilen polimer kompozitin T_g'sinin saf PLA T_g'sine göre daha yüksek olması polimer matrisindeki moleküller arası etkileşimlerin geliştiğini göstermektedir. Ancak bu süreç koşulları ve POSS türüyle PLA filmlerinin ısıl kararlılığını önemli ölçüde geliştirecek yeterli bir dolun elde edilememiştir.

Anahtar Kelimeler: Silika kafes, CO₂ uyumlu, organik–inorganik hibrit malzemeler, ikili sistem, geçiş basıncı.

To My Dearest Parents,

ACKNOWLEDGMENTS

I would like to express my sincere gratitude to my supervisor Assoc. Prof. Dr. Çerağ Dilek Hacıhabiboğlu for her invaluable guidance, encouragement and advices through my studies. It was my honor to be her first master student. I greatly appreciate working with her and her endless support.

I would also like to thank to Prof. Dr. Levent Yılmaz for his invaluable advices and helpful comments.

I would like to thank to Mihrican Açıkgöz from Department of Chemical Engineering for DSC and TGA analysis, for teaching me how to use the instruments and giving me the opportunity to use them.

I also thank to my lab mates Novendra and Cansu Demirtaş for helping me through my laboratory studies, for their suggestions and their enjoyable friendship.

I am also thankful to all the administrative and technical staff of Department of Chemical Engineering METU.

The study was supported financially by The Scientific and Technological Research Council of Turkey (TUBITAK) under scholarship code 110M465.

Above all, I owe my parents a great debt of gratitude for their endless love, support and encouragement through whole my life no matter what happens.

And heartfelt thanks to my friends with whom I shared unforgettable memories in Ankara and thanks for their understanding, patience and precious friendship

TABLE OF CONTENTS

ABSTRACT	v
ÖZ	vii
ACKNOWLEDGMENTS	x
TABLE OF CONTENTS.....	xi
LIST OF FIGURES	xiii
LIST OF TABLES	xvi
NOMENCLATURE.....	xvii
CHAPTERS	
1. INTRODUCTION	1
1.1 Polyhedral Oligomeric Silsesquioxane (POSS).....	1
1.2 Supercritical Fluids (SCF).....	2
1.2.1 Supercritical Carbon Dioxide.....	4
1.2.2 Solubility in Supercritical Carbon Dioxide.....	5
1.3 The modeling of solubility in supercritical CO ₂	6
1.4 Impregnation	11
2. LITERATURE SURVEY	13
2.1 Applications of POSS in Polymer Processing	13
2.2 scCO ₂ Impregnation in Polymers.....	15
2.3 POSS-scCO ₂ Systems	17
3. EXPERIMENTAL METHODS.....	19
3.1 Materials.....	19
3.2 Solubility Experiments.....	20
3.2.1 Experimental Set-Up.....	20
3.2.2 Cloud and Dew Point Measurements	21

3.3 Impregnation	23
3.3.1 Materials	23
3.3.2 Film Preparation	24
3.3.3 scCO ₂ Treatment	24
3.4 Characterization of POSS and PLA	24
3.4.1 Scanning Electron Microscopy (SEM).....	25
3.4.2 Differential Scanning Calorimetry (DSC).....	25
3.4.3 Thermal Gravimetric Analysis (TGA)	25
4. RESULTS AND DISCUSSION	27
4.1 L-V Equilibria of Methacryl POSS-CO ₂ Binary System	27
4.2 L-V Equilibria of Isooctyl POSS-CO ₂ Binary System.....	31
4.3 S-V Equilibria of Octaisobutyl POSS-CO ₂ Binary System	34
4.4 Effects of Temperature and Pressure on CO ₂ Density at Phase Separation ..	35
4.5 Modeling of Solubility	39
4.6. Thermal Characterization of POSS	50
4.7 SC Impregnation of PLA with POSS-CO ₂ Solutions.....	51
5. CONCLUSION	69
REFERENCES	73
APPENDICES	83
A. DSC ANALYSIS RESULTS	83

LIST OF FIGURES

FIGURES

Figure 1. 1 POSS structures; (a) random structure; (b) ladder structure; (c), (d) and (e) cage structure; (f) partial-cage structure [2]	1
Figure 1. 2 Variation in density of CO ₂ with pressure and temperature [8].....	3
Figure 3. 1 Chemical structures of a) octamethyl POSS, b) methacryl POSS, c) isooctyl POSS, d) octaisobutyl POSS.	19
Figure 3. 2 Experimental set-up for the solubility measurements.	21
Figure 4. 1 The dew points of methacryl POSS–CO ₂ binary system (□) at 308K and (◇) at 323K, (○) the repeated dew points. Curves represent regression fits of the data.	31
Figure 4. 2 The dew points of isooctyl POSS–CO ₂ binary system (□) at 308K and (◇) at 323K, the repeated dew points data (Δ) at 308K, (○) at 323K. Curves represent regression fits of the data.	33
Figure 4. 3 The dew points of octaisobutyl POSS–CO ₂ binary system (□) at 308K and (◇) at 323K, the repeated dew points data (Δ) at 308K, (○) at 323K. Curves represent regression fits of the data.....	33
Figure 4. 4 ScCO ₂ densities at the dew points of (a) methacryl POSS-CO ₂ and (b) isooctyl POSS-CO ₂ , and the cloud points of (c) octaisobutyl POSS-CO ₂ binary systems , for (■) 308K and (◆) 323K.....	36
Figure 4. 5 ScCO ₂ densities at the dew and cloud points of (■) trifluoropropyl POSS-CO ₂ , (✱) octaisobutyl POSS-CO ₂ , (▲) isooctyl POSS-CO ₂ , (◆) methacryl POSS-CO ₂ binary systems, for a) 308K, b) 323K.	38
Figure 4. 6 Plots of lnS versus lnP for a) methacryl POSS b) isooctyl POSS c) octaisobutyl POSS using Chrastil model at (●) 308K, (◆) 323K.....	41
Figure 4. 7 Plots of lnS versus lnP for a) methacryl POSS b) isooctyl POSS c) octaisobutyl POSS using del Valle model at (●) 308K, (◆) 323K.	42
Figure 4. 8 Plots of ln y_2 versus ρ for a) methacryl POSS b) isooctyl POSS c) octaisobutyl POSS using K-J model at (●) 308K, (◆) 323K.....	43
Figure 4. 9 Plots of $103 \cdot T \cdot \ln(y_2 P)$ versus lnP for a) methacryl POSS b) isooctyl POSS c) octaisobutyl POSS using MST model at (●) 308K, (◆) 323K.....	44

Figure 4. 10 Plots of $\ln(y_{2P}/Pref)$ versus $\rho - pref$ for a) methacryl POSS b) isooctyl POSS c) octaisobutyl POSS using Bartle model at (●) 308K, (◆) 323K.....	45
Figure 4. 11 Self-consistency tests for methacryl POSS solubility in scCO ₂ using five different models: (a) Chrastil model; (b) del Valle Aguilera model; (c) K-J model; (d) MST model; and (e) Bartle model. Experimental results: (●) 308K, (◆) 323K; calculated results (-).....	47
Figure 4. 12 Self-consistency tests for isooctyl POSS solubility in scCO ₂ using five different models: (a) Chrastil model; (b) del Valle; (c) K-J model; (d) MST model; and (e) Bartle model. Experimental results: (●) 308K, (◆) 323K; calculated results (-).....	48
Figure 4. 13 Self-consistency tests for octaisobutyl POSS solubility in scCO ₂ using five different models: (a) Chrastil model; (b) del Valle; (c) K-J model; (d) MST model; and (e) Bartle model. Experimental results: (●) 308K, (◆) 323K; calculated results (-).....	49
Figure 4. 14 POSS TGA curves in nitrogen.....	50
Figure 4. 15 Cross section of unprocessed neat PLA with magnifications of a) 2000x, b) 5000x, (PLA-N).....	55
Figure 4. 16 Cross section of PLA processed with F-POSS-CO ₂ solution at 13.8MPa and 323K for 3hours with magnifications of a) 2000x, b) 5000x, (PLA-1A).....	55
Figure 4. 17 Cross section of PLA processed with F-POSS-CO ₂ solution at 13.8MPa and 323K for 24 hours with magnifications of a) 2000x, b) 5000x, (PLA-2A).....	56
Figure 4. 18 Cross section of PLA processed with F-POSS-CO ₂ solution at 13.8MPa and 308K for 3hours with magnifications of a) 2000x, b) 5000x, (PLA-3A).....	56
Figure 4. 19 EDX measurement for the detection of Si and F on a) PLA-1A (323K, 3hr) b) PLA-2A (323K, 24hr), c) PLA-3A (308K, 24hr).....	57
Figure 4. 20 Cross section of PLA processed with octaisobutyl POSS-CO ₂ solution at 13.8 MPa and 323K for 3 hours with magnifications of a) 2000x, b) 5000x, (PLA-1B).....	58
Figure 4. 21 Cross section of PLA processed with octaisobutyl POSS-CO ₂ solution at 13.8 MPa and 323K for 24 hours with magnifications of a) 2000x, b) 5000x, (PLA-2B).....	59
Figure 4. 22 Cross section of PLA processed with octaisobutyl POSS-CO ₂ solution at 13.8 MPa and 308K for 24 hours with magnifications of a) 2000x, b) 5000x, (PLA-3B).....	59
Figure 4. 23 EDX measurement for the detection of Si on a) PLA-1B (323K, 3 hr), b) PLA-2B (323K, 24 hr), c) PLA-3B (308K, 24 hr).....	60

Figure 4. 24 TGA curves of, unprocessed neat PLA, scCO ₂ processed neat PLA, F-POSS impregnated PLA and octaisobutyl POSS impregnated PLA at 323K and 13.8 MPa for 3 h.	61
Figure 4. 25 TGA curves of neat F-POSS and octaisobutyl POSS, neat PLA, processed PLA and impregnated PLA at 323K and 13.8 MPa for 24 h.	63
Figure 4. 26 TGA curves of neat F-POSS and octaisobutyl POSS, neat PLA, processed PLA and impregnated PLA at 308K and 13.8 MPa for 24 h.	64
Figure A. 1 DSC plot of PLA-N Run 1.....	83
Figure A. 2 DSC plot of PLA-1 Run 1.	84
Figure A. 3 DSC plot of PLA-1A Run 1.....	84
Figure A. 4 DSC plot of PLA-1B Run 1.....	85
Figure A. 5 DSC plot of PLA-2 Run 1.	85
Figure A. 6 DSC plot of PLA-2A Run 1.....	86
Figure A. 7 DSC plot of PLA-2B Run 1.....	86
Figure A. 8 DSC plot of PLA-3 Run1.	87
Figure A. 9 DSC plot of PLA-3A Run 1.....	87
Figure A. 10 DSC plot of PLA-3B Run 1.....	88

LIST OF TABLES

TABLES

Table 1. 1 Physical data for gases, SCFs and liquid states [11]	4
Table 3. 1 Materials used in the study	20
Table 3. 2 Properties of PLA	23
Table 4. 1 The dew and cloud point pressures of POSS-CO ₂ binary systems at 308K and 323K, and the corresponding carbon dioxide densities.	28
Table 4. 2 Different parameters of the POSS-CO ₂ binary systems obtained by using the Chrastil, del Valle, K-J, MST and Bartle models.	40
Table 4. 3 Thermal Decomposition Temperatures for the POSS	51
Table 4. 4 SCI process condition.....	53
Table 4. 5 The degradation temperatures of PLA treated at 323K and 13.8 MPa for 3h.	62
Table 4. 6 The degradation temperatures of scCO ₂ -F-POSS processed at 323K and 13.8 MPa for 24 h.....	64
Table 4. 7 The degradation temperatures of PLA treated at 308K and 13.8 MPa for 24h.	66
Table 4. 8 Thermal properties of different types of PLA.	66

NOMENCLATURE

scCO ₂	Supercritical Carbon dioxide
T _c	Critical temperature
T _m	Melting point temperature, °C
T _g	Glass transition Temperature, °C
T _{5%}	Degradation temperature at 5% weight loss, °C
T _{max}	Maximum degradation rate temperature, °C
ΔH _f	Heat of fusion, J/g
X _c	Percent Crystallinity, %
ΔH _{Relax}	Relaxation enthalpy
P	Pressure, MPa
P _c	Critical pressure
P _{ref}	Reference pressure
ρ _{ref}	Reference density
SCF	Supercritical Fluid
[A]	Molar concentration of a solute in SCF, mol/lit
[B]	Molar concentration of solvent in SCF, mol/lit
[AB _k]	Molar concentration of the solvato complex in SCF, mol/lit
k	Association number
a,b,c,d	Constant parameters of density based models
K _{eq}	Equilibrium constant
E	Enhancement factor
ΔH _{solv}	Heat of solvation
ΔH _{vap}	Heat of vaporization
ΔH	Total heat of reaction (ΔH _{solv} + ΔH _{vap})
MW _A	Molecular weight of solute
MW _B	Molecular weight of solvent

g, q_v, q_s, q	Constants in Equations
S	Mass concentration, g/L
ρ	Solvent density, g/L
y_2	Solubility mole fraction of solute in supercritical fluid
R	Gas constant
K-J Model	Kumar and Johnston Model
MST Model	Mendez-Santiago and Teja Model
Del Valle Model	del Valle and Aguilera Model
$y_{i,exp}$	Experimental mole fraction solubility corresponding to point i
$y_{i,cal}$	Calculated solubility corresponding to point i
N	Number of experimental data points.

Subscript and Superscript

Cal	Calculated value
exp	Experimental value
ref	Reference

Abbreviations

POSS	Polyhedral Oligomeric Silsesquioxane
PP	Polypropylene
PS	Polystyrene
PLA	Poly (lactic) acid
PMMA	Poly (methyl methacrylate)
PEGM	Poly (ethylene glycol) methacrylate
PEG	Poly (ethylene glycol)
PLGA	Poly (lactic acid-co-glycolic acid)
SAN	Styrene acrylonitrile
F-POSS	Trifluoropropyl POSS
AARD%	Average Absolute Relative Deviation Percentage
SEM	Scanning Electron Microscopy
EDX	Energy Dispersive X-ray Spectroscopy

TGA	Thermal Gravimetric Analysis
DSC	Differential Scanning Calorimetry
SFC	Supercritical Fluid Chromatography
EOS	Equations of state
THF	Tetrahydrofuran

CHAPTER 1

INTRODUCTION

1.1 Polyhedral Oligomeric Silsesquioxane (POSS)

Polyhedral oligomeric silsesquioxane is one of the silsesquioxane molecules and these molecules refer to all structures with the chemical formula of $R_nSi_nO_{1.5n}$ where R group may be hydrogen or an organic functional group such as alkyl, alkylene, aryl, arylene, hydroxyl or epoxide groups [1]. Silsesquioxanes can be classified as random, ladder, cage and partial-cage structures, as shown in Figure 1.1.

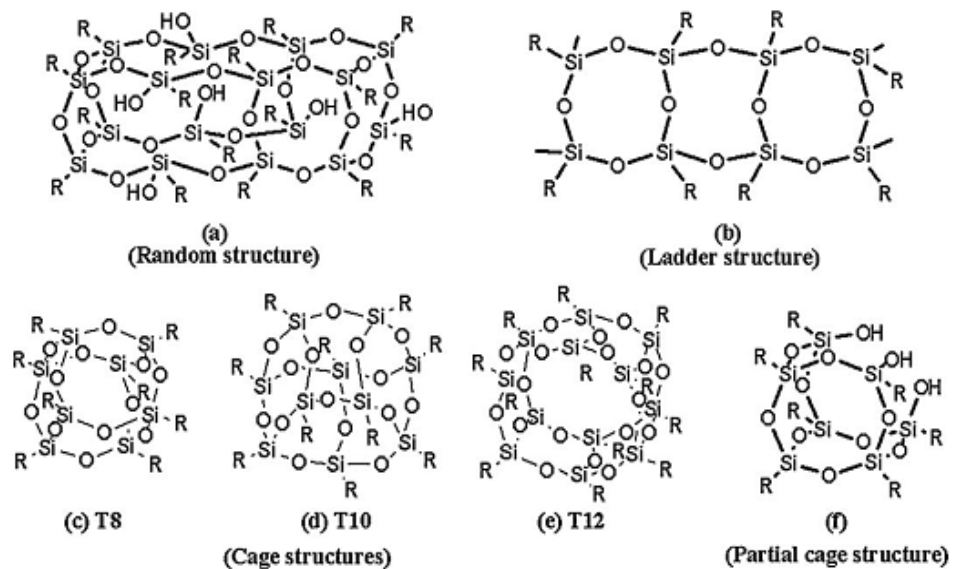


Figure 1. 1 POSS structures; (a) random structure; (b) ladder structure; (c), (d) and (e) cage structures; (f) partial-cage structure [2]

The cage-like structures of silsesquioxanes are usually called Polyhedral Oligomeric Silsesquioxanes which are abbreviated as POSS. The cage may generally contain eight, T8, ten, T10, or twelve, T12, (Figure 1.c, 1.d, 1.e) Si atoms but, the most commonly studied is the one with the 8 Si atoms. Due to its inorganic (silica) and organic groups (R) attached to each Si atom on the cage structure; the POSS possess hybrid material properties. They have been widely used in polymer applications as nanofillers [3,4]. Unlike most fillers or silicones, functional organic groups which are responsible for interactions of POSS with polymer chains enhance the compatibility of POSS molecules with the polymer matrix. This also serves to increase their dispersion within the polymer matrix. Additionally, POSS molecules with different reactivities used for polymer blending or copolymerization can be formed by varying these functional groups attached to Si atoms [2]. Different from traditional organic compounds, POSS derivatives are odorless, non-volatile and environmentally benign materials. When added to polymers, POSS can enhance many properties of the material, such as the mechanical properties, thermal stability, flame retardancy, oxidation resistance and low dielectric constant [5]. POSS-containing polymers have wide range of applications such as in packaging materials, biomedicine, catalyst support, coatings, membrane materials, electronics, optics, magnetic nano devices. Recently, POSS structures have significant importance for their use in biomedical applications, such as carriers for drugs. They are also used as imaging reagents due to their unique structure and size, biocompatibility, non-toxicity and excellent mechanical properties [6,7].

1.2 Supercritical Fluids (SCF)

Fluid is expressed as supercritical fluid (SCF) when the temperature and pressure of fluid is increased to values above its critical temperature (T_c) and the pressure (P_c), respectively. In this region, fluid cannot be condensed to form a liquid even with extremely high pressure and cannot evaporate to form a gas at increased temperatures [8].

One of the most important properties of SCFs is its tunable density. The density of SCF can exhibit dramatic variation with small changes in either pressure or

temperature in the vicinity of the critical points [9]. Figure 1.2 shows the variation of density as a function of pressure for carbon dioxide. This behavior also explains the large compressibility of SCFs at constant temperature in that region.

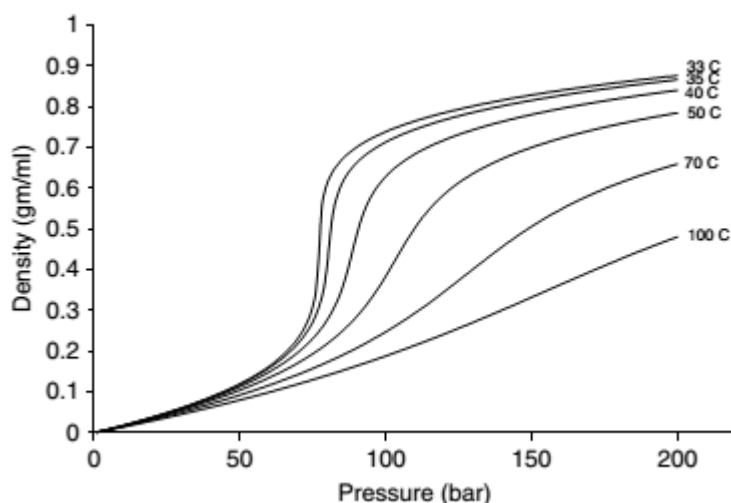


Figure 1. 2 Variation in density of CO₂ with pressure and temperature [8].

It is known that, the solvent power of a SCF is proportional to its density [10]. For solubility consideration, SCF does not have such high density as conventional liquid solvents. However, it can be changed from gas-like state to liquid-like state by increasing the pressure of the system at constant temperature. Hence, in general, the density and solvent power of a SCF are like those of a liquid near the critical region, while transport properties such as mass, momentum and thermal diffusivities lie between those of gases and liquids. The liquid-like density improves solubility character of SCF and gas-like transport properties of diffusivity and viscosity eliminate the mass transfer limitations of liquid solvents and allow rapid equilibration. Therefore, SCFs are of particular concern to industrial area due to its environmentally benign nature and the quality and purity of the end products. Physical properties of different fluid states are compared in Table 1.

Table 1. 1 Physical data for gases, SCFs and liquid states [11]

State	Density(g/ml)	Dynamic viscosity (g/cm.s)	Diffusion Coefficient (cm²/s)
Gas (ambient)	0.0006-0.002	0.0001-0.0030	0.100000-0.40000
Supercritical fluid (T_c, P_c)	0.2000-0.500	0.0001-0.0003	0.0007
Liquid (ambient)	0.6000-1.600	0.0020-0.0300	0.000002-0.00002

1.2.1 Supercritical Carbon Dioxide

Carbon dioxide (CO₂) is the most preferably used solvent in supercritical fluid technology since it offers many advantages compared to other SCF and organic solvents. The most important one is that it can decrease or eliminate the use of organic solvents in chemical processes. Therefore, it can prevent the emissions of volatile organic compounds which are associated with organic solvent use. It can be simply converted to gas state by releasing the pressure further there is no need to evaporation or separation to remove solvent residue. It is non-flammable, non-explosive, non-toxic, and inexpensive. It has relatively low critical temperature of 304 K and pressure of 74 bar [10]. Due to its low critical temperature, it prevents the degradation of heat sensitive material during processing. Its relatively low critical pressure allows lower cost of equipment which is required to supply high pressure. In addition, supercritical CO₂ has a zero surface tension which allows good wetting on the surface.

In general CO₂ is known as nonpolar solvent but it has some polarity due to having C=O bond and strong quadrupole moment which is enough to dissolve materials that has some groups such as fluoride, hydroxide or carbonyl [12]. Therefore, estimating the phase behavior of materials like alkanes or alkenes is not explicit. Co-solvents are usually used to improve the polarity of CO₂ and increase the solubility power of CO₂ for polar or heavy molecules.

Currently, in order to decaffeinate coffee or extract hops supercritical CO₂ has been widely used in food industry [13]. Besides, it is also used commercially in drying and cleaning processes such as microelectromechanical systems (MEMS) and in analytical scale, and used as a mobile phase in Supercritical Fluid Chromatography (SFC) to separate the components [12,14]. Other applications include polymer foaming, polymer impregnation, crystallization of plastics, chemical reactions, metal de-binding, powder coatings, dyeing of textiles, particle formation, and separation of oils from refinery sludge [15–19].

1.2.2 Solubility in Supercritical Carbon Dioxide

In order to design or develop environmentally benign material processing applications using supercritical fluid systems, knowledge of the phase behavior of the systems and solubility of novel materials in the SCF are the most significant and required criterion. The yield, rate, design and economy of the processes can be improved by using the solubility data. Solubility can be typically defined as mole fraction or the weight fraction of a solute in the supercritical phase which is in equilibrium with the bulk solute. The extent of solubility required can be different depending upon the process of interest. For instance, high solubility is desired for supercritical extraction processes while it is not preferred for particle formation using the supercritical anti-solvent precipitation process [20,21]. Solubility of solutes in scCO₂ is based on several properties of both solute and solvent such as solvent density and polarity, solute vapor pressure, molecular weight, molecular structure and polarity [22]. Particularly, solubility of solids and liquids in compressed gases (i.e supercritical fluids) can be varied majorly according to the small changes in temperatures and/or pressure that will affect the solvent density, solvent power, and other density-dependent parameters such as enthalpy, entropy and diffusivity.

Typically, solubility of solids or low volatile compounds increases with increasing pressure due to increase in density of CO₂ [8]. However, effect of temperature on the solubility is more complex because, there can be two temperature dependent factors to be considered: vapor pressure of the solute and density of supercritical carbon dioxide. As the temperature of the system increases solvent density (solvent power)

decreases while solute vapor pressure increases. Generally, in the low pressure region with greater compressibility, decrease in solvent density has dominant effect, and solubility decreases with increasing temperature. In the high pressure region, increase in the vapor pressure of the solute dominates, thus solubility increases with temperature [23]. This phenomenon can be observed in the phase behavior of many systems [8].

1.3 The modeling of solubility in supercritical CO₂

Experimental determination of solute solubilities in supercritical carbon dioxide at each operating conditions including different temperature and pressure is onerous and time consuming [20,24]. Because of that there are limited amount of experimental data in the literature. Therefore, mathematical models draw considerable interest to accurately predict the phase behavior of the systems. Equations of state models (EOS) and semi-empirical density based models are the two major approaches that have been commonly used to correlate the solubility data. EOS modeling requires the knowledge of pure component parameters of the solutes such as the critical temperature, critical pressure, acentric factor and the vapor pressure of the solute [25,26].

Thermodynamic properties of many organic or inorganic-organic hybrid materials which have complex structure are not known and group contribution methods used generally for estimation of thermodynamic properties do not give highly accurate estimations for that kind of complex structures. Therefore, the correlation of solubility data of these compounds with EOS accurately is not possible [27]. Solubility of these materials in supercritical CO₂ can be commonly modeled by using semi empirical models. Semi-empirical models do not require the knowledge of solute properties requested for an EOS and use only available variables such as pressure, temperature and density of SCF [27,28]. These relations are widely used for solubility of solute in SCF and give very successful result in correlating existing solubility data generally at solvent region of 10 MPa to about 30 MPa [26,29]. These models fail inevitably at higher pressures where more extreme density regimes exist such as liquid-like solvent density (1000 g.dm⁻³) [29].

1.3.1 Chrastil

The most commonly used density based model was proposed by Chrastil in 1982 [30]. The hypothesis behind the model is that one molecule of solvato complex AB_k is formed by the association of one molecule of a solute A with k molecules of a solvent B, where AB_k is in equilibrium with the system. This relationship is established between the logarithm of solubility and logarithm of density linearly.



At the equilibrium, K_{eq} is the equilibrium constant:

$$K_{eq} = \frac{[AB_k]}{[A][B]^k} \quad (1)$$

By using logarithms the expression can be written as:

$$\ln K_{eq} + \ln[A] + k \ln[B] = \ln[AB]_k \quad (2)$$

[A] is the solute concentration,

[B] is the solvent concentration,

[AB] is the concentration of the solvato complex

k is an association number.

K_{eq} is expressed logarithmically:

$$\ln K_{eq} = \frac{\Delta H_{solv}}{RT} + q_s \quad (3)$$

where ΔH_{solv} denotes the heat of solvation, R denotes ideal gas constant, T denotes the absolute temperature, and q_s is a constant.

The logarithm of the solute vapor concentration can be approximated by the Clausius-Clapeyron equation:

$$\ln[A] = \frac{\Delta H_{vap}}{RT} + q_v \quad (4)$$

where ΔH_{vap} is the heat of vaporization of the solute and q_v is a constant.

Equations 2, 3 and 4 can be used to obtain:

$$\frac{\Delta H}{RT} + q + k \ln[B] = \ln[AB_k] \quad (5)$$

where ΔH is the total reaction heat, q is a constant and they equal to:

$$\Delta H = \Delta H_{solv} + \Delta H_{vap} \text{ and } q = q_s + q_v$$

Concentration is transformed from mol/L to g/L by dividing into the molecular weights:

$$[AB]_k = \frac{S}{MW_A + kMW_B} \quad (6)$$

$$[B] = \frac{\rho}{MW_B} \quad (7)$$

MW_A and MW_B are the molecular weight of solute, A, and solvent, B, respectively. S (g/L) is the mass concentration of the solute, and ρ (g/L) is the solvent density.

Equations 6 and 7 are used in Eq. 5 to obtain:

$$\frac{\Delta H}{RT} + q + k \ln \rho - k \ln MW_B = \ln S - \ln(MW_A + kMW_B) \quad (8)$$

The Chrastil equation takes the following form:

$$S = \rho^k \exp\left(\frac{a}{T} + b\right) \quad (9)$$

Where k is an association number, T is the temperature in K, a depends on the heat of solvation and the heat of vaporization of the solute, and b is a function of the molecular weights of the solute and scCO₂, they are expressed as:

$$a = \frac{\Delta H}{R} \quad (10)$$

$$b = \ln(MW_A + kMW_B) + q - k \ln MW_B \quad (11)$$

Model parameters, k , a , and b can be obtained by the fitting of experimental data.

In Chrastil model, S is transformed to mole fraction (y_2) to compare the correlation models more easily on the same basis:

$$S = \frac{y_2 \rho MW_{solute}}{MW_{SCF}(1 - y_2)} \quad (12)$$

1.3.2 Del Valle and Aguilera

Del Valle and Aguilera equation [31] is modified version of Chrastil's equation which is derived especially for the solubility of vegetable oils to be estimated in compressed CO₂. They proposed the following modification to compensate for the change in the enthalpy of vaporization ΔH_{vap} with temperature:

$$S = \rho^k \exp\left(\frac{a}{T} + b + \frac{c}{T^2}\right) \quad (13)$$

Other than c , which is function of $1/T^2$ and introduced by Del Valle and Aguilera, all variables have the same meaning as in the Chrastil model. This equation also provides wider temperature ranges to be used in solubility estimations.

1.3.3 Kumar and Johnston

Similar to Chrastil model new linear relationship between $\ln y_2$ and ρ was proposed by Kumar and Johnston (1988) [32]:

$$\ln y_2 = k\rho + \frac{a}{T} + b \quad (14)$$

$$y_2 = \exp(k\rho + \frac{a}{T} + b) \quad (15)$$

1.3.4 Mendez-Santiago and Teja

Mendez-Santiago and Teja [33] proposed a new density based model for solid solubility which is based on the theory of dilute solutions derived from the linear relationship between $T \ln(E)$ and ρ (Eq. 16).

$$T \ln E = T \ln \left(y_2 \frac{P}{P_2^{sub}} \right) = b + k\rho \quad (16)$$

Where E is the enhancement factor which requires knowledge of the sublimation pressure, P_2^{sub} , and they are often not available for nonvolatile solutes. Therefore, Clausius–Clapeyron expressions $E = y_i P / P_i^s$ and $\ln(P_i^s) = A + B/T$ were incorporated into Eq.16 to use the model with compounds whose sublimation pressure is unknown:

$$T \ln(y_2 P) = b + k\rho + aT \quad (17)$$

where y_2 is the mole fraction solubility of the solute in the scCO₂; ρ is the density of the scCO₂; T and P are the operating temperature and pressure; a , b , k are the adjustable parameters obtained by the fitting of experimental data. Moreover, when experimental data are plotted in the form of $T \ln(y_2 P) - aT$ versus ρ , the entire mole fraction (y_2) values at different temperatures fit in a single straight line. Therefore, the model can also be used to check the consistency of experimental data. However, applications of the model existing in the literature show that the model can fail to correlate to solubility data at low density regions [29,34,35].

1.3.5 Bartle

Bartle et al.[36] presented a semi-empirical model to correlate the solubility data in SCF. The Bartle equation is given as:

$$\ln\left(\frac{y_2 P}{P_2^v}\right) = k\rho + a' \quad (18)$$

Here y_2 is the mole fraction solubility; T is the absolute temperature (K), P is the system pressure, ρ is the density of scCO₂ at the operating temperature and pressure (g/L). Due to the lack of knowledge of vapor pressure of some solutes (P_2^v), Bartle et al. used reference pressure P_{ref} which is assumed as the standard pressure ($P_{ref} = 0.1\text{MPa}$),

$$\ln\left(\frac{y_2 P}{P_{ref}}\right) = k(\rho_1 - \rho_{ref}) + \frac{a}{T} + b \quad (19)$$

Where ρ_{ref} is a reference density for which a value of 700 kg/m³. a , b , and k are the empirical parameters. ρ_{ref} is used to reduce the sensitivity of a and b because of the possible experimental error in the solubility data. Parameter a is related to the enthalpy of vaporization of the solute, ΔH_{vap} , by the expression $\Delta H_{vap} = -Ra$, where R is the gas constant.

1.4 Impregnation

Impregnation is a method of saturating a material with desired molecules of compounds. scCO₂ technique in the case of using supercritical carbon dioxide solution leads to eliminating the organic solvents used in traditional methods [37,38]. Therefore, there is no need to further purification steps to remove the organic solvent. This advantage makes scCO₂ the most preferred solvent especially for drug delivery systems with polymers [39]. Apart from the drug impregnation the most significant example is the dye impregnation into polymer matrix [40,41].

For supercritical impregnation process, there are two possible mechanisms to be followed [42,43]. One of them is based on the deposition of the solute compound in scCO₂ phase into polymer matrix. Firstly, polymer is exposed to scCO₂ for a period of time because the polymers exposed to the scCO₂ swell and exhibit increase in chain mobility which induce the transport of compounds into the polymer matrix. Secondly, excess amount of solute is dissolved in scCO₂ and the solute-CO₂ solution which is in equilibrium with the excess solute is conducted to the polymer for solute transfer. And finally, CO₂ is released by controlled depressurization to entrap the solute molecules into the polymer matrix. These steps can be followed separately or together relating to the process technology selected and this mechanism is very applicable for the system containing highly soluble solutes in SCF.

The other mechanisms depend on the compatibility between solute and polymer, in other words partitioning of solutes between polymer and SCF. In this case even solute solubility is very low in SCF, the affinity of solute molecules for polymer becomes driving force for the impregnation process [44,45].

CHAPTER 2

LITERATURE SURVEY

2.1 Applications of POSS in Polymer Processing

POSS are mostly used as fillers in polymeric blends and nanocomposites [46–48]. Other applications include surface modification and coating [49,50] and formation of polymeric films [51].

In the study of Baldi et al. isooctyl, octaisobutyl and octamethyl POSS were used to prepare POSS/Polypropylene (PP) blends to investigate the effect of alkyl group length of POSS on the mechanical behaviour of POSS/PP blends. Addition of octamethyl-POSS increased the Young's modulus and decreased the yield strength in comparison with neat PP. On the other hand, isooctyl and octaisobutyl POSS were decreased both Young's modulus and the yield strength by increasing the POSS content [46].

In the preparation of Poly (methyl methacrylate) (PMMA) nanocomposites by S.R. Jin et al., octaisobutyl methacryl and octasilane POSS were used and effects of these types of POSS for PMMA films at two different film thicknesses were investigated. Methacryl POSS/PMMA exhibited the most effective behaviour in both T_g and relaxation enthalpy (ΔH_{Relax}) because of the physical aging [47].

Dielectric properties of nanostructured PP-(octamethyl and isooctyl) POSS compounds which were produced with melt state compounding were investigated by M. Takala et al. Relative permittivity, loss factor and volume resistivity measurements showed that, octamethyl POSS improved the dielectric properties of PP. Octamethyl POSS increased the breakdown strength and permittivity values

according to pure PP. However, increase in breakdown strength for PP with isooctyl POSS was not high as such in octamethyl POSS compound. Also with higher amount of octamethyl POSS, higher loss factor values were obtained and at lower frequencies reduced volume resistivity were obtained. However, improvements obtained with isooctyl POSS were not significant as compared to PP/octamethyl POSS compounds [48].

In the study of Ciesielczyk et al. innovative hybrid filler was obtained by chemical functionalization of silica surface with incorporation of methacryl POSS and silane and this modification led to increase in hydrofobic nature and dispersive character of the filler. Additionally, decrease in surface area of hybrid filler was obtained after the functionalization. Bifunctionalized inorganic fillers with improved properties provide wide range of applications of polymer composites and reduce the cost of their production [49].

In recent study by H Mahfuz et al., octaisobutyl POSS was used as a reinforcement material in the modification of fiber/matrix interface of carbon/vinyl ester composites by the coating of carbon fiber. Mechanical tests have showed that interlaminar shear strength and low velocity impact strength have improved by addition of POSS. Coating with POSS also reduces water absorption and preserve the composite properties [50].

Another application by Y.H. La et al. is for preparation of thin and durable hydrogel films with a hydrophilic poly (ethylene glycol) methacrylate (PEGM) by addition of methacryl POSS which contains UV-curable methacrylate groups as a multifunctional cross-linker. By adjusting the weight ratio of methacryl-POSS and PEGM, the water uptake of the crosslinked POSS-PEGM films could increase from 8% to 90%. Following improvement in the water uptake and also water permeability of the film was obtained by using polyethylene glycol (PEG) to form molecular-scale pores within the crosslinked film after extraction of the PEG. The coated polysulfone (PSF) ultra-filtration (UF) membranes with nanoporous and water permeable POSS-PEGM demonstrated great anti-fouling efficiency for oil-water emulsions or a bovine serum albumin system [51].

In the study of Fina et al. octamethyl-, octaisobutyl- and octaisooctyl-POSS were used to prepare polypropylene (PP)/POSS nanocomposites by melt blending technique. They investigated the effect of functional group chain length of POSS on the morphological and thermal properties of PP based nanocomposites. It was observed from the SEM images that compatibility of POSS with PP matrix and extent of dispersion of POSS inside polymer matrix were improved by increase in chain length from octamethyl-POSS to octaisobutyl-POSS. However, further increase in alkyl chain length with octaisooctyl-POSS did not make any improvement. Octamethyl and octaisobutyl-POSS were found to have influence over crystallization behavior of nanocomposites; octamethyl POSS as a nucleating agent and octaisobutyl-POSS inducing polymer polymorphism. Regarding thermal characterization, in order to see the effect of POSS addition on the thermal degradation behavior, thermogravimetric analysis performed in nitrogen and air. In nitrogen media, the addition of POSS does not show significant change to the degradation behaviour of the composite. However, in the presence of air, maximum degradation temperature of PP is shifted to higher temperatures especially with the addition of octaisobutyl POSS which can form silica residue on the surface of the polymer by oxidation of its more reactive organic part according to octamethyl group [52].

2.2 scCO₂ Impregnation in Polymers

Impregnation process of polymers with scCO₂ overcomes the difficulties arising from use of conventional solvents. They would not be appropriate for many polymers due to their surface tension and viscosity [53]. For impregnation by scCO₂, dissolving of polymers with conventional solvents and the further processes like heating and blending are not required due to the easy penetration of scCO₂ into polymers and demonstrating high permeation rate in almost every polymer [54]. The polymers exposed to the scCO₂ swell and exhibit increased chain mobility which accelerates the incorporation of solutes into the polymer matrix. Solute used in polymer impregnation processes generally include, dyes for textile industry, drugs for controlled release systems, organometallic precursors for reduction of

polymers, and monomers and initiators for polymer blends [41,55–57]. The exposure of polymer to the scCO₂ leads to decrease in T_g of the polymer and increasing the processability of them. Additionally, extent of the polymer swelling, diffusion rate and partitioning of substances can be tuned by changing the solvent power of CO₂ with the pressure and temperature adjustments [44].

scCO₂ impregnation of solutes into polymers which are poly (vinyl chloride) (PVC) (Berens et al. 1992; Muth et al. 2000) [45,58], poly(vinylpyrrolidone) (PVP) (Kazarian & Martirosyan 2002; Manna et al. 2007; Banchemo et al. 2009; Hussain & Grant 2012) [59–62], polycarbonate (PC) (Berens et al. 1992; Muth et al. 2000; Hasell et al. 2008) [45,58,63], poly (methyl methacrylate) (PMMA) [(Kazarian et al. 1997; West et al. 1998; Ngo et al. 2003; Üzer et al. 2006; Hussain & Grant 2012; Andanson et al. 2009)] [41,62,64–67] and poly(ethylene terephthalate) (PET) (Kazarian et al. 1999; Sicardi et al. 2000; Fleming et al. 2005) [40,68,69] are processed more easier because of their amorphous or semi-crystalline nature. Berens et al. have reported that the impregnation of additives into polymer is more effective at high pressure for these polymers and obviously, the additives must be soluble in CO₂ medium. However, the amount of impregnated additives within the polymer is more about the affinity of additives for the polymers [45].

Biodegradable and biocompatible polymers have also investigated for impregnation process due to their utility in drug delivery systems and biosurface modifications. Poly(lactic acid) (PLA) and poly(lactic acid-co-glycolic acid) (PLGA) (Cabezas et al. 2012; Liu et al. 2005; Guney & Akgerman 2002; López-Periago et al. 2008; Sugiura et al. 2005; Yoda et al. 2011) [37,56,70–73] are the most commonly used polymers in many kinds of biodegradable polymers for scCO₂ impregnation of pharmaceuticals such as ibuprofen and indomethacin (nonsteroidal anti-inflammatory drugs), 5-fluorouracil [38,71] for chemotherapy, β -estradiol for estrogen hormone therapy [74].

2.3 POSS-scCO₂ Systems

In order to develop scCO₂ processing techniques applying novel materials such as POSS, thermodynamic phase behaviors of these materials with CO₂ are needed to be studied. Recently, POSS with CO₂-philic fluoroalkyl groups (F-POSS) was investigated for its solubility in scCO₂. Solid-vapor phase equilibrium curves of the binary system were determined with the cloud point measurements. It was found that at temperature and pressure ranges of 308–323K and 8.3–14.8 MPa, F-POSS exhibits solubility in scCO₂ up to 4.4% by weight and 0.17% by mole. F-POSS solubility in scCO₂ decreases with increasing temperature. Using the obtained phase behavior data of F-POSS-CO₂ binary system, process conditions were determined for the surface coating application without use of any organic solvents. A uniform coating of F-POSS aggregates was obtained by F-POSS deposition on the PMMA sheet in scCO₂ [75].

In Eriş et al. study [57], the F-POSS solubility data [75] were used to design a process where a F-POSS fiber was extracted to create a microchannel in an aerogel for optofluidic applications. Primarily, the fibers were prepared by melt and freeze processing of F-POSS powder in a U-shaped mold. U-shaped fibers were placed into silica solution and then solution was waited for gelation and aging processes. Since F-POSS is known as soluble in scCO₂, the fibers could extract from silica alcogel during supercritical drying of wet silica alcogel by scCO₂. The extraction of POSS fibers formed U-shaped hollow channel within the gel structure and in order to fill the channels with water aerogel surface was turned into hydrophobic by reaction of silanol groups at the surface of the aerogel with hexamethyldisilazane in the presence of scCO₂. They obtained optofluidic waveguides by coupling of light into the water-filled channel and monitoring the channel output.

Costeux et al. worked on production of homogeneous nanocellular foams by scCO₂ foaming process of thermoplastic polymers in order to improve the thermal insulation properties of them. They investigated the effect of adding additives such as POSS and silica nanoparticles on polymer foaming and reported enhanced cell nucleation density for PMMA (polymethyl methacrylate) and SAN (styrene

acrylonitrile) copolymers with addition of methacryl POSS and silica nanoparticles by three orders of magnitude. At pressures above 300 bar and the temperature at or below 40°C, lowest density nanocellular foams were obtained by addition of methacryl POSS to the PMMA copolymer. However in this study, there is no information on phase behavior of methacryl POSS-CO₂. Therefore, it is not known that whether methacryl POSS completely removed from polymer at the operating conditions.

CHAPTER 3

EXPERIMENTAL METHODS

3.1 Materials

Octamethyl POSS (94.0%, Figure 3.1.a), methacryl POSS (97.2%, Figure 3.1.b), isooctyl POSS (99.0%, Figure 3.1.c), and octaisobutyl POSS (99.4%, Figure 3.1.d) were supplied from Hybridplastics. All the POSS types were used in the experiments without further purification. Carbon dioxide (99.9%) was supplied from Linde. Octamethyl POSS and octaisobutyl POSS with bulk densities of 0.59 g/cm^3 and 0.63 g/cm^3 respectively are in powder form. Isooctyl POSS and methacryl POSS are viscous liquids with densities of 1.01 g/cm^3 and 1.2 g/cm^3 and viscosities of 19 and 18 Poise at 298 K, respectively. Both the density and viscosity data were supplied by the manufacturer. The solubilities of POSS in supercritical carbon dioxide have been measured by cloud or dew point experiments.

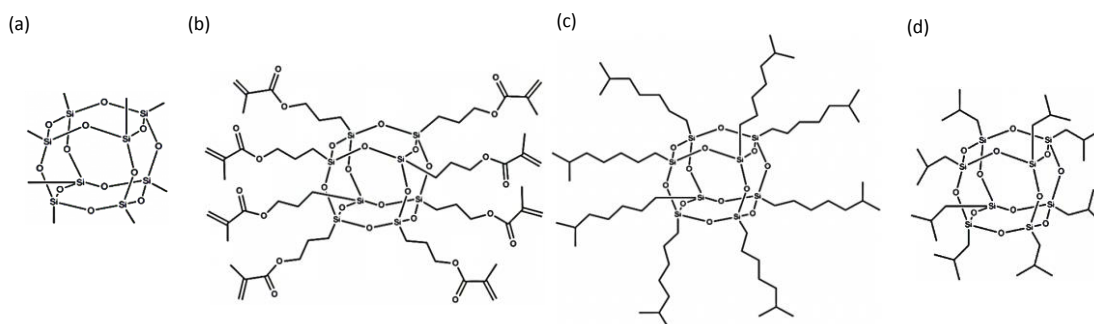


Figure 3. 1 Chemical structures of a) octamethyl POSS, b) methacryl POSS, c) isooctyl POSS, d) octaisobutyl POSS.

Table 3. 1 Materials used in the study

Materials	Appearance	Vendor	MW(g/mol)	Density(g/cm ³)
POSS				
Octamethyl	powder	Hybrid Plastics	536.96	0.59
Methacryl	Viscous liquid		1433.97	1.01
Isooctyl	Viscous liquid		1322.46	1.20
Octaisobutyl	powder		873.60	0.63
CO ₂ (99.99%)	liquid	Linde	-	-

3.2 Solubility Experiments

3.2.1 Experimental Set-Up

The dew and cloud point measurements of POSS-CO₂ binary systems were performed using a high-pressure set-up, which is represented schematically in Figure 3.2. The set-up contained a custom-made jacketed stainless steel high-pressure vessel with two sapphire windows, a rupture disc, and two needle valves. The inner volume of the high-pressure vessel is 46.15±0.07 cm³. A syringe pump (Teledyne ISCO-260D) was used to charge CO₂ into the vessel. The temperature of the ISCO pump reservoir was controlled with a water circulating heater (Polyscience, 9112) within a range of ±0.01 K. The syringe pump pressure accuracy was within ±0.05 MPa. Prior to the measurements, the syringe pump was loaded with CO₂ from a CO₂ cylinder with dip tube. A thermocouple (Omega Engineering KMQXL-IM150U-150) was used to measure the temperature of the high-pressure vessel contents to an accuracy

of $\pm 0.5\text{K}$. The temperature of the vessel was controlled by a water circulating heater (Polyscience, 9112) within a range of $\pm 0.01\text{ K}$. The vessel pressure was measured using a pressure transducer (Omega Engineering PX419) to an accuracy of $\pm 0.03\text{ MPa}$. The set-up included a magnetic stir plate to mix the contents of the vessel continuously.

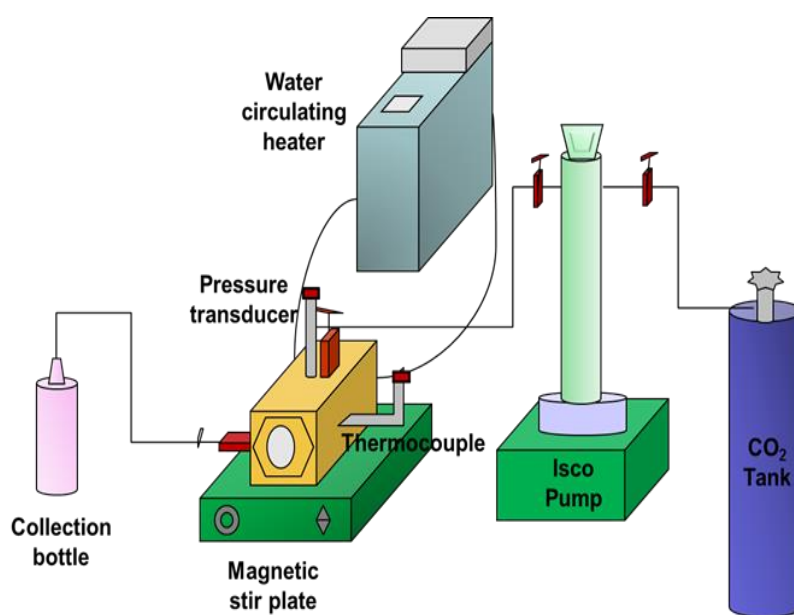


Figure 3. 2 Experimental set-up for the solubility measurements.

3.2.2 Cloud and Dew Point Measurements

The solubilities of POSS in scCO₂ have been obtained by cloud and dew point measurements for liquid POSS and solid POSS, respectively. Both measurement procedures were identical except the phase of the solute that segregated from the homogenous mixture. Initially, the high pressure vessel was loaded with POSS, which was weighed to an accuracy of $\pm 0.0001\text{g}$. The vessel was sealed and its temperature was increased to the desired value by the water circulating heater. The temperature of the ISCO pump reservoir was also set to the desired value. Next, the

vessel was connected to the syringe pump with high-pressure tubing carrying a check valve to avoid reverse flow. After setting the pressure of the ISCO pump to the desired value, the tubing between the vessel and the syringe pump was loaded with CO₂ using the syringe pump operating at constant-pressure mode. Before introducing CO₂ into the vessel through the vessel inlet valve, the volume of the pump reservoir filled with CO₂ was recorded. Next, CO₂ was loaded into the vessel slowly until the vessel pressure was equalized to the syringe pump pressure. The inlet valve was then closed and the volume of the pump reservoir filled with CO₂ was recorded one more time to calculate the volume displacement, which gave the volume of the CO₂ loaded into the vessel. The weight of CO₂ loaded into the cell was determined from the density of CO₂ at the constant loading temperature and pressure, obtained from the NIST Chemistry WebBook [76] and the loaded CO₂ volume. The composition of POSS in the binary system was determined from the loaded weights of POSS and the charged CO₂. The ISCO pressure was selected such that the loading resulted in a desired CO₂ density in the vessel allowing CO₂ to dissolve all the solute loaded in the cell. Therefore, after charging the system with carbon dioxide, the loaded POSS was completely dissolved in the supercritical fluid, while the content of the cell was mixed continuously. Next, slow and isothermal depressurization of the system was started through a slightly opened exit valve, while the contents of the vessel were vigorously and continuously stirred. The vigorous and continuous mixing and the slow depressurization rate of approximately 0.007 MPa/s maintained the solution to remain in a single homogenous phase with unchanged-solution composition. The cloud or dew pressure was recorded immediately when POSS phase segregated from the single-phase solution, which caused cloudiness that was visually detectable. Once the phase segregation pressure was recorded, the experiment was ended, and the vessel was discharged and cleaned thoroughly. This procedure was repeated at 308 and 323K for each investigated POSS at various concentrations. Some of the solubility experiments were chosen randomly and were repeated. The repeated experiments were performed on different days by following all the steps of the solubility measurements described above. The highest measurement error was ± 0.54 MPa, which was obtained in the repeated dew pressure measurements of the isooctyl POSS-CO₂ binary system. The accuracy and reliability of the measurement

technique was previously verified by reproducing the literature data of the extensively studied liquid-vapor equilibria of the ethanol-CO₂ binary system [75]. This technique was also used and explained in detail in the previous studies of the phase equilibria measurements of hexamethyldisilazane-CO₂, hexamethyldisiloxane-CO₂ and hydroxy-terminated poly(dimethylsiloxane)-CO₂ binary systems [77–79].

3.3 Impregnation

3.3.1 Materials

Poly(lactic acid) (PLA) with 5% D-lactide stereoisomer content in granular form was purchased from NaturaPlast, France. The selected transparent PLA has average molecular weight of (M_w) 278000 and polydispersity (M_w/M_n) of 1.78. Table 3.1 shows the properties of PLA provided by the manufacturer (NaturePlast PLI-005).

Table 3. 2 Properties of PLA

Physical Properties	Value
Density (g/ml)	1.25 (± 0.05)
Melt Temperature ($^{\circ}\text{C}$)	144-155
Degradation Temperature ($^{\circ}\text{C}$)	240-250

The additives used in this study for PLA impregnation process were trifluoropropyl POSS (F-POSS) ($(\text{C}_3\text{H}_4\text{F}_3)_8(\text{SiO}_{1.5})_8$, MW = 1193.15 $\text{g}\cdot\text{mol}^{-1}$) octaisobutyl POSS ($\text{C}_{32}\text{H}_{72}\text{O}_{12}\text{Si}_8$, MW = 873.60 $\text{g}\cdot\text{mol}^{-1}$) in powder form were provided by Hybridplastics, Hattiesburg, Mississippi, USA. The polymeric films were prepared by solvent casting using chloroform (99-99,4% purity, Sigma-Aldrich, Taufkirchen, Germany). Carbon dioxide (99.99%) was obtained from Linde Gas (Kocaeli, Turkey).

3.3.2 Film Preparation

Polymeric films with 0.60 mm thickness were prepared by solvent casting method before starting the supercritical CO₂ impregnation process. A sealed gas bottle was used to prevent evaporation of chloroform which was used to dissolve the PLA. In order to obtain homogeneous solution the solution was mixed continuously with a magnetic stirrer. Then the solution was poured on to a glass plate and waited overnight at an ambient pressure and temperature for the evaporation of solvent. The final film was obtained and cut into desired pieces.

3.3.3 scCO₂ Treatment

The high pressure set up used for the impregnation experiments was the same as previously presented experimental set up that was schematically illustrated in Figure 3.2. Firstly, excess amount of POSS and magnetic stirrer bar were loaded in the high pressure vessel and then PLA was positioned. A metal mesh sheet was inserted between the POSS and PLA to prevent the physical contact. The procedure for charging CO₂ to the vessel was given in detail in Chp 3.2.2. However, in this part there is no need to record the volume. Then, in order to allow the POSS to penetrate into polymer matrix, the system was left 3 hours and overnight at adjusted temperature and pressure at which POSS determined as soluble with the solubility experiments. Rapid depressurization of the system was carried out while the contents of the vessel were continuously stirred. After releasing CO₂ to atmospheric pressure the vessel was opened, POSS impregnated polymer was taken out and POSS precipitation occurred on the surface of the polymer was removed gently by hand.

3.4 Characterization of POSS and PLA

The morphology of the cross section of the whole PLA samples were analyzed and imaged by scanning electron microscope (SEM). Differential scanning calorimetry (DSC) and thermal gravimetric analysis (TGA) were performed to understand the effect of F-POSS and octaisobutyl POSS addition on the thermal properties of PLA.

3.4.1 Scanning Electron Microscopy (SEM)

In this study, polymer film morphologies were observed by scanning electron microscopy (SEM) analysis (FEI Quanta-400 F). In order to analyze the cross section, PLA films were broken in liquid nitrogen and were placed vertically on carbon tape. The samples were prepared to analysis by gold/palladium coating to have an electrically conductive layer. SEM images were taken between 500x to 5000x magnifications.

3.4.2 Differential Scanning Calorimetry (DSC)

In this study, Shimadzu DSC-60 analyzer was used for the DSC analysis. The temperature of the samples was increased from room temperature to 200°C for PLA and to 350°C for powder form POSS (octaisobutyl and octamethyl POSS) with a heating rate of 10°C/min, under nitrogen flow with a flow rate of 60 ml/min. Then, the sample was cooled back to room temperature. Melting and crystallization temperatures, heat of fusion and percent crystallinity of the polymers were determined from the DSC curves.

3.4.3 Thermal Gravimetric Analysis (TGA)

In this study, Shimadzu DTG-60H thermal gravimetric analysis device was used for the TGA of all types of POSS, neat PLA and the processed PLA. The samples were continuously weighed while being heated from room temperature to 700°C and 500°C for POSS and PLA samples respectively with a constant heating rate of 10°C/min. The samples were held under nitrogen atmosphere during the analysis and the flow rate of the nitrogen gas was held at 60 ml/min.

CHAPTER 4

RESULTS AND DISCUSSION

4.1 L-V Equilibria of Methacryl POSS-CO₂ Binary System

In order to investigate the effect of the functional organic groups on the solubility of POSS in supercritical carbon dioxide, four different structures were investigated including octamethyl POSS, methacryl POSS, isooctyl POSS and octaisobutyl POSS. In an earlier study it was shown that POSS with fluoropropyl groups attached to the silicon atoms had a significant solubility in scCO₂ at moderate pressures [75]. Among the POSS structures reported in this work, octamethyl POSS was found to be insoluble in scCO₂. This shows that CO₂-philic groups attached to the silicon atoms of POSS can enhance interaction of POSS with CO₂ such as in the trifluoropropyl POSS-CO₂ binary system. In this study, carbonyl functionality is one of the functionalities that were selected to observe their contributions on the solubility of POSS in scCO₂. For this aim, methacryl POSS which has carbonyl functionalities incorporated in the methacrylate groups was selected. Figure 4.1 shows the measured solubility isotherms of methacryl POSS in scCO₂. In this figure mole fractions of solubilized POSS at various dew pressures are plotted at 308 and 323K. The plotted data is given in Table 4.1. In Figure 4.1, the region on the right-hand side of the solubility isotherm, which represents the higher pressure region, represents the conditions at which the binary mixture exists as a single phase. At these conditions POSS is completely dissolved in scCO₂. At lower pressures, two isotherms converge to each other. Solubility in supercritical fluids is influenced strongly by the system temperature and pressure due to the change in the density, and thus the solvent power of the supercritical fluid. An isothermal increase in pressure increases the CO₂ density, which in turn increases its solvent power. This

corresponds to an increase in the solubility of the methacryl POSS in scCO₂. The solubility of methacryl POSS, on the other hand, decreases with an isobaric increase in temperature. As the temperature of a single-phase binary system increases, the density, thus the solvent power of supercritical CO₂ decreases rapidly. The decrease in the scCO₂ density due to an isobaric increase in temperature can have a dominant negative contribution on the solubility of the solute in scCO₂, compared to the positive contribution of the increase in the solute vapor pressure [23]. This is also the case for methacryl POSS-scCO₂ binary system at the studied temperature, pressure and composition ranges. As the temperature of a single phase binary system is increased at constant pressure, to retain the system at single phase, where methacryl POSS completely dissolves in scCO₂, density of the system has to be increased subsequently by increasing the pressure.

Table 4. 1 The dew and cloud point pressures of POSS-CO₂ binary systems at 308K and 323K, and the corresponding carbon dioxide densities.

308K			
Methacryl POSS weight fraction (±0.8%)	Methacryl POSS mol fraction	Pressure (MPa)	CO₂ density (g/cm³)
0.0014	0.00004	17.51	0.8433
0.0029	0.00009	19.71	0.8633
0.0024	0.00007	20.53	0.8700
0.0042	0.00013	22.61	0.8855
0.0090	0.00028	26.48	0.9101
0.0128	0.00040	28.50	0.9214
0.0132	0.00041	29.32	0.9256

Table 4.1 (continued)

Isooctyl POSS weight fraction ($\pm 0.8\%$)	Isooctyl POSS mol fraction	Pressure (MPa)	CO₂ density (g/cm³)
0.0043	0.00015	11.31	0.7517
0.0066	0.00022	12.84	0.7829
0.0085	0.00029	13.43	0.7928
0.0108	0.00036	14.26	0.8051
0.0135	0.00046	15.42	0.8203
0.0161	0.00054	16.18	0.8292
0.0200	0.00068	17.22	0.8404
Octaisobutyl POSS weight fraction ($\pm 0.8\%$)	Octaisobutyl POSS mol fraction	Pressure (MPa)	CO₂ density (g/cm³)
0.0013	0.00006	9.03	0.6644
0.0019	0.00010	10.02	0.7135
0.0027	0.00013	11.82	0.7634
0.0030	0.00015	12.86	0.7833
0.0035	0.00018	13.24	0.7897
323K			
Methacryl POSS weight fraction ($\pm 0.8\%$)	Methacryl POSS mol fraction	Pressure (MPa)	CO₂ density (g/cm³)
0.0009	0.00003	17.65	0.7517
0.0017	0.00005	19.68	0.7804
0.0025	0.00008	22.89	0.8154
0.0029	0.00009	23.03	0.8167
0.0033	0.00010	26.13	0.8433
0.0046	0.00014	26.54	0.8464

Table 4.1 (continued)

Isooctyl POSS weight fraction ($\pm 0.8\%$)	Isooctyl POSS mol fraction	Pressure (MPa)	CO₂ density (g/cm³)
0.0044	0.00015	16.28	0.7276
0.0060	0.00020	16.51	0.7320
0.0073	0.00024	16.81	0.7375
0.0125	0.00042	18.01	0.7573
0.0135	0.00046	19.02	0.7717
0.0181	0.00061	20.13	0.7859
0.0195	0.00066	20.15	0.7861
Octaisobutyl POSS weight fraction ($\pm 0.8\%$)	Octaisobutyl POSS mol fraction	Pressure (MPa)	CO₂ density (g/cm³)
0.0009	0.00007	10.89	0.4944
0.0019	0.00016	12.20	0.5970
0.0027	0.00022	13.01	0.6366
0.0033	0.00027	13.64	0.6603
0.0046	0.00038	14.47	0.6858
0.0053	0.00044	15.18	0.7042

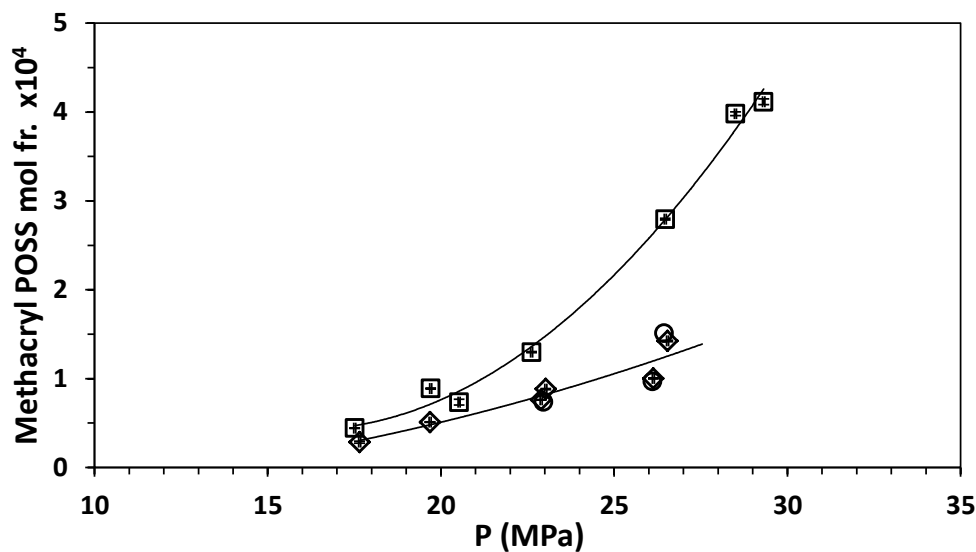


Figure 4. 1 The dew points of methacryl POSS–CO₂ binary system (□) at 308K and (◇) at 323K, (○) the repeated dew points. Curves represent regression fits of the data.

The solubility of methacryl POSS can be attributed to the carbonyl functionalities in the groups attached to the silicon atoms. Carbonyl functionalities can contribute to the solubility of molecules in scCO₂ [80–86]. Ab Initio calculations and IR spectroscopic analysis attribute the CO₂ affinity of molecules consisting of carbonyl functionalities to the Lewis acid-base interactions between the electron acceptor CO₂ and electron donor carbonyl [80,81,87]. The solubility of polymethyl methacrylate (PMMA) is attributed to this specific interaction[80,81], which can also enable solubility of methacryl POSS in scCO₂.

4.2 L-V Equilibria of Isooctyl POSS-CO₂ Binary System

Addition of alkyl side chains to CO₂-soluble polymers can decrease the solubility of the polymer in scCO₂ as the length of the added side chain increases [88]. However, if the alkyl side chains are branched, the effect on the solubility of the polymer is reversed. Due to the branched alkyl chains, the free volume of the polymer increases, which has an entropic contribution on solubility [88,89]. This can also be simply

explained with the solubility parameter model [90]. As the free volume of the polymer increases, its cohesive energy density decreases, decreasing the difference between the solubility parameters of the polymer and CO₂. Consequently, the solubility of the polymer in scCO₂ increases. In this study, the effect of the branched alkyl chains on the solubility of POSS was studied by studying two POSS structures, one with isooctyl groups and the other with isobutyl groups, attached to the silicon atoms. Figure 4.2 shows the dew pressures of the isooctyl POSS-CO₂ binary system at 308 and 323K, representing the solubility of isooctyl POSS in scCO₂. The data plotted in the figure is also given in Table 4.1. Similar to methacryl POSS, the solubility of isooctyl POSS in scCO₂ increases with an isothermal increase in pressure, and decreases with an isobaric increase in temperature. Compared to the solubility of methacryl POSS in scCO₂ at the same temperature and pressure, the solubility of isooctyl POSS in scCO₂ is about an order of magnitude higher, which is valid for both 308K and 323K. On the other hand, compared to trifluoropropyl POSS solubility in scCO₂ [75], isooctyl POSS has about an order of magnitude lower solubility. At 308K, methacryl POSS solubility of 3×10^{-4} mole fraction in scCO₂ is obtained at 27 MPa, while for isooctyl POSS and trifluoropropyl POSS, the same solubility can be obtained at about 13.5 MPa and 8.5 MPa respectively.

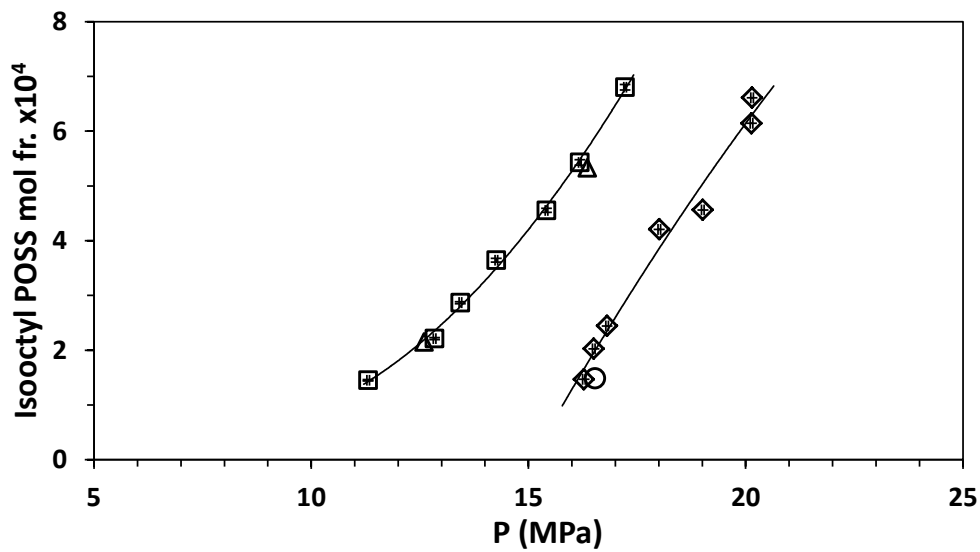


Figure 4. 2 The dew points of isooctyl POSS–CO₂ binary system (□) at 308K and (◇) at 323K, the repeated dew points data (Δ) at 308K, (○) at 323K. Curves represent regression fits of the data.

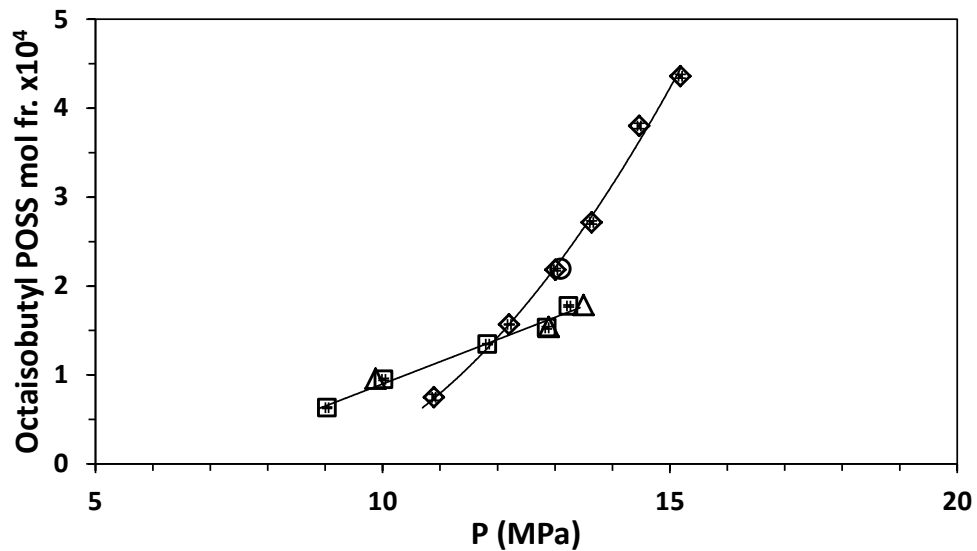


Figure 4. 3 The dew points of octaisobutyl POSS–CO₂ binary system (□) at 308K and (◇) at 323K, the repeated dew points data (Δ) at 308K, (○) at 323K. Curves represent regression fits of the data.

4.3 S-V Equilibria of Octaisobutyl POSS-CO₂ Binary System

The cloud points of octaisobutyl POSS-scCO₂ binary system, representing the solubility of octaisobutyl POSS in scCO₂, are shown in Figure 4.3 for 308 and 323K. A crossover pressure, at which two isotherms intersect, was found to be at about 12 MPa. At pressures higher than the crossover pressure, the solubility of octaisobutyl POSS in scCO₂ increases with increasing temperature due to the increased solid vapor pressure in the relatively dense and incompressible region. Below the crossover point, the solubility of octaisobutyl POSS in scCO₂ decreases with an increase in temperature, which shows that the decrease in the density and thus solvent power of carbon dioxide with increased temperature predominates over the increase in the vapor pressure of octaisobutyl POSS. Consequently, the solubility of octaisobutyl POSS decreases in scCO₂.

Solubility of octaisobutyl POSS in scCO₂ is comparable to that of isooctyl POSS at 308K, with the former being slightly less than the latter at pressures over 12 MPa. At 328K, however, the difference between the solubilities of two POSS types in scCO₂ becomes significant; with octaisobutyl POSS becoming more soluble than isooctyl POSS, approaching to the solubility of trifluoropropyl POSS [75]. At 328K, in the concentration range of 1.5×10^{-4} - 4.2×10^{-4} by mole fraction of solute, the solubility isotherm of octaisobutyl exists at about 3 MPa lower compared to the isooctyl POSS solubility isotherm. In order to reach a solubility of about 4×10^{-4} by mole, the system pressure is required to be around 13, 15, and 18 MPa for trifluoropropyl POSS [75], octaisobutyl POSS and isooctyl POSS respectively. The reason of the opposite solubility behaviors of octaisobutyl POSS and isooctyl POSS at 308 and 323K is the temperature effect, which is different for the two components as explained earlier. With temperature increasing to 323K, the increase in the solubility of octaisobutyl POSS in scCO₂ is attributed to the predominating effect of vapor pressure increase of octaisobutyl POSS, while for the isooctyl solubility, the predominating effect is the solvent density decrease. Therefore, at the lower temperature, while isooctyl POSS was slightly more soluble than octaisobutyl POSS in scCO₂, at the higher temperature, the solubility of octaisobutyl POSS in the

supercritical solvent exceeds that of isooctyl POSS. At 323K, the solubility of methacryl POSS, which is the least soluble among all the POSS types studied, reaches only up to about 1×10^{-4} at 26 MPa. To reach a solubility of 1.5×10^{-4} mole fraction at 308K, the required pressure is about 23 MPa for methacrylPOSS, while it is about 11 MPa and 13 MPa for isooctyl and octaisobutyl POSS. At 323K, to reach 1.5×10^{-4} mole fraction solubility, the required pressure is about 16.3 MPa for isooctyl and 12.1 MPa for octaisobutyl, while up to 27 MPa, methacryl POSS does not reach this solubility

4.4 Effects of Temperature and Pressure on CO₂ Density at Phase Separation

The effect of CO₂ density on the solubilities of methacryl POSS, isooctyl POSS and octaisobutyl POSS in scCO₂ is shown in Figure 4.4 a, b and c respectively. The figures show the solubility isotherms of POSS at 308K and 323K, which are plotted against the CO₂ density at the cloud or dew points of the binary systems. At constant CO₂ density, the solubility increases with increasing temperature, associated with the increase in the vapor pressures of the solutes, which is most significant in the solute-CO₂ binary systems of octaisobutyl POSS-CO₂ and isooctyl POSS-CO₂ (Figure 4.4.b and Figure 4.4.c).

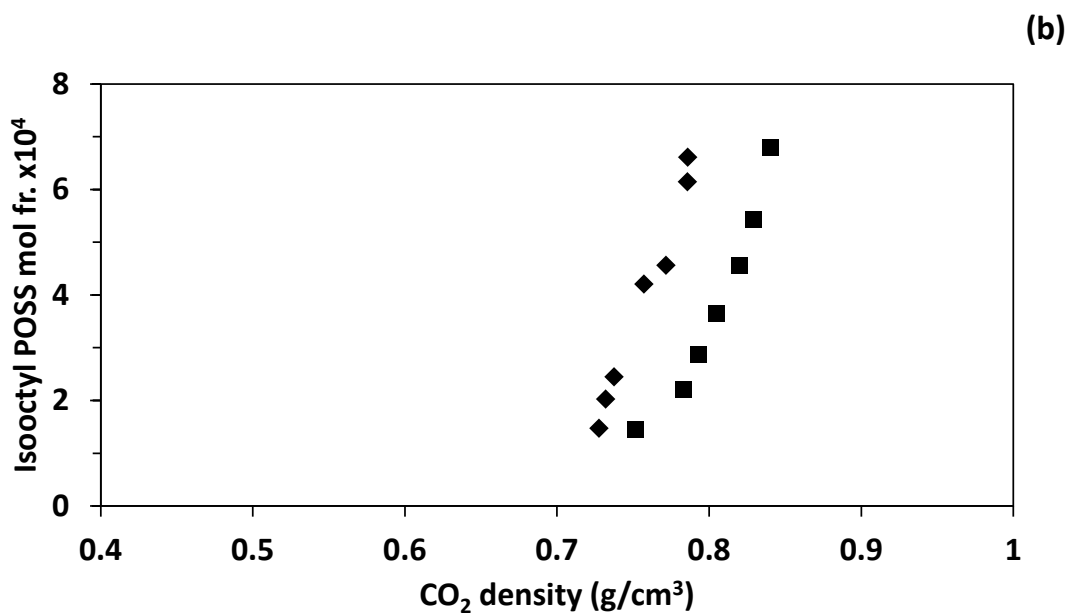
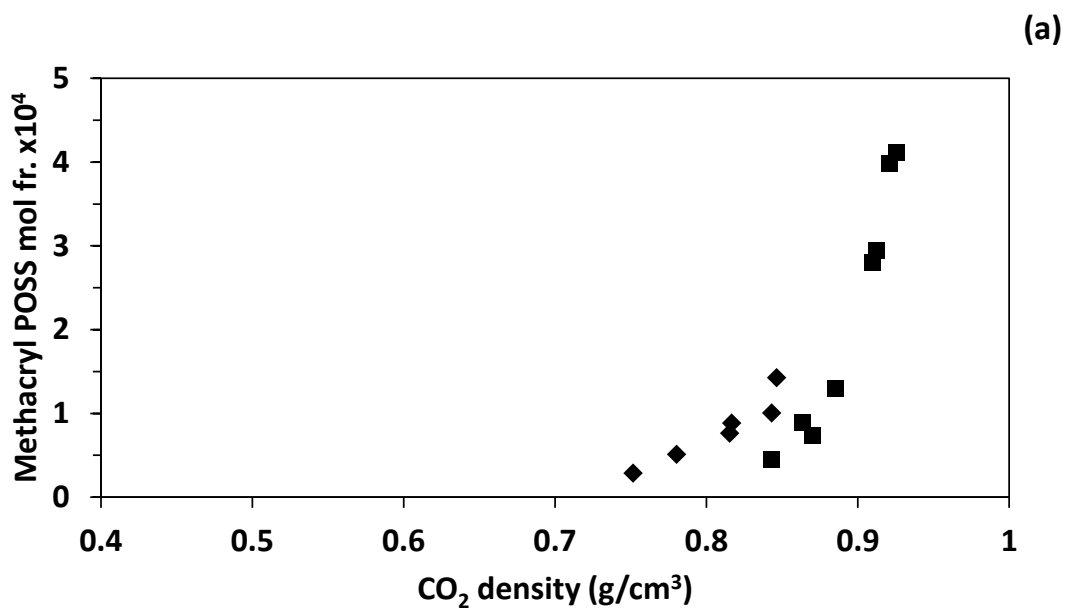


Figure 4. 4 scCO₂ densities at the dew points of (a) methacryl POSS-CO₂ and (b) isooctyl POSS-CO₂, and the cloud points of (c) octaisobutyl POSS-CO₂ binary systems , for (■) 308K and (◆) 323K

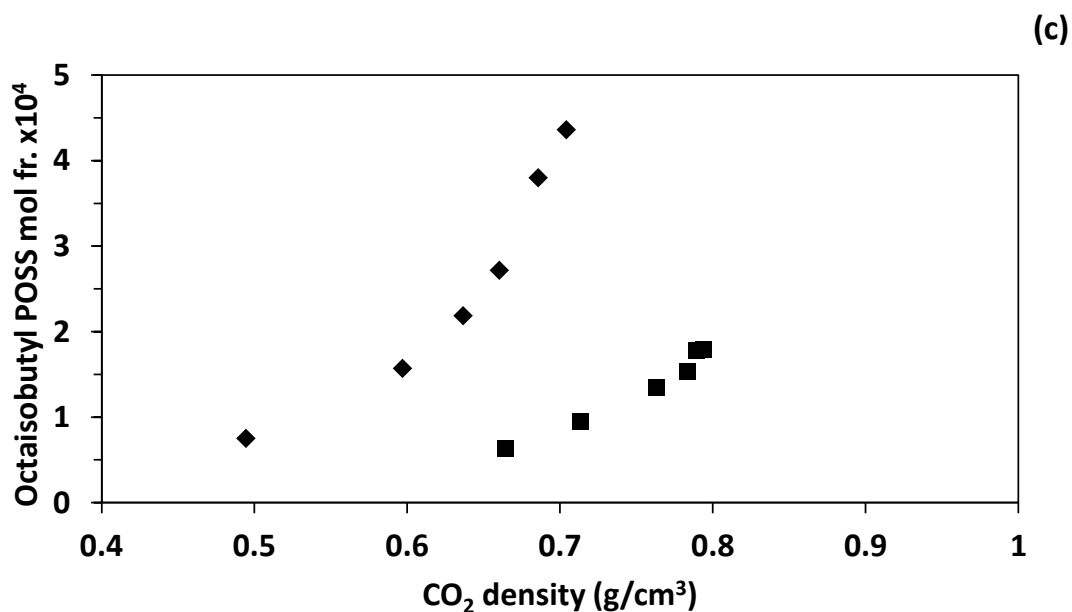


Figure 4. 4 (continued)

Figure 4.5 shows POSS solubility versus scCO₂ density at the cloud or bubble points of all the studied POSS types and trifluoropropyl POSS [75] at 308K (Figure 4.5.a) and 323K (Figure 4.5.b). At both temperatures, to reach the same solubility value, trifluoropropyl POSS requires the lowest solvent density, thus solvation power of scCO₂ compared to the other POSS types, while methacryl POSS requires the highest. At 308K, in the scCO₂ density range of 0.76-0.79 g/ml, the solubility isotherms of isooctyl POSS and isooctabutyl POSS overlap, as both solutes require a similar solvent power for dissolution. As temperature is increased to 323K, the difference between the required densities for the dissolutions of the two POSS types becomes significantly different. The solubility isotherm of octaisobutyl POSS exists at lower scCO₂ densities approaching that of trifluoropropyl POSS due to its increased solubility at 323K, exceeding that of isooctyl POSS.

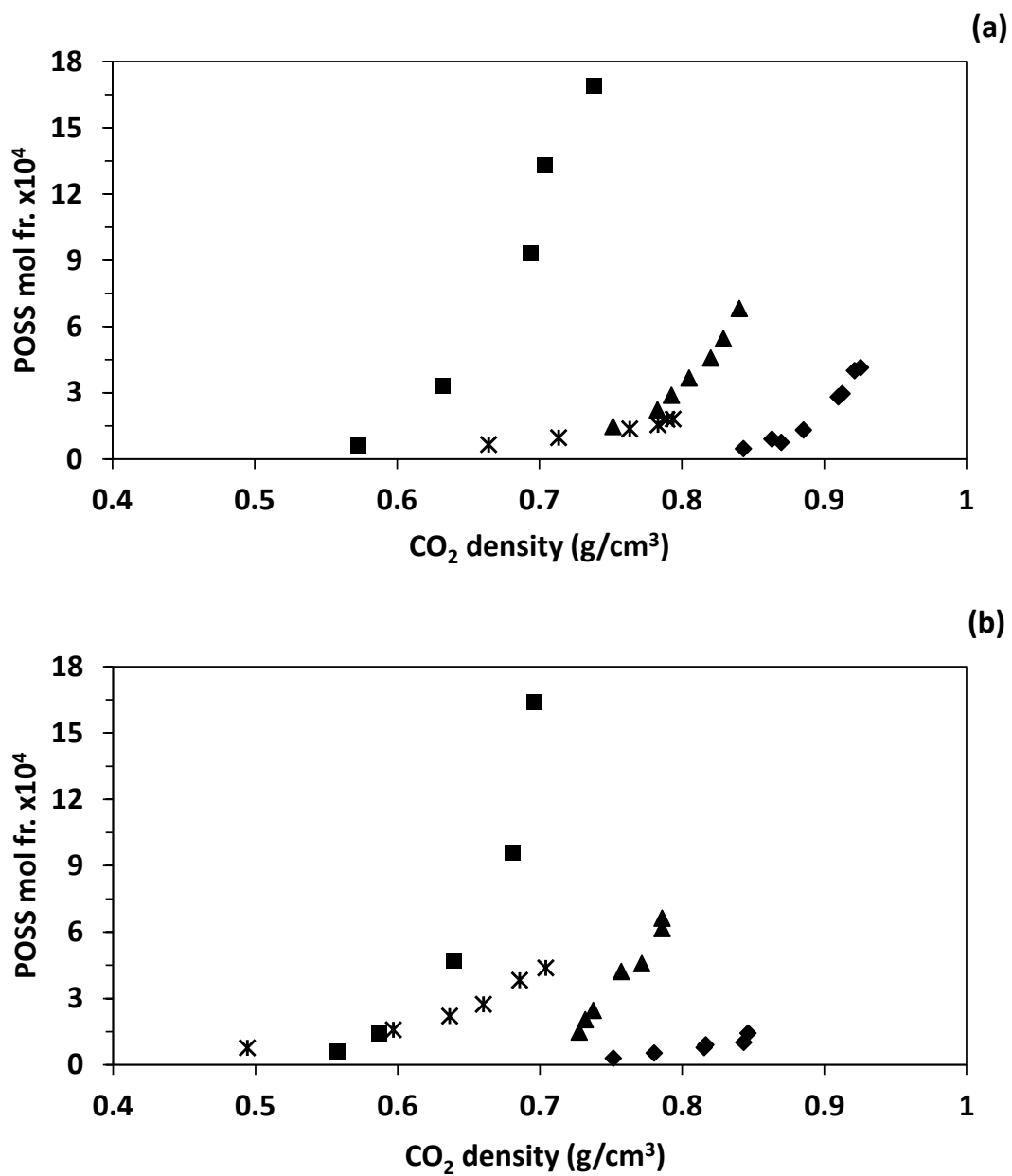


Figure 4. 5 scCO_2 densities at the dew and cloud points of (■) trifluoropropyl POSS-CO₂ [75], (*) octaisobutyl POSS-CO₂, (▲) isooctyl POSS-CO₂, (◆) methacryl POSS-CO₂ binary systems, for a) 308K, b) 323K.

4.5 Modeling of Solubility

The solubility data of methacryl POSS, isooctyl POSS, octaisobutyl POSS and trifluoropropyl POSS (F-POSS) were correlated using density based models. The models of Chrastil, Kumar-Johnston, Del Valle-Aguilera, Mendez-Santiago and Teja, and Bartle were fitted to experimental data using MATLAB. Information about these models was given in Chp 1. in detail. If the correlation equations are rewritten and presented briefly:

$$\ln S = k \ln \rho + \frac{a}{T} + b \quad (\text{Chrastil, 1982})$$

$$\ln S = k \ln \rho + \frac{a}{T} + b + \frac{c}{T^2} \quad (\text{Del Valle and Aguilera, 1988})$$

$$\ln y_2 = k \rho + \frac{a}{T} + b \quad (\text{Kumar and Johnston, 1988})$$

$$T \ln(y_2 P) = k \rho + aT + b \quad (\text{Mendez-Santiago and Teja, 1999})$$

$$\ln \left(\frac{y_2 P}{P_{ref}} \right) = k (\rho_1 - \rho_{ref}) + \frac{a}{T} + b \quad (\text{Bartle, 1990})$$

The accuracy of the calculations is evaluated with average absolute relative deviation percentage (AARD%). It is the objective function that gives the error between the experimentally measured solubility data and the solubility calculated by the density based equations:

$$AARD\% = \frac{100}{N} \sum_{i=1}^N \left(\left| \frac{y_{i,cal} - y_{i,exp}}{y_{i,exp}} \right| \right) \quad (20)$$

where $y_{i,exp}$ is the experimental mole fraction solubility of the solute for experimental point i , and $y_{i,cal}$ is the calculated solubility corresponding to point i , and N is the number of experimental data points

Table 4. 2 Different parameters of the POSS-CO₂ binary systems obtained by using the Chrastil, del Valle, K-J, MST and Bartle models.

Methacryl POSS	<i>k</i>	<i>a</i>	<i>b</i>	<i>c</i>	AARD%
Models					
Chrastil	0.260x10 ²	-0.770x10 ⁴	-0.150x10 ³	-	0.212x10 ²
del Valle	0.260x10 ²	-0.770x10 ⁴	0.182	-0.150x10 ³	0.212x10 ²
K-J	-0.916x10 ¹	0.280x10 ⁻¹	-0.754x10 ⁴	-	0.196x10 ²
MST	-0.194x10 ⁵	0.106x10 ²	0.242x10 ²	-	0.197x10 ²
Bartle	0.214 x 10 ²	-0.104x10 ⁵	0.350x10 ⁻¹	-	0.207x10 ²
Isooctyl POSS	<i>k</i>	<i>a</i>	<i>b</i>	<i>c</i>	AARD%
Models					
Chrastil	0.165x10 ²	-0.617x10 ⁵	-0.882x10 ²	-	0.733x10 ¹
del Valle	0.165x10 ²	-0.701x10 ⁵	0.132x10 ⁶	-0.868x10 ²	0.733x10 ¹
K-J	-0.315x10 ¹	0.190x10 ⁻¹	-0.631x10 ⁴	-	0.782x10 ¹
MST	-0.152x10 ⁵	0.769x10 ¹	0.216x10 ²	-	0.832x10 ¹
Bartle	0.224x10 ²	-0.936x10 ⁴	0.250x10 ⁻¹	-	0.798x10 ¹
Octaisobutyl POSS	<i>k</i>	<i>a</i>	<i>b</i>	<i>c</i>	AARD%
Models					
Chrastil	0.690 x 10 ¹	-0.107x10 ⁴	-0.108x10 ¹	-	0.577x10 ¹
del Valle	0.659 x 10 ¹	-0.106x10 ⁴	0.199 x10 ⁵	-0.933x10 ¹	0.585x10 ¹
K-J	0.217 x 10 ²	0.800x10 ⁻²	-0.114x10 ⁵	-	0.585x10 ¹
MST	-0.161x10 ⁵	0.353x10 ¹	0.348x10 ²	-	0.537x10 ¹
Bartle	0.367x10 ²	-0.135x10 ⁵	0.110x10 ⁻¹	-	0.532x10 ¹

Table 4.2 exhibits the AARD% values and k , a , b and c , are adjustable parameters obtained by the fitting of the experimental solubility data. Highlighted values represent the lowest AARD% for each type of POSS.

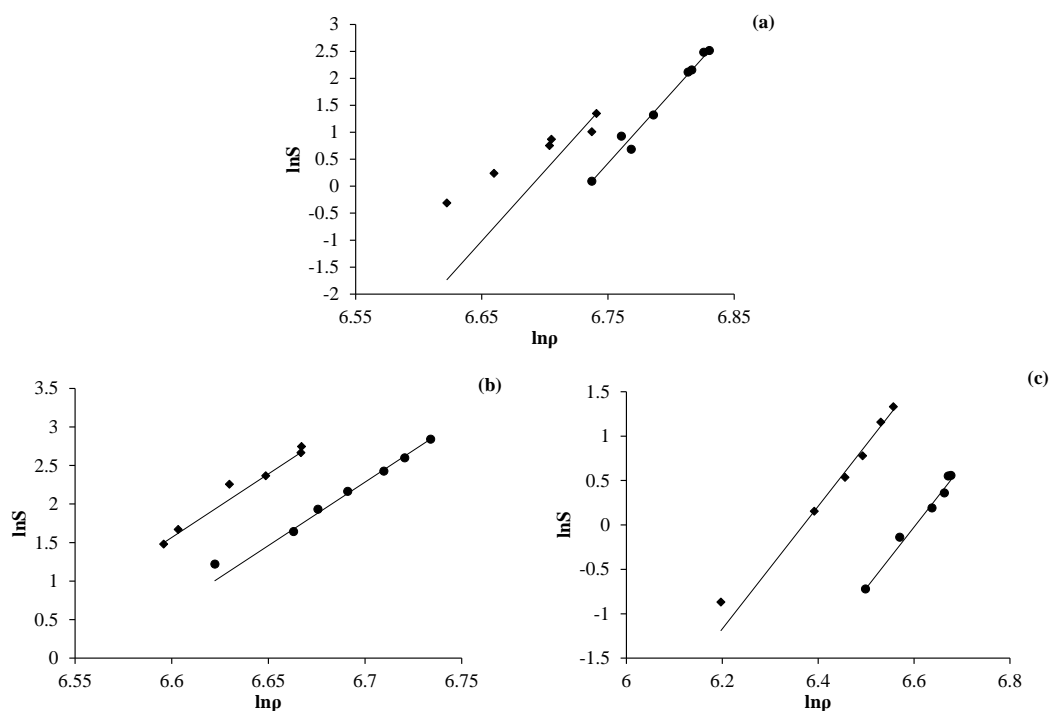


Figure 4. 6 Plots of $\ln S$ versus $\ln \rho$ for a) methacryl POSS, b) isooctyl POSS, c) octaisobutyl POSS using Chrastil model. Experimental results: (●) 308K, (◆) 323K; model results (—).

The correlated solubility results for methacryl POSS-CO₂, isooctyl POSS-CO₂ and octaisobutyl POSS-CO₂ binary systems obtained by using the Chrastil model are shown in Table 4.2. As can be seen, AARD% values obtained for the three of POSS vary in the range of 0.212×10^2 and 0.577×10^1 for Chrastil model. Also, Figure 4.6 exhibits the plots of POSS solubilities, $\ln S$, as a function of $\ln \rho$ at temperatures of 308K, 323K. It shows that the POSS solubilities in scCO₂ change linearly as a logarithmic function of pure CO₂ density at that process conditions. With the lowest overall AARD% value of 0.577×10^1 Chrastil model gives the best fit to the octaisobutyl POSS solubility data. However, the application of the models for

methacryl POSS-CO₂ binary system show that the model can fail to correlate to solubility data at low density regions [29,34,35].

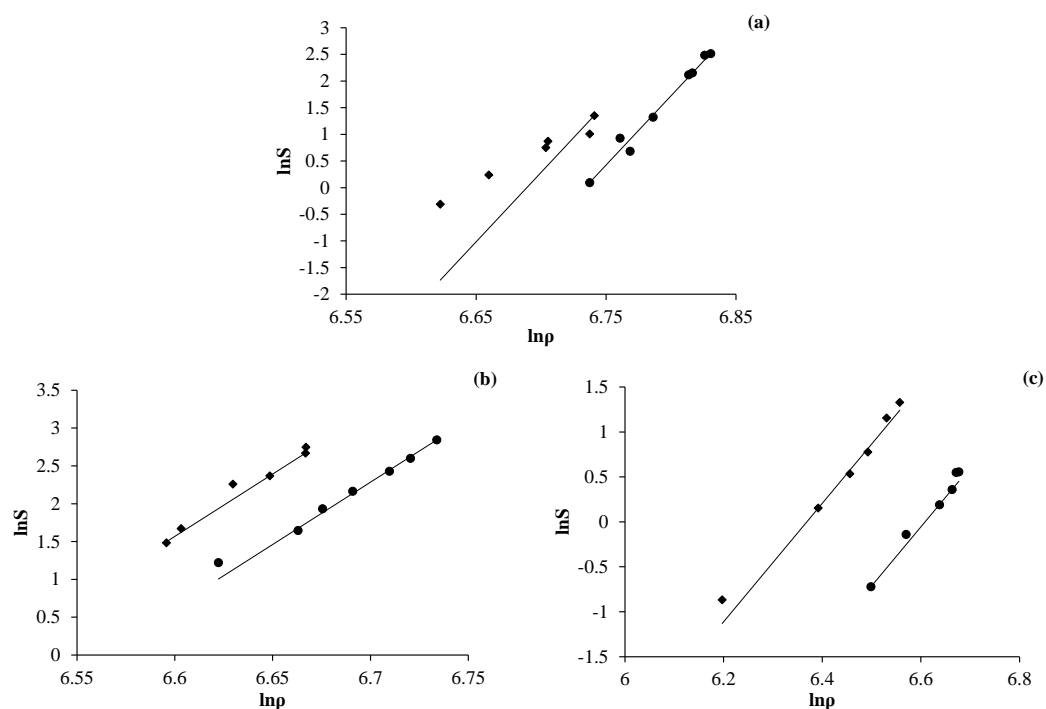


Figure 4. 7 Plots of $\ln S$ versus $\ln \rho$ for a) methacryl POSS, b) isooctyl POSS, c) octaisobutyl POSS using del Valle model. Experimental results: (●) 308K, (◆) 323K; model results (—) .

Using another density based model, del Valle and Aguilera model, the correlated solubility results for methacryl POSS-CO₂, isooctyl POSS-CO₂ and octaisobutyl POSS-CO₂ binary systems obtained as shown in Table 4.2. Figure 4.7 exhibits the plots of POSS solubilities, $\ln S$, as a function of $\ln \rho$ at temperatures of 308K, 323K. The Chrastil model were extended and modified with an additional term of $1/T^2$. However, once these two correlation results given on the Table 4.2 are compared with regard to AARD%, it is observed that except for octaisobutyl POSS there is no difference between the AARD% values obtained for the methacryl POSS and

isooctyl POSS. As in the Table 4.2, AARD% values obtained vary in the range of 0.212×10^2 and 0.585×10^1 .

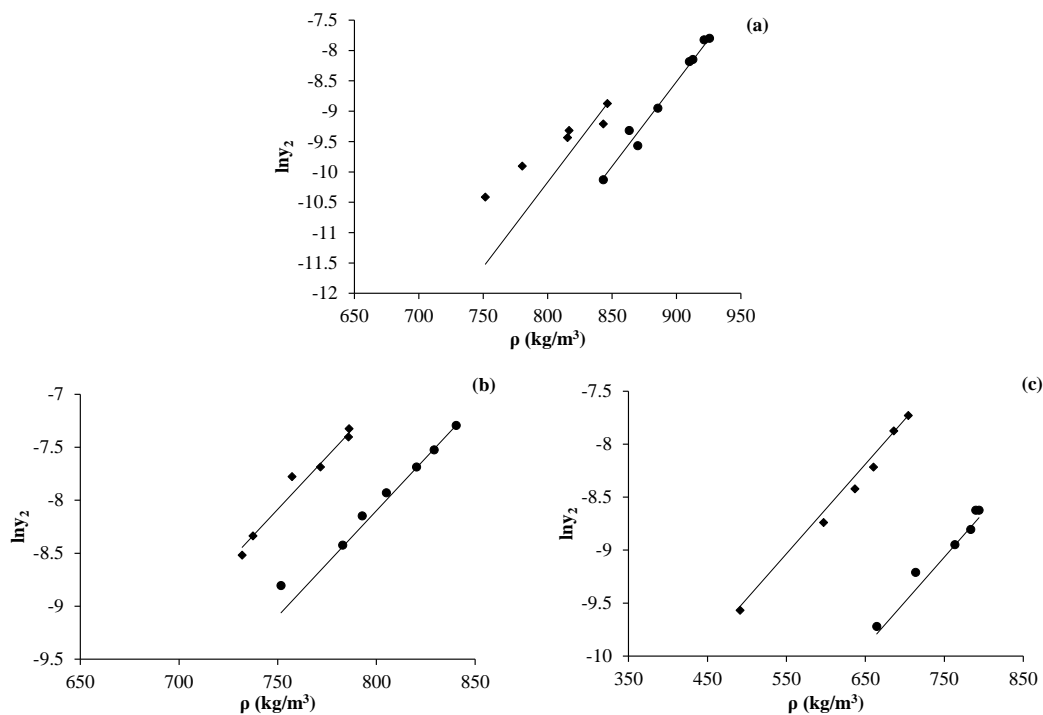


Figure 4. 8 Plots of $\ln y_2$ versus ρ for a) methacryl POSS, b) isooctyl POSS, c) octaisobutyl POSS using K-J model. Experimental results: (●) 308K, (◆) 323K; model results (—).

The solubility data of methacryl POSS, isooctyl POSS, octaisobutyl POSS in $scCO_2$ were correlated using Kumar and Johnston model. As shown in the Table 4.2, K-J model gave better result than the Chrastil model for methacryl POSS and octaisobutyl POSS. The AARD% values obtained for the three of POSS range from 0.585×10^1 to 0.196×10^2 . Also, Figure 4.8 exhibits the plots of POSS solubilities, $\ln y_2$, as a function of ρ at temperatures of 308K and 323K. It shows that the POSS solubilities in $scCO_2$ change linearly as a function of pure CO_2 density at that process conditions. With the lowest overall AARD% value of 0.585×10^1 K-J model gives the best fit to the octaisobutyl POSS solubility data.

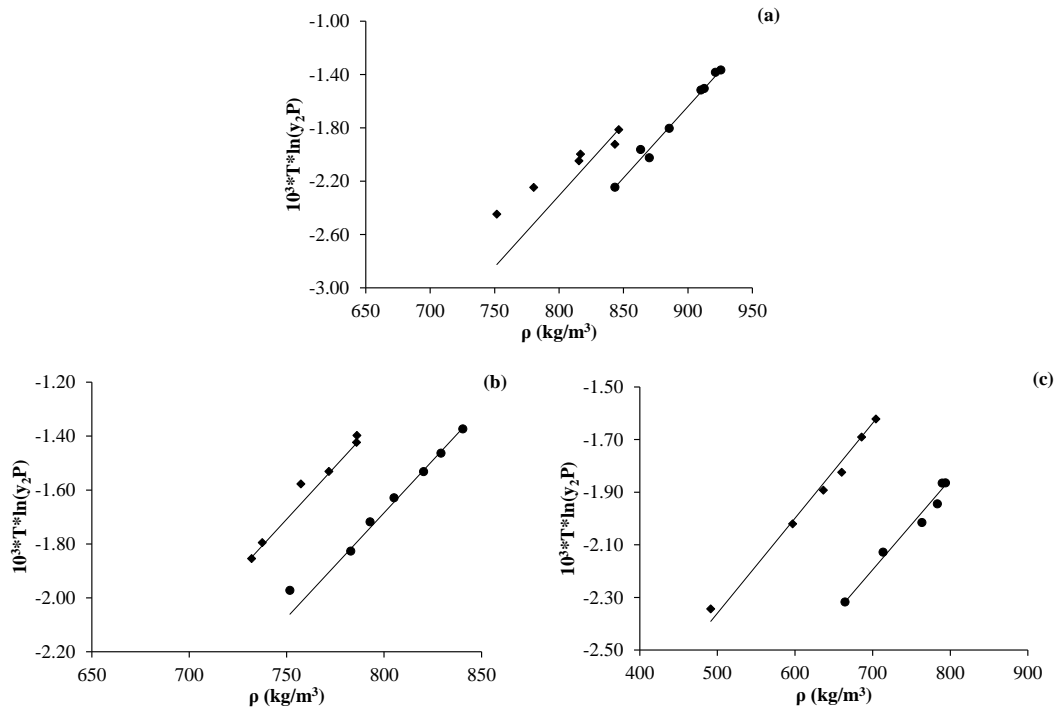


Figure 4.9 Plots of $10^3 T \ln(y_2 P)$ versus $\ln p$ for a) methacryl POSS, b) isooctyl POSS, c) octaisobutyl POSS using MST model. Experimental results: (●) 308K, (◆) 323K; model results (—).

The solubility data of methacryl POSS-CO₂, isooctyl POSS-CO₂ and octaisobutyl POSS-CO₂ binary systems correlated with Méndez-Santiago and Teja model are shown in Table 4.2. Also, Figure 4.9 exhibits the plots of $10^3 T \ln(y_2 P)$ as a function of ρ at temperatures of 308K and 323K. MST model also considers the effect of pressure and temperatures on the solubility. As it is seen, AARD% values obtained for the three of POSS vary in the range of 0.197×10^2 and for MST model. Therefore, taking into account of pressure and temperature does not make notable sense as can be understood from the range. With the lowest overall AARD% value of 0.537×10^1 MST model gives the best fit to the octaisobutyl POSS experimental solubility data.

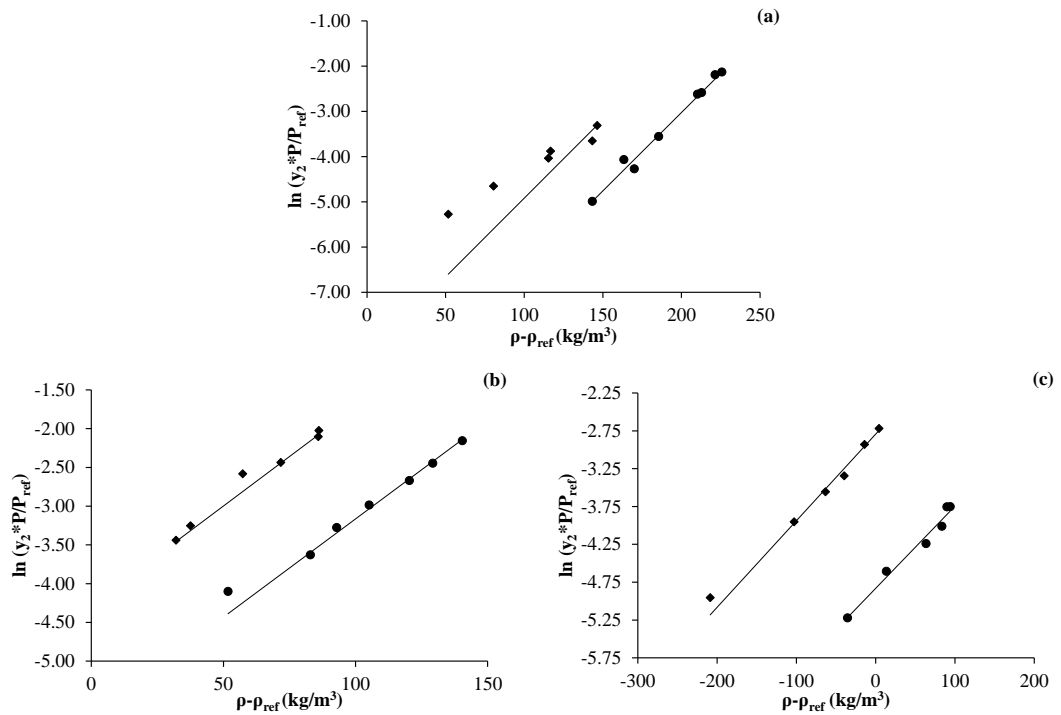


Figure 4.10 Plots of $\ln(y_2 P/P_{ref})$ versus $\rho - \rho_{ref}$ for a) methacryl POSS, b) isooctyl POSS, c) octaisobutyl POSS using Bartle model. Experimental results: (●) 308K, (◆) 323K; model results (–) .

Similar to MST model, Bartle correlation also considers the effect of pressure on the solubility. The correlated solubility data for methacryl POSS, isooctyl POSS and octaisobutyl POSS are shown in Table 4.2. Also, Figure 4.10 exhibits the plots of $\ln(y_2 P/P_{ref})$ as a function of $\rho - \rho_{ref}$ at temperatures of 308K and 323K. As it is seen, AARD% values obtained range from 0.532×10^1 to 0.207×10^2 for Bartle model. Hence, considering the pressure effect does not make significant improvement as can be understood from the range. With the lowest overall AARD% value of 0.532×10^1 Bartle model gives the best fit to the octaisobutyl POSS experimental solubility data. Among all the models used the lowest AARD% value belongs to Bartle model which is used for the octaisobutyl POSS solubility data. It is obvious that lowest accuracy obtained belongs to methacryl POSS correlated by Chrastil and del Valle and Aguilera models. MST and Bartle models take the temperature and pressure effect into consideration for the solubility in scCO₂. Due to the temperature and pressure

dependence of solvent density, relationship between logarithm of solubility ($\ln y_2$) and ρ is more complex. Therefore, Bartle and MST models may be able to correlate the experimental data better than the others.

4.5.1 Consistency

In addition to the correlation method, Méndez-Santiago and Teja (1999) et al. also examined the consistency of experimental data. In terms of self-consistency test, all the experimental solubility data at different temperatures fit into a single straight line representing the model. It gives the chance to compare the solute solubility data obtained and calculated data. Figure 4.11, Figure 4.12, Figure 4.13 illustrate the comparison of methacryl POSS, isooctyl POSS and octaisobutyl POSS solubility data to their calculated data by Chrastil, del Valle, K-J, MST and Bartle models, respectively.

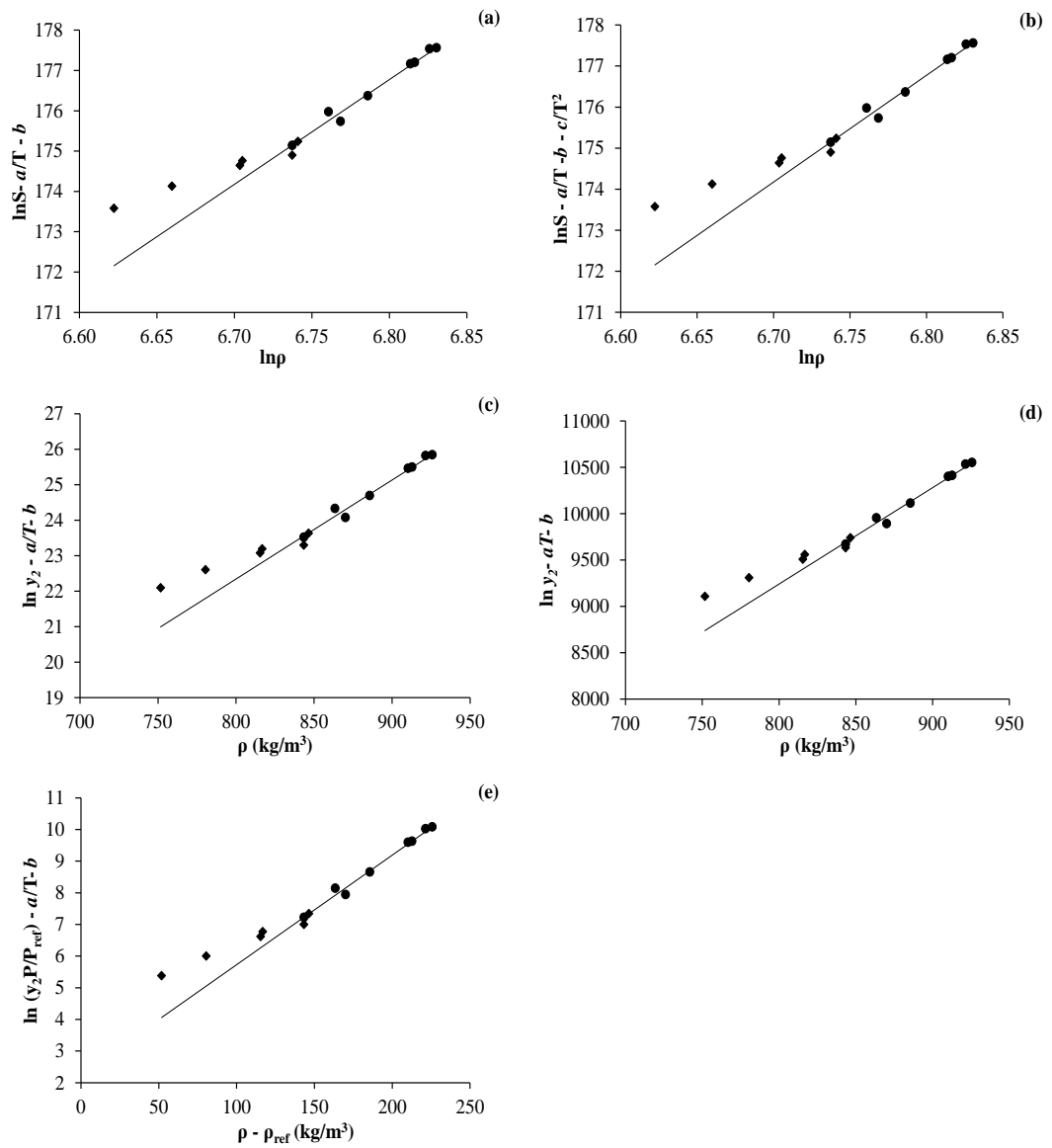


Figure 4.11 Self-consistency tests for methacryl POSS solubility in scCO₂ using five different models: (a) Chrastil; (b) del Valle; (c) K-J; (d) MST; and (e) Bartle models. Experimental results: (●) 308K, (◆) 323K; model results (—).

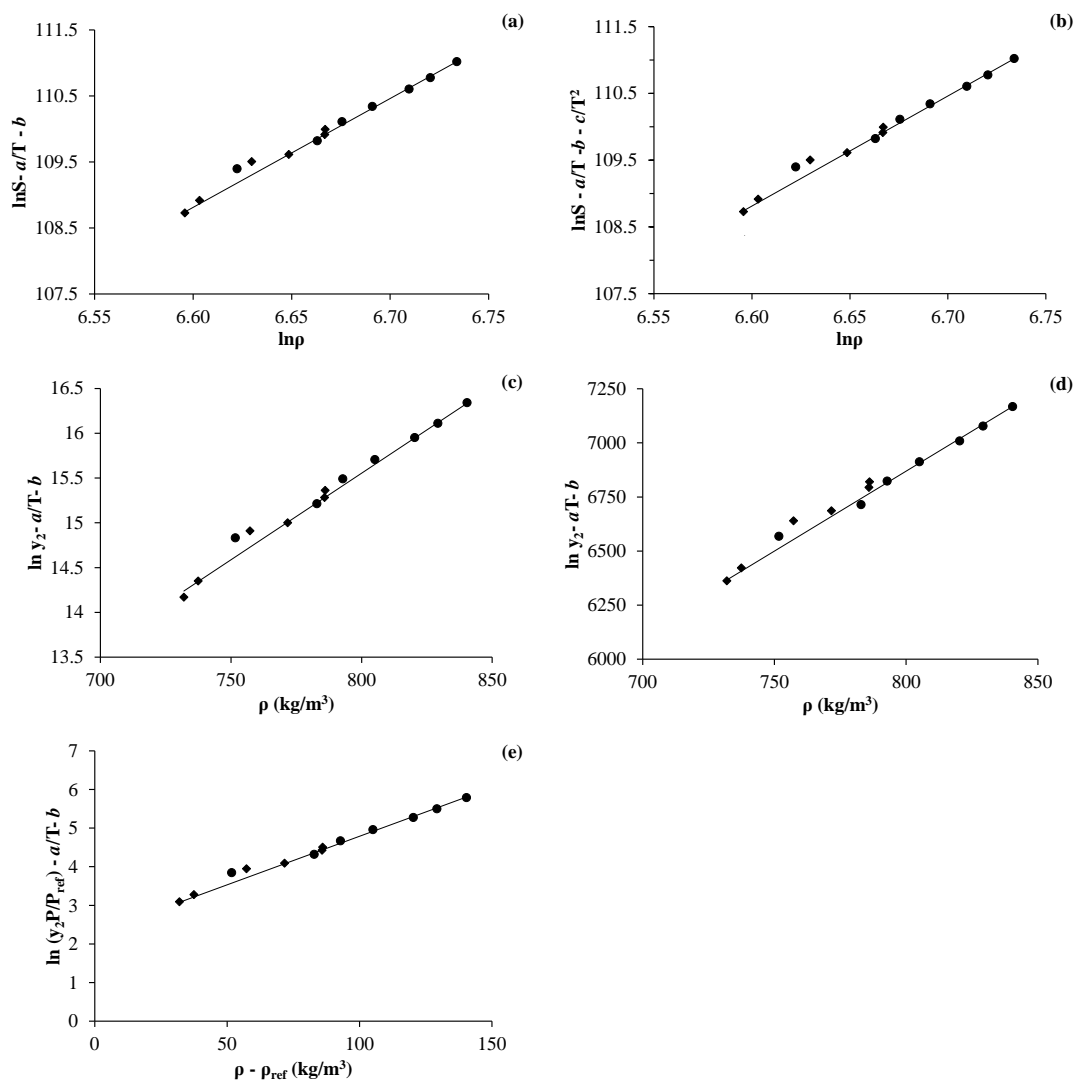


Figure 4. 12 Self-consistency tests for isooctyl POSS solubility in scCO₂ using five different models: (a) Chrastil; (b) del Valle; (c) K-J; (d) MST; and (e) Bartle models. Experimental results: (●) 308K, (◆) 323K; model results (-).

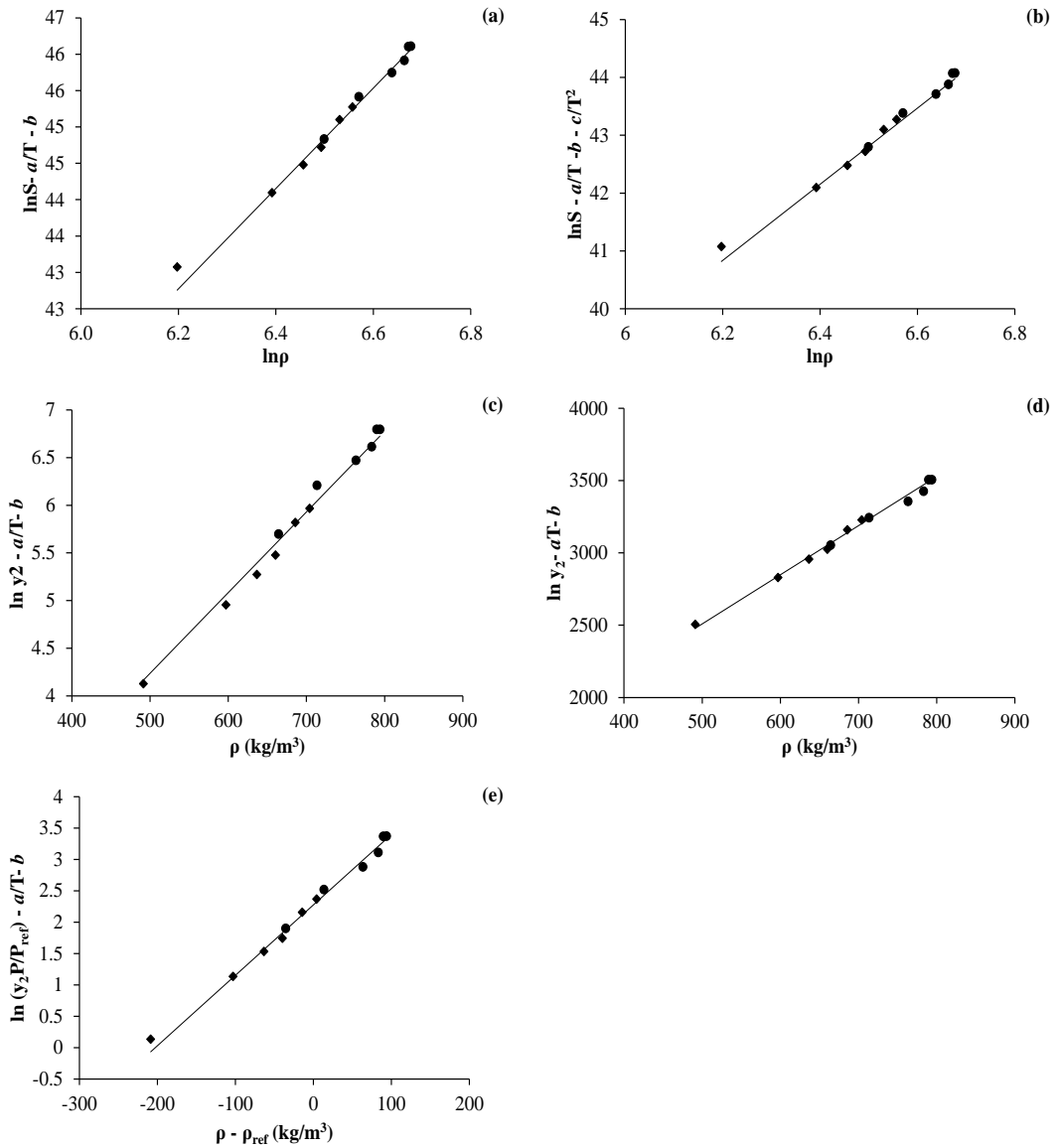


Figure 4.13 Self-consistency tests for octaisobutyl POSS solubility in scCO₂ using five different models: (a) Chrastil; (b) del Valle; (c) K-J; (d) MST; and (e) Bartle models. Experimental results: (●) 308K, (◆) 323K; model results (—).

The results show that linear trend can be obtained in the self-consistency of octaisobutyl POSS-CO₂ and isooctyl POSS-CO₂ binary systems showing that this model can be used to predict the solubility data in the vicinity of the experimental conditions. However, these five different semi-empirical models deviate from the linear trend in the study of methacryl POSS-CO₂ binary system at the region of low

CO₂ density. Formerly this behavior was also observed in the literature for 2,3,5,6-Tetrachloropyridine-CO₂ binary system by Cui et al. [34].

4.6. Thermal Characterization of POSS

In this work, thermal degradation behaviors of all types of POSS were investigated to see the effect of molecular structure on the degradation temperature and thermal stability. The measurements were performed using TGA by heating samples from room temperature to 700°C under nitrogen atmosphere. Figure 4.14 shows the thermogravimetric curves of each POSS used in the study.

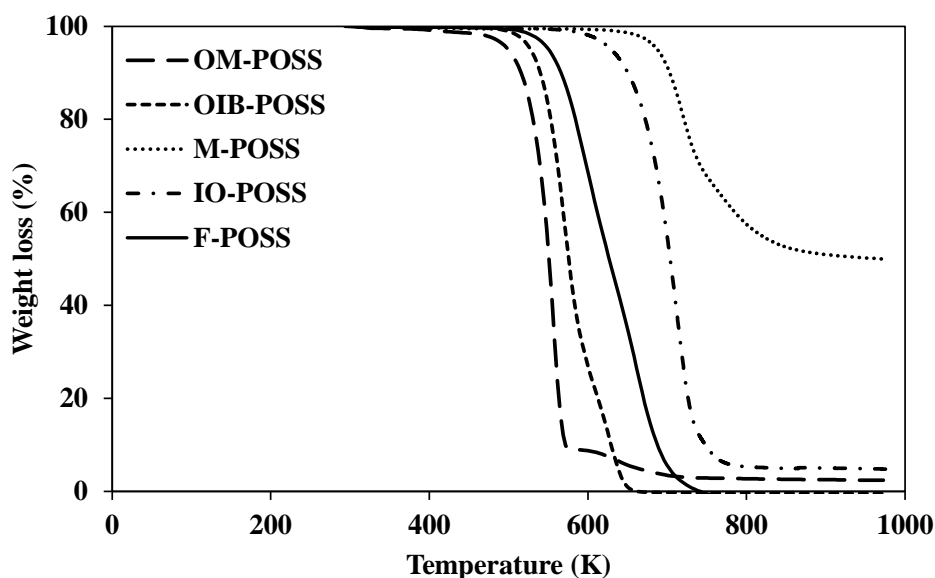


Figure 4. 14 POSS TGA curves in nitrogen.

Except for the methacryl POSS, almost complete weight loss occurs at 823 K in a single step [91]. About 50% weight loss for methacryl POSS is less than the fraction of methacryl groups attached to Si atoms in the material. Indeed the reaction proceeds until the organic functional groups degrade and inorganic Si-O remains as residue. This can be ascribed to the presence of hydroxyl groups which are formed as a consequence of incomplete condensation reactions during the production of methacryl POSS cage mixture [92]. Methacryl POSS was found to be the most

thermally stable one, while octamethyl POSS was the least. It can be attributed to the functional group size effect on volatility [93]. Also, in the literature octamethyl POSS which has very simple structure was noticed to exhibit almost complete sublimation [94], while POSS that have longer alkyl chain evaporate above melting temperature [95]. Moreover, the evaporation of the compounds as well as the decomposition and rearrangement due to formation of larger siloxane structures result in weight loss of R_8T_8 derivatives; which are larger than the organic fractions (Bolln et. al.). These can explain the amount of residue of the POSS with octaisobutyl, octamethyl and isooctyl groups. The melting temperatures supplied from the manufacturer for the solid octamethyl and octaisobutyl POSS are 543 K and 553 K, respectively. The melting temperature of F-POSS is taken from the literature as 462 K [75]. They start to degrade upon heating and exhibit at least 10% weight loss before they melt. 2%, 5% and 10% weight loss temperatures of octamethyl POSS, octaisobutyl POSS, trifluoropropyl POSS, isooctyl POSS and methacryl POSS were observed in TGA analysis and represented in Table 4.3. Table clearly shows the dependence of the thermal stability of POSS on molecular weight. Among all the POSS, octamethyl POSS which has the lowest molecular weight start to degrade at lowest temperature. As given sequentially in the Table 4.3, it is seen that thermal degradation temperature increases with increasing molecular weight.

Table 4. 3 Thermal Decomposition Temperatures for the POSS

POSS type	MW(g/mol)	T(K) at 2% weight loss	T(K) at 5% weight loss	T(K) at 10% weight loss
Octamethyl	536.96	471	500	516
Octaisobutyl	873.60	512	528	540
Trifluoropropyl	1193.16	530	550	566
Isooctyl	1322.46	602	630	651
Methacryl	1433.97	664	688	703

4.7 SC Impregnation of PLA with POSS-CO₂ Solutions

One of the issues studied within the scope of the study is using the obtained solubility and phase equilibrium data of POSS-CO₂ binary systems to design an environmentally friendly material processing application. scCO₂ has a plasticizer effect on polymers which have affinity to CO₂ such as PMMA, Polystyrene (PS), and PLA. Due to the molecular interactions, scCO₂ can dissolve in these polymers and decreases glass transition temperature by increasing the chain mobility [42,43,96–98]. In this part of this work, a preliminary study was conducted to investigate the possibility of supercritical impregnation (SCI) process to deposit POSS particles into a polymer matrix using this advantage of scCO₂. The goal is to perform the deposition with an environmentally benign manner without the use of hazardous and toxic solvents like tetrahydrofuran (THF) and chloroform, and without application of high temperatures for melt processing, which might cause the degradation of the polymer and/or the functional groups of the additives.

PLA was chosen as the polymer matrix due to its biodegradable and biocompatible nature, while F-POSS and octaisobutyl POSS, which are in a powder form and exhibit the highest CO₂-affinity among all the POSS types, were selected to be impregnated into the PLA.

Using the obtained phase behavior data of F-POSS-CO₂ from literature, and octaisobutyl POSS-CO₂ binary systems conducted in this work, process conditions were determined for the impregnation application. F-POSS starts to degrade at about 448 K [75] while melting process temperature of many polymers are above that value. For PLA used, recommended heat treatment temperature by manufacturer is about 353 K, which is lower than the starting degradation temperature of F-POSS. Therefore, supercritical impregnation process can also prevent the degradation of heat sensitive additives.

The PLA film thicknesses prepared by solvent casting method were 0.60±0.05 mm. PLA impregnation experiments with F-POSS and octaisobutyl POSS were performed at 13.8 MPa and two different temperatures, 308K and 323K while the

system was depressurized at a flow rate of about 12 MPa/min. During impregnation, excess amount of POSS is needed in the system to provide efficient impregnation, so the supercritical phase is saturated with POSS. As the operating pressure increases, higher amount of POSS is needed to saturate the system. While higher pressure allows better penetration into the polymer matrix, it also causes higher amounts of POSS to be lost as waste during the depressurization. Rapid venting rate was preferred to have better precipitation and to avoid POSS loss during the venting. The process conditions of all the experiments performed are listed as in the Table 4.4.

Table 4. 4 SCI process condition

POSS type	Waiting Time	Amount (g)	Pressure (MPa)	Temperature (K)	Venting Time (MPa/min)
Trifluoro-Propyl					
PLA-1A	3h	1.5	13.8	323	1.2
PLA-2A	24h	1.5	13.8	323	1.2
PLA-3A	24h	1.5	13.8	308	1.2
Octaisobutyl					
PLA-1B	3h	0.3	13.8	323	1.2
PLA-2B	24h	0.3	13.8	323	1.2
PLA-3B	24h	0.3	13.8	308	1.2

4.7.1 Morphological Analysis

The morphological characteristics of the impregnated PLA samples with F-POSS and octaisobutyl POSS at three different conditions were investigated by scanning electron microscopy (SEM). The waiting time of PLA in the F-POSS-CO₂ solution was determined as 3 hours and 24 hours. Figure 4.15 shows the cross section area of the neat PLA (PLA-N). Figure 4.16 and Figure 4.17 show the cross section area of PLA exposed to F-POSS-CO₂ solution at a pressure of 13.8 MPa and a temperature

of 323K for 3 hours and 24 hours, respectively. As seen from the SEM images the amount of POSS loaded into PLA which was impregnated for 24 hours is significantly higher than the PLA impregnated for 3 hours. However, considering the dispersity, formation of F-POSS aggregates is very high in this sample. In order to verify that the aggregates were F-POSS, EDX analysis was performed which had, confirmed the presence of F and Si atoms that belongs the F-POSS structure in PLA (Figure 4.19 a and Figure 4.19 b). Au and Pd peaks come from the gold/palladium coating of PLA surface. The EDX analysis also verifies that more POSS was loaded into the PLA matrix with the supercritical impregnation conducted for 24 hours (Figure 4.19 b) compared to the PLA processed for 3 hours (Figure 4.19 a). Gravimetric analysis was intended to be used to measure the loaded amount; however, it was found that the weight of the PLA decreases during the supercritical processing which did not allow the gravimetric method to verify the loaded amount of F-POSS accurately.

The other parameter studied with F-POSS was the temperature. In this part of the study, the effect of temperature on impregnation was investigated by decreasing the processing temperature to 308K while keeping the waiting time constant at 24 hours. Figure 4.18 shows the cross section area of PLA kept in F-POSS-CO₂ solution at a pressure of 13.8 MPa and a temperature of 308K for 24 hours. The images show that the lower temperature leads to better results in terms of F-POSS loading, which is also verified by the EDX analysis (Figure 4.19 b and Figure 4.19 c). The reason for a higher loading achieved at lower temperature could be the higher solubility of F-POSS at 308K compared to 323K. However better dispersion was obtained at 323K with 24 hours exposure time.

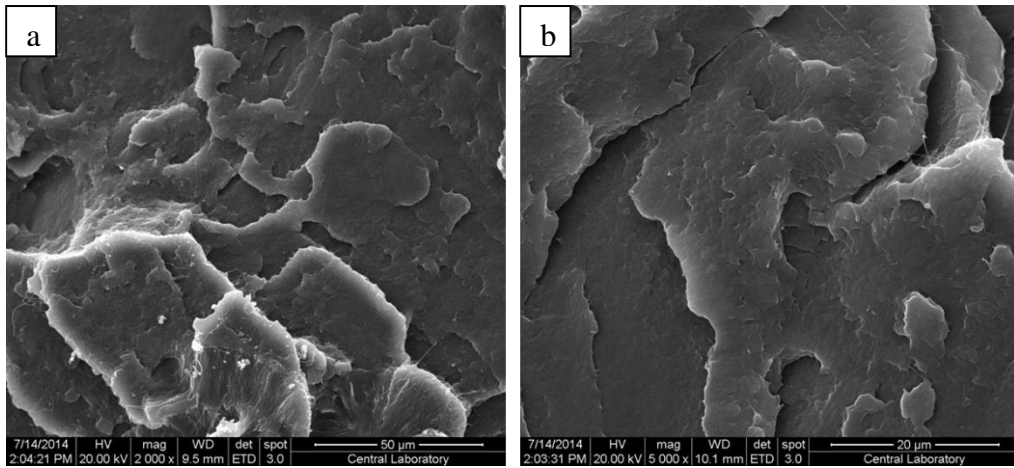


Figure 4. 15 Cross section of unprocessed neat PLA with magnifications of a) 2000x, b) 5000x, (PLA-N).

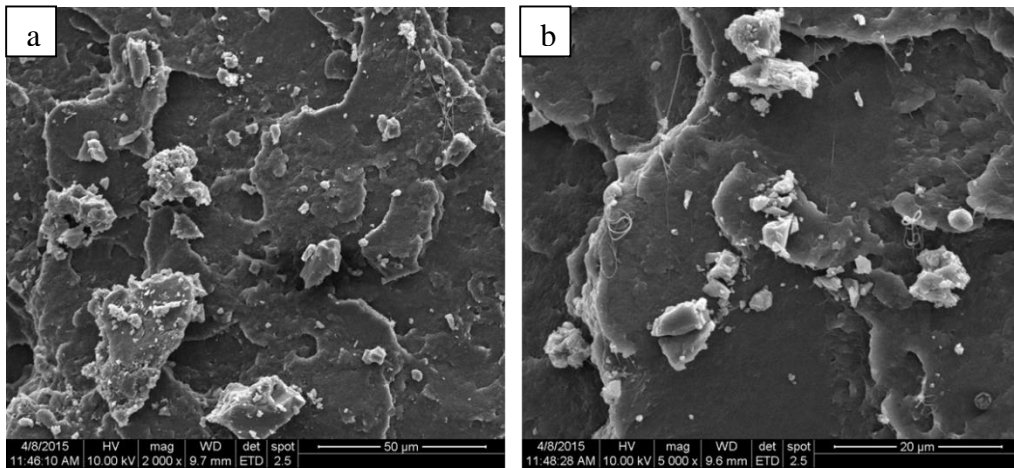


Figure 4. 16 Cross section of PLA processed with F-POSS-CO₂ solution at 13.8 MPa and 323K for 3hours with magnifications of a) 2000x, b) 5000x, (PLA-1A).

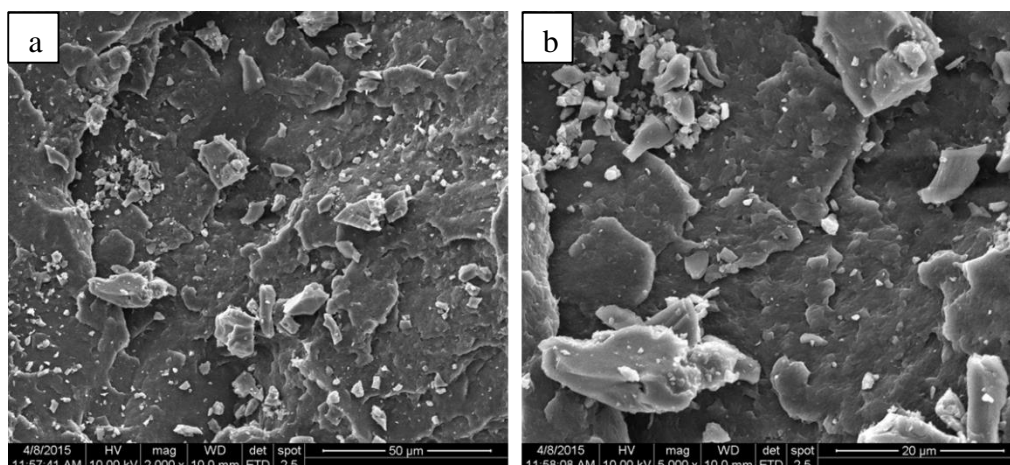


Figure 4. 17 Cross section of PLA processed with F-POSS-CO₂ solution at 13.8 MPa and 323K for 24 hours with magnifications of a) 2000x, b) 5000x, (PLA-2A).

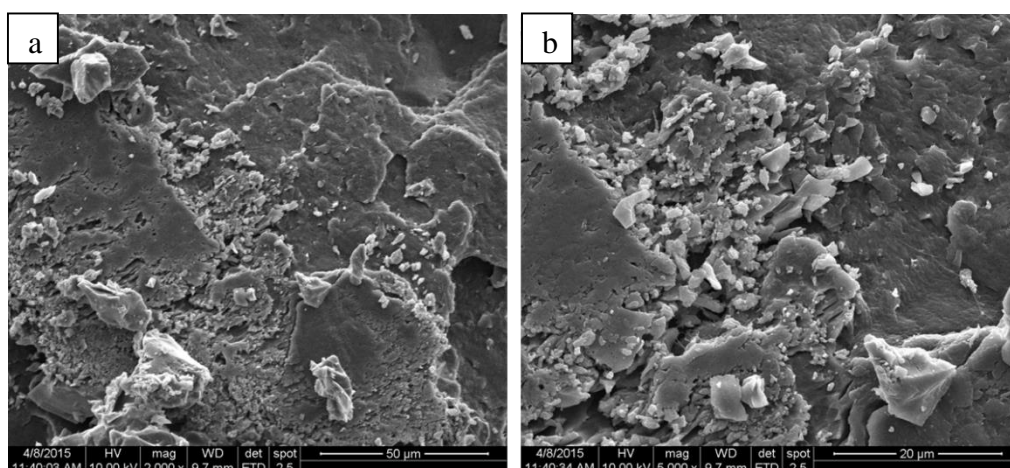


Figure 4. 18 Cross section of PLA processed with F-POSS-CO₂ solution at 13.8 MPa and 308K for 24 hours with magnifications of a) 2000x, b) 5000x, (PLA-3A).

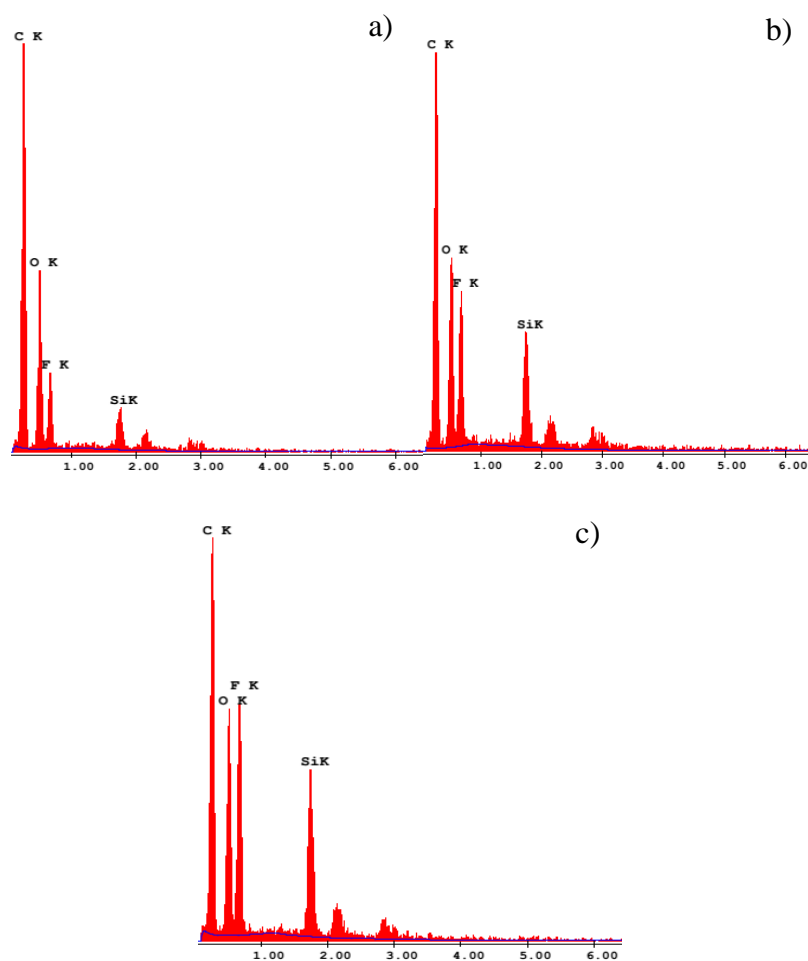


Figure 4. 19 EDX measurement for the detection of Si and F on a) PLA-1A (323K, 3hr), b) PLA-2A (323K, 24hr), c) PLA-3A (308K, 24hr).

Similar to experiments performed with F-POSS the studied parameters were waiting time, which was either 3 hours or 24 hours, and temperature which was 308K and 323K for the octaisobutyl POSS impregnation as well. Figure 4.20 and Figure 4.21 show the cross section area of PLA exposed to octaisobutyl POSS-CO₂ solution at a pressure of 13.8 MPa and a temperature of 323K for 3 hours and 24 hours, respectively. As they are compared with each other, it is seen that 24 hours exposure led to more amount of octaisobutyl POSS loading than 3 hours exposure. This is also verified with EDX analysis as seen in Figure 4.23 a and b.

When we compare the loadings of the two additives F-POSS and octaisobutyl POSS, at 13.8 MPa, 323K for 24 hours, impregnation performed with F-POSS was more efficient than the impregnation performed with octaisobutyl POSS as can be seen in SEM analysis (Figures 4.17 and 4.21) and EDX analysis, (Figures 4.19 b and 4.23 b). This can be explained with about two times greater solubility of F-POSS in scCO₂ at 323K compared to octaisobutyl POSS.

The PLA was kept in the saturated octaisobutyl POSS-CO₂ solutions for 24 hours at two different temperatures, 308K and 323K similar to the study conducted with F-POSS to study the effect of temperature on the impregnation performance. Figure 4.22 shows the cross section area of PLA, exposed to octaisobutyl POSS-CO₂ solution at a pressure of 13.8 MPa and a temperature of 308K for 24 hours. EDX results (Figure 4.23) revealed the presence of POSS in PLA. According to the SEM images and EDX results, POSS loading efficiency at 323K is better than that of at 308K. This can be explained with a higher solubility of octaisobutyl POSS in scCO₂ at 323K than at 308K at 13.8 MPa, which is above the crossover pressure in the phase behavior diagram of octaisobutyl POSS-CO₂ binary system given in Figure 4.3.

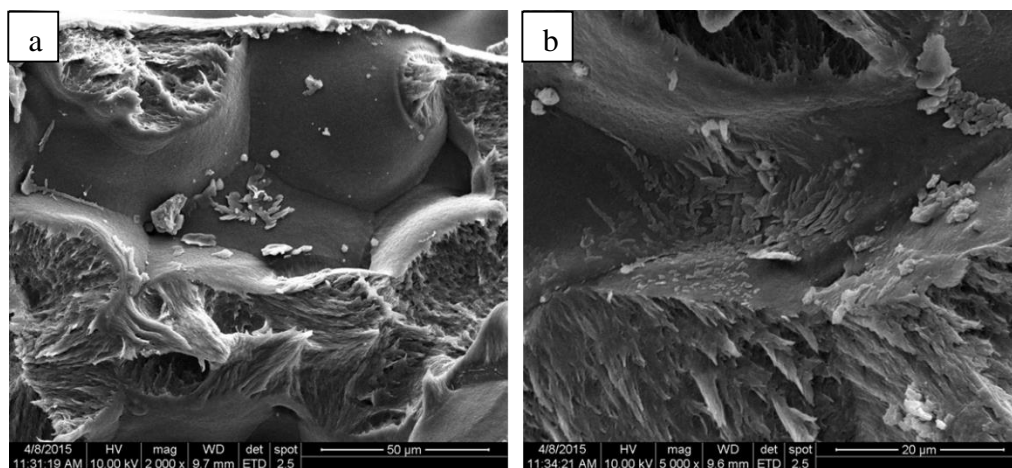


Figure 4. 20 Cross section of PLA processed with octaisobutyl POSS-CO₂ solution at 13.8 MPa and 323K for 3 hours with magnifications of a) 2000x, b) 5000x, (PLA-1B).

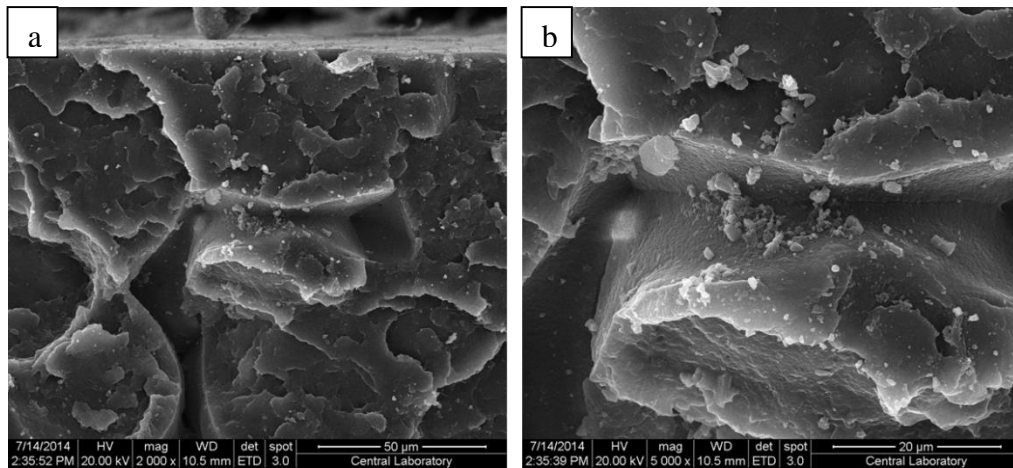


Figure 4. 21 Cross section of PLA processed with octaisobutyl POSS-CO₂ solution at 13.8 MPa and 323K for 24 hours with magnifications of a) 2000x, b) 5000x, (PLA-2B).

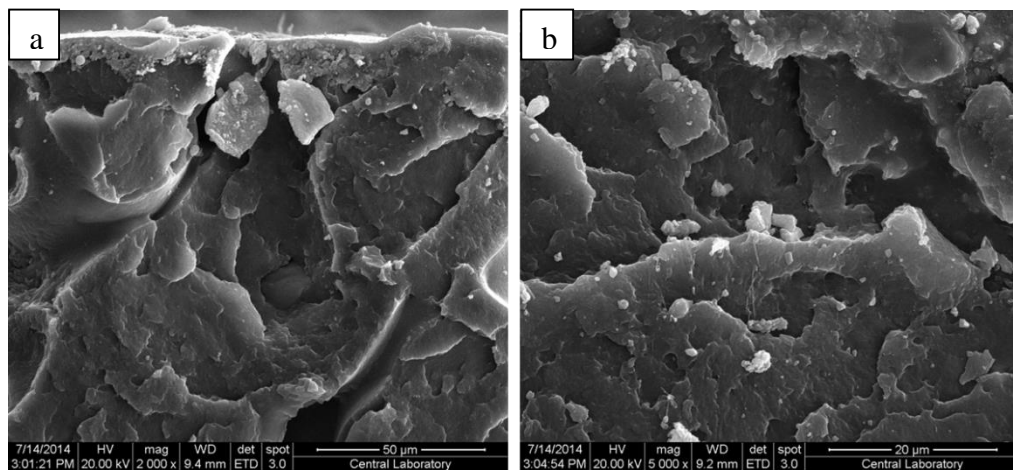


Figure 4. 22 Cross section of PLA processed with octaisobutyl POSS-CO₂ solution at 13.8 MPa and 308K for 24 hours with magnifications of a) 2000x, b) 5000x, (PLA-3B)

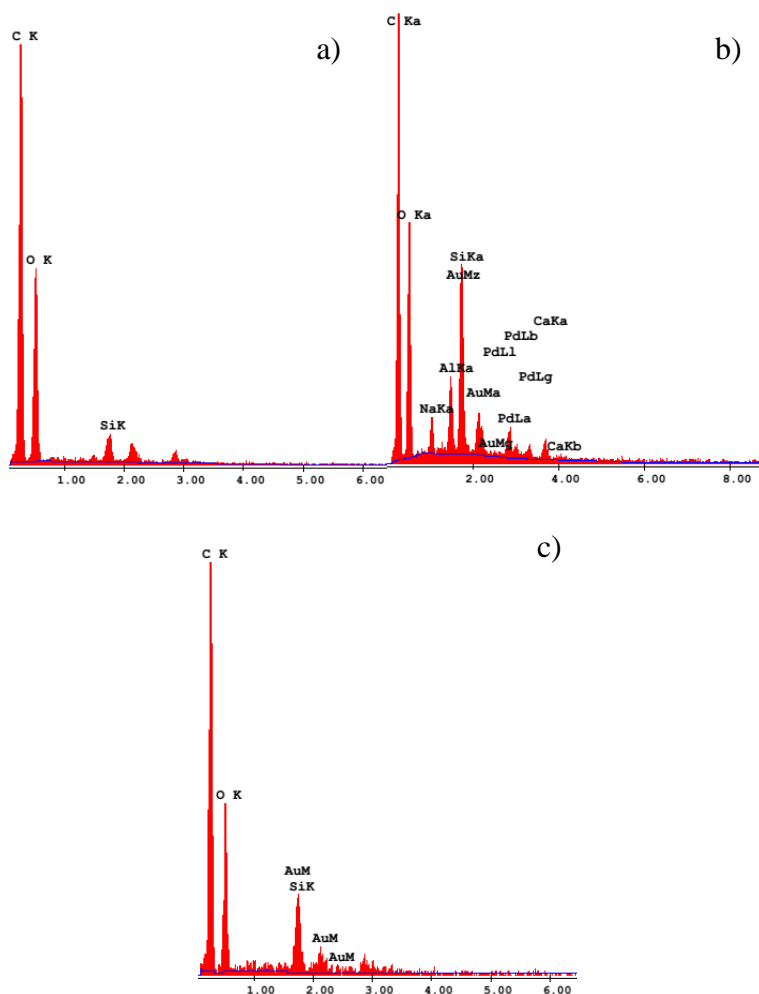


Figure 4. 23 EDX measurement for the detection of Si on a) PLA-1B (323K, 3 h), b) PLA-2B (323K, 24 hr), c) PLA-3B (308K, 24 h)

4.7.2 Thermal Properties

In this study, thermal stability of PLA and effect of F-POSS and octaisobutyl POSS on thermal stability of PLA were also investigated. TGA thermograms were categorized according to process conditions performed, effect of each POSS type was evaluated and contributions of each were compared. Figure 4.24, 4.25 4.26 show the TGA curves of pure POSS, neat PLA film, PLA films exposed only to scCO₂ and PLA impregnated with POSS at different conditions.

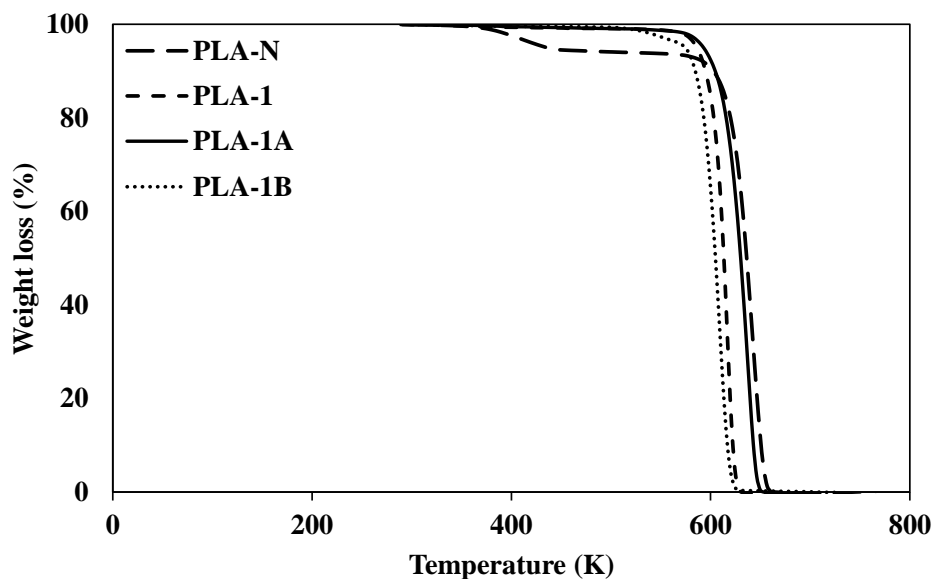


Figure 4.24 TGA curves of, unprocessed neat PLA, scCO₂ processed neat PLA, F-POSS impregnated PLA and octaisobutyl POSS impregnated PLA at 323K and 13.8 MPa for 3 h.

Figure 4.24 shows the TGA curves of two PLA samples without POSS, one is unprocessed and the other is pure scCO₂ processed, and two PLA samples, one processed with F-POSS-CO₂ solution and the other processed with octaisobutyl POSS-CO₂ solution. All the processed samples were processed for 3 hours at 323K and 13.8 MPa. PLA-1 represents the neat PLA processed with scCO₂, PLA-1A represents the PLA processed with F-POSS-CO₂ solution, and PLA-1B represents the PLA processed with octaisobutyl POSS-CO₂ solution. The first degradation step was observed between 373 and 443K and at this range 5% weight loss of neat PLA film occurred. The steep weight loss started at the temperature of 603K and 100 % weight loss was observed before the temperature reaches 673K. After the treatment of neat PLA (PLA-N) films by exposure to the supercritical carbon dioxide, the first step weight loss is not seen. Therefore, the first step weight loss observed for the neat PLA film could be due to release of chloroform used in the sample preparation or the release of water trapped in the PLA. During the scCO₂ processing of the samples PLA-1, PLA-1A, PLA-1B, the trapped chloroform or water was extracted, so the

first step weight loss was clearly not seen on their TGA plots. When F-POSS was added to the PLA with supercritical impregnation technique, it was seen that its thermal stability was slightly reduced by 1.3% with respect to scCO₂ processed neat PLA. However, addition of octaisobutyl POSS increased the thermal stability of scCO₂ processed neat PLA by about 3.5%. The maximum degradation rate temperatures (T_{max}) of samples are listed in Table 4.5. T_{max} values of all samples were found by taking the first derivative of the weight loss curves. As explained earlier, SEM and EDX analysis show that POSS could be loaded into the PLA matrix with the supercritical impregnation technique conducted for 3 hours. However, according to the results based on the T_{max} of the samples, a sufficient loading was not achieved to improve the thermal stability of the neat PLA (PLA-N).

Table 4. 5 The degradation temperatures of PLA treated at 323K and 13.8 MPa for 3h.

PLA Type	T_{max} (K)
PLA-N	643
PLA-1	617
PLA-1A	609
PLA-1B	638

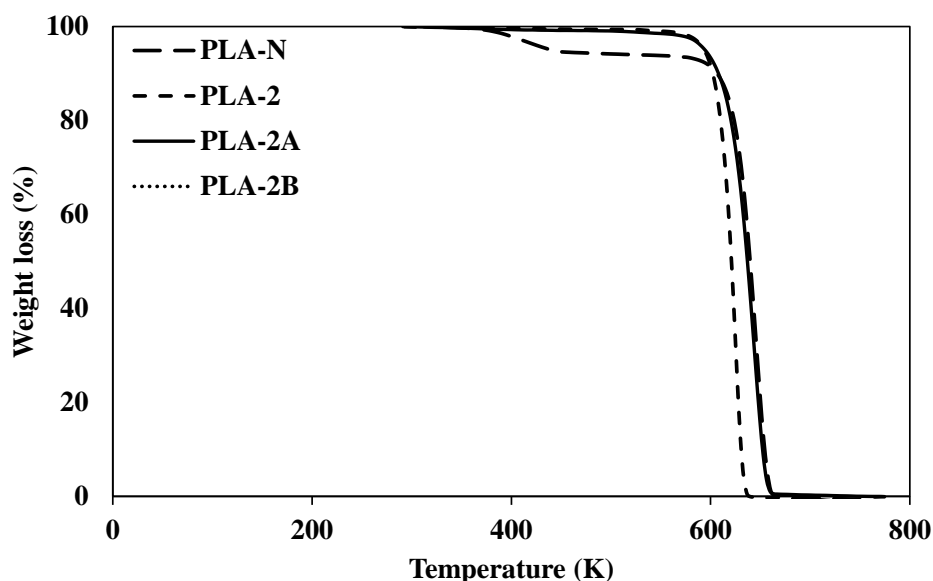


Figure 4. 25 TGA curves of neat F-POSS and octaisobutyl POSS, neat PLA, processed PLA and impregnated PLA at 323K and 13.8 MPa for 24 h.

Figure 4.25, similar to the previous figure, shows the TGA curves of two PLA samples without POSS, one is unprocessed neat PLA (PLA-N) and the other is pure scCO₂ processed (PLA-2), and two PLA samples, one processed with F-POSS-CO₂ solution (PLA-2A) and the other processed with octaisobutyl POSS-CO₂ (PLA-2B) solution. Here, the supercritical process duration of all the processed samples are 24 hours at 323K and 13.8 MPa. Similar to the Figure 4.24, after the treatment of neat PLA (PLA-N) films by exposure to the supercritical carbon dioxide, the first step weight loss between 373- 443 K was not seen. Therefore, the first step weight loss observed for the neat PLA film could be due to release of chloroform used in the sample preparation or the release of water trapped in the PLA. During the scCO₂ processing of the samples PLA-2, PLA-2A, PLA-2B the trapped chloroform or water was extracted, so the first step weight loss was clearly not seen on their TGA plots. As the neat PLA (PLA-N) and scCO₂ processed neat PLA (PLA-2) is compared it is seen that the scCO₂ treatment reduced the maximum degradation rate temperature (T_{max}) by about 3.5%. However, 2.5% and 3.5% increase in the thermal stability of the scCO₂ processed neat PLA were obtained by addition of F-POSS and octaisobutyl POSS, respectively. T_{max} of scCO₂ processed neat PLA (PLA-2) with

increased with octaisobutyl POSS (PLA-2B) and became equal to that of neat PLA. The maximum degradation rate temperatures (T_{max}) of samples are listed in the Table 4.6. Even though SEM and EDX analysis results show that POSS could be loaded into the PLA matrix with the supercritical impregnation technique conducted for 24 hours, the results based on T_{max} of the samples show that still a sufficient loading was not achieved to improve the thermal stability of neat PLA.

Table 4. 6 The degradation temperatures of scCO₂-F-POSS processed at 323K and 13.8 MPa for 24 h.

PLA Type	T_{max} (K)
PLA-N	643
PLA-2	621
PLA-2A	637
PLA-2B	643

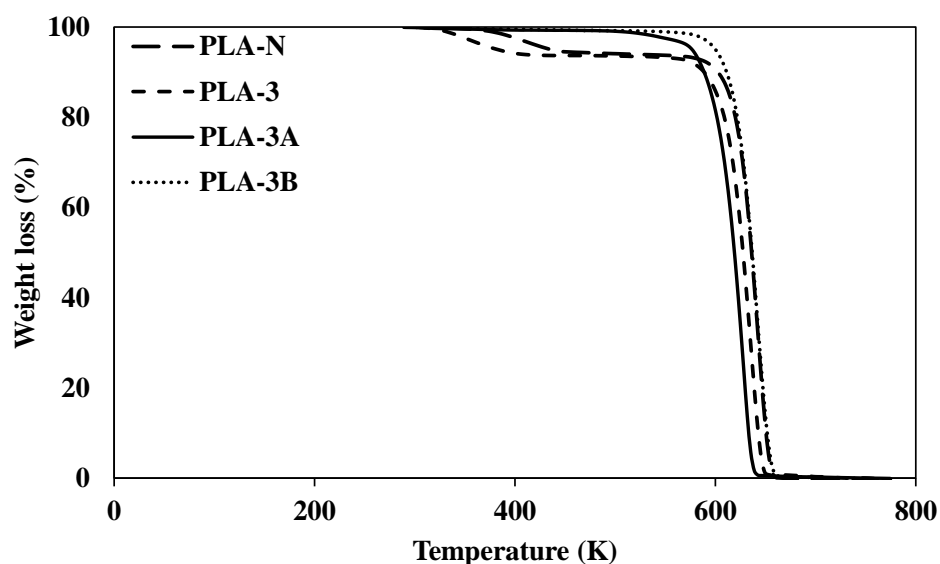


Figure 4. 26 TGA curves of neat F-POSS and octaisobutyl POSS, neat PLA, processed PLA and impregnated PLA at 308K and 13.8 MPa for 24 h.

As the temperature is decreased the solubility of F-POSS in scCO₂ increases at 13.8 MPa, while the solubility of octaisobutyl POSS decreases. Also, as the temperature is decreased the solubility of CO₂ in the polymer decreases while its diffusivity increases. So in order to see if impregnation temperature affects the thermal stability of the loaded PLA, the TGA analysis was performed to the samples processed at a different temperature. The TGA curves of the PLA samples that were processed for 24 hours at 308K and 13.8 MPa are given in Figure 4.26. PLA-3 represents the neat PLA processed with scCO₂, PLA-3A represents the PLA processed with F-POSS-CO₂ solution, and PLA-3B represents the PLA processed with octaisobutyl POSS-CO₂ solution. At those conditions the TGA curve of neat PLA processed with scCO₂ (PLA-3) demonstrated that thermal stability was reduced and shifted to lower temperature by about 8 K. The processed neat PLA (PLA-3) started to degrade first at a temperature of 323K and ended at a temperature of 413 K. It was expected as in the previous conditions that exposure of neat PLA to scCO₂ would eliminate the first degradation step however; it did not obtained with this process condition. This can be due to the lower process temperature (308K) which may not be sufficient to enable the release of water or chloroform from PLA. The prominent step of weight loss occurred between the temperature ranges of 583-648 K. The thermal stability of the scCO₂ processed neat PLA (PLA-3) was reduced by 1% after addition of F-POSS. However, addition of octaisobutyl POSS increased the thermal stability of scCO₂ processed neat PLA by about 3.5%. T_{max} of PLA processed with octaisobutyl POSS-CO₂ (PLA-2B) increased and became equal to that of neat PLA. The maximum degradation rate temperatures (T_{max}) of samples are listed in the Table 4.7, showing that similar to processing at 323K, processing at 308K does not have a significant effect on T_{max} of neat PLA (PLA-N).

As a result of thermal analysis of the samples that processed at three different conditions, it is observed that F-POSS addition increased the thermal stability only at 323K and 13.8 MPa with 24 hours exposure time. This may be attributed to the SEM result (Figure 4.17) which showed the better dispersion of F-POSS in the PLA matrix at this condition.

Table 4. 7 The degradation temperatures of PLA treated at 308K and 13.8 MPa for 24h.

PLA Type	T _{max} (K)
PLA-N	643
PLA-3	635
PLA-3A	629
PLA-3B	642

Glass transition temperatures (T_g), melting temperatures (T_m), enthalpy of fusion (ΔH_f) of unprocessed neat PLA (PLA-N), the neat PLA processed with scCO₂ (PLA-1, PLA-2, PLA-3), PLA processed with F-POSS-CO₂ solution (PLA-1A, PLA-2A, PLA-3A, and PLA processed with octaisobutyl POSS-CO₂ solution (PLA-1B, PLA-2B, PLA-3B) were investigated by DSC analysis. DSC plots of all samples are given in Appendix. Thermal properties of all samples studied are tabulated in Table 4.8.

Table 4. 8 Thermal properties of different types of PLA.

PLA Type	T _g (K)	T _m (K)	ΔH_f (J/g)
13.8 MPa, 323K, 3h			
PLA-N	327	441	46.22
PLA-1	338	441	43.41
PLA-1A	338	442	36.85
PLA-1B	338	442	38.74
13.8 MPa, 323K, 24h			
PLA-N	327	441	46.22
PLA-2	332	442	33.01
PLA-2A	336	442	35.75
PLA-2B	336	442	45.41

Table 4. 8 (continued)

13.8 MPa, 308K, 24h			
PLA-N	327	441	46.22
PLA-3	334	440	42.58
PLA-3A	339	442	35.73
PLA-3B	337	443	38.81

The T_g results presented in Table 4.8 shows that glass transition temperature (T_g) of neat PLA increased after scCO₂ processing. In literature, it has been shown that scCO₂ can plasticize the polymer chains which corresponds to increase in free volume of polymer [99]. It leads to decrease in T_g . However, depressurization of CO₂ induces the rearrange of polymer chains to reach more stable state. The rubbery polymer turns into glassy state [56]. Except for the samples processed at 323K for 3 h, further increase in T_g was obtained with impregnated PLA samples compared to the neat PLA processed with scCO₂. Especially, long exposure time of PLA to POSS-CO₂ solutions made this increase apparent. The greatest increase in T_g was obtained with the F-POSS impregnated PLA (PLA-3A) at 308K, 13.8 MPa for 24 hours. However, for the octisobutyl POSS impregnated PLA, the greatest increase in T_g was obtained at 323K, 13.8 MPa for 24 hours. This can be explained with a higher solubility of octaisobutyl in scCO₂ at 323K than at 308K at 13.8 MPa and the higher solubility of F-POSS at 308K compared to 323K. At both cases more loading was probably achieved due to the higher solubility of POSS in scCO₂.

Using supercritical carbon dioxide at three different conditions and also using two different types of POSS did not make significant change to melting temperatures of PLA.

CHAPTER 5

CONCLUSION

The solubilities of octamethyl, methacryl, isooctyl and octaisobutyl POSS in scCO₂ were studied to observe the contribution of carbonyl and branched alkyl functionalities to the solubility of POSS in scCO₂. Solubility curves of the POSS-CO₂ binary systems have been obtained by dew point and cloud point measurements at 308 and 323K up to 30 MPa. Among the studied POSS structures, octamethyl POSS, which has no specific interaction with CO₂, was found to be insoluble in scCO₂. The rest of the POSS types, which are methacryl, isooctyl and octaisobutyl POSS, are soluble in the supercritical solvent, showing that CO₂-philic functionalities with specific interactions or entropic contributions are required to solubilize the POSS in scCO₂. The solubility of both methacryl and isooctyl POSS in scCO₂ decrease with isobaric increase in temperature due to the decrease in the density of scCO₂. Isooctyl POSS exhibits nearly an order of magnitude higher solubility than methacryl POSS at both temperatures. Octaisobutyl-CO₂ binary system exhibits a crossover point at 12 MPa. Above this pressure, octaisobutyl becomes more soluble with increasing temperature due to predominating effect of its increased solute vapor pressure. Below the crossover pressure, with increasing temperature, decreasing density and so the solvent power of CO₂ is dominating the solubility of POSS despite the increase in its vapor pressure. Solubilities of isooctyl and octaisobutyl POSS are similar to each other at 308K while octoisobutyl has higher solubility at 323K.

Obtained data show that the solubility of POSS in scCO₂ can be due to the specific interactions between the groups attached to the silicon atoms and CO₂, and also the

entropic contributions as in the case of isooctyl and octaisobutyl POSS with branched alkyl groups.

After the solubility experiments the obtained phase behavior data of methacryl POSS, isooctyl POSS, and octaisobutyl POSS were correlated using density based models. Mendez-Santiago and Teja model, Chrastil model, Bartle model, del Valle and Aguilera model, and Kumar and Johnston models were used to correlate. They all gave good fit to the solubility data; while the lowest AARD% value, which is 5.32, was obtained with Bartle model for the octaisobutyl POSS experimental data.

The solubility data of POSS in scCO₂ reported in this work and also data of F-POSS [75] can be used in the design of environmentally benign impregnation process using POSS and the supercritical fluid systems. In the preliminary impregnation studies conducted with the most CO₂-soluble POSS in this work, morphological analyses show that POSS can be deposited into PLA at the conditions where POSS can be solubilized in the supercritical fluid. Lower temperature leads to better F-POSS loading which is believed to be due to the higher solubility of F-POSS at 308K compared to 323K. However, better homogeneous dispersity was obtained with the F-POSS at 13.8 MPa, 323K for 24 hours exposure. Thermal characterization of the impregnated PLA films and the neat PLA film were performed by DSC and TGA instruments. The effect of POSS addition on the glass transition temperature, melting temperature and thermal stability were investigated. Analysing the PLA samples after processing with pure scCO₂, it was observed that treatment with scCO₂ increased the T_g of the polymer. Further increase in T_g was obtained with the impregnated PLA samples compared to the scCO₂ processed neat PLA. Especially PLA that have 24 hours exposure time to POSS-CO₂ solution made this difference apparent with an increase of 10K in T_g compared to the neat PLA. Despite the increase in T_g, the melting temperatures remained almost the same. When the neat PLA and scCO₂ processed neat PLA were compared, TGA analysis showed that the scCO₂ treatment generally reduced the maximum degradation rate temperature (T_{max}). There was no significant contribution by octaisobutyl POSS and F-POSS to the thermal stability of the neat PLA probably due to insufficient amounts of POSS

loaded during the processes, except addition of octaisobutyl POSS compensated the decrease resulted from the scCO₂ treatment of neat PLA and increased the thermal stability of scCO₂ processed neat PLA up to that of neat PLA.

REFERENCES

- [1] G. Li, L. Wang, H. Ni, C.U. Pittman, Polyhedral Oligomeric Silsesquioxane (POSS) Polymers and Copolymers: A Review, *Journal of Inorganic and Organometallic Polymers*. 11 (2001) 123–154–154. doi:10.1023/A:1015287910502.
- [2] S.W. Kuo, F.C. Chang, POSS Related Polymer Nanocomposites, *Progress in Polymer Science (Oxford)*. 36 (2011) 1649–1696. doi:10.1016/j.progpolymsci.2011.05.002.
- [3] J. Wu, P.T. Mather, POSS Polymers: Physical Properties and Biomaterials Applications, *Polymer Reviews*. 49 (2009) 25–63. doi:10.1080/15583720802656237.
- [4] M. Joshi, B.S. Butola, Polymeric Nanocomposites—Polyhedral Oligomeric Silsesquioxanes (POSS) as Hybrid Nanofiller, *Journal of Macromolecular Science, Part C: Polymer Reviews*. 44 (2004) 389–410. doi:10.1081/MC-200033687.
- [5] E. Ayandele, B. Sarkar, P. Alexandridis, Polyhedral Oligomeric Silsesquioxane (POSS)-Containing Polymer Nanocomposites, *Nanomaterials*. 2 (2012) 445–475. doi:10.3390/nano2040445.
- [6] W. Zhang, A.H.E. Müller, Architecture, Self-Assembly and Properties of Well-defined Hybrid Polymers Based on Polyhedral Oligomeric Silsequioxane (POSS), *Progress in Polymer Science*. 38 (2013) 1121–1162. doi:10.1016/j.progpolymsci.2013.03.002.
- [7] H. Hussain, S.M. Shah, Recent Developments in Nanostructured Polyhedral Oligomeric Silsesquioxane-based Materials via “Controlled” Radical Polymerization, *Polymer International*. 63 (2014) 835–847. doi:10.1002/pi.4692.
- [8] R.B. Gupta, J.-J. Shim, *Solubility in Supercritical Carbon Dioxide*, 1st Editio, CRC Press, 2006.
- [9] Y.-P. Sun, *Supercritical Fluid Technology in Materials Science And Engineering Synthesis, Properties, and Applications*, Marcel Dekker, Inc., 2002.

- [10] M.A. Mchugh, V.J. Krukonis, *Supercritical Fluid Extraction*, 2nd Editio, Butterworth-Heinemann, 1994.
- [11] L.T. Taylor, *Supercritical Fluid Extraction*, John Wiley, New York, 1996.
- [12] X. Zhang, S. Heinonen, E. Levänen, Applications of Supercritical Carbon Dioxide in Materials Processing and Synthesis, *RSC Adv.* 4 (2014) 61137–61152. doi:10.1039/C4RA10662H.
- [13] H. Peker, M. Srinivasan, J. Smith, B. McCoy, Caffeine Extraction Rates from Coffee Beans with Supercritical Carbon Dioxide, *AIChE Journal.* 38 (1992) 761–770. doi:10.1002/aic.690380513.
- [14] M. Perrut, *Supercritical Fluid Applications: Industrial Developments and Economic Issues*, *Industrial & Engineering Chemistry Research.* 39 (2000) 4531–4535. doi:10.1021/ie000211c.
- [15] H. Machida, M. Takesue, R.L. Smith, *Green Chemical Processes with Supercritical Fluids: Properties, Materials, Separations and Energy*, *Journal of Supercritical Fluids.* 60 (2011) 2–15. doi:10.1016/j.supflu.2011.04.016.
- [16] F. Lin, D. Liu, S.M. Das, N. Prempeh, Y. Hua, J. Lu, Recent Progress in Heavy Metal Extraction by Supercritical CO₂ Fluids, *IEC.Res.* (2014). doi:10.1021/ie4035708.
- [17] D. Gnanasekaran, K. Madhavan, B.S.R. Reddy, Developments of Polyhedral Oligomeric Silsesquioxanes (POSS), POSS Nanocomposites and Their Applications: A Review, *Journal of Scientific & Industrial Research.* 68 (2009) 437–464.
- [18] K. Tanaka, Y. Chujo, *Chemicals-Inspired Biomaterials: Developing Biomaterials Inspired by Material Science Based on POSS*, 1239 (2013) 1231–1239. doi:10.1246/bcsj.20110162.
- [19] Y. Arai, T. Sako, Y. Takebayashi, *Supercritical Fluids Molecular Interactions, Physical Properties, and New Applications*, Springer, Berlin, 2002.
- [20] H. Sim Yeoh, G. Hean Chong, N. Mohd Azahan, R. Abdul Rahman, T.S. Yaw Choong, Solubility Measurement Method and Mathematical Modeling in Supercritical Fluids, *Engineering Journal.* 17 (2013) 67–78. doi:10.4186/ej.2013.17.3.67.
- [21] P.S. Bhosale, H.A. Stretz, Gold Nanoparticle Deposition Using CO₂ Expanded Liquids : Effect of Pressure Oscillation and Surface - Particle Interactions, (2008) 12241–12246.

- [22] W.H. Teoh, R. Mammucari, N.R. Foster, Solubility of Organometallic Complexes in Supercritical Carbon Dioxide: A Review, *Journal of Organometallic Chemistry*. 724 (2013) 102–116. doi:10.1016/j.jorganchem.2012.10.005.
- [23] K. Johnston, C. Eckert, An analytical Carnahan-Starling-van der Waals Model for Solubility of Hydrocarbon Solids in Supercritical Fluids, *AIChE Journal*. 27 (1981) 773–779. <http://onlinelibrary.wiley.com/doi/10.1002/aic.690270511/abstract>.
- [24] L. Nasri, S. Bensaad, Z. Bensefati, Modeling the Solubility of Dihydroxybenzoic Acid and Methylbenzoic Acid Isomers in Supercritical Carbon Dioxide, *International Journal of Thermodynamics*. 17 (2014) 81–85. doi:10.5541/ijot.513.
- [25] M. Sauceau, J.J. Letourneau, D. Richon, J. Fages, Enhanced Density-based Models for Solid Compound Solubilities in Supercritical Carbon Dioxide with Cosolvents, *Fluid Phase Equilibria*. 208 (2003) 99–113. doi:10.1016/S0378-3812(03)00005-0.
- [26] M. Škerget, Solubility of Solids in Sub- and Supercritical Fluids: A Review, *Journal of Chemical & Engineering Data*. 56 (2011) 694–719. doi:10.1021/je1011373.
- [27] Z. Tang, J. Jin, Z. Zhang, H. Liu, New Experimental Data and Modeling of the Solubility of Compounds in Supercritical Carbon Dioxide, *Industrial & Engineering Chemistry Research*. 51 (2012) 5515–5526. doi:10.1021/ie2016224.
- [28] B. Hadi, H.-A. Ali, L. Nader, Thermodynamic Modeling of Solid Solubility in Supercritical Carbon Dioxide: Comparison Between Mixing Rules, *Chemical Industry and Chemical Engineering Quarterly*. 19 (2012) 74–74. doi:10.2298/CICEQ120203074B.
- [29] C.B. Kautz, G.M. Schneider, J. Shim, D. Tuma, Solubilities of a 1,4-Bis(alkylamino)-9,1-anthraquinone Series in Compressed Carbon Dioxide, (2008) 2356–2371.
- [30] J. Chrastil, Solubility of Solids and Liquids in Supercritical Gases, *Journal of Physical Chemistry*. 86 (1982) 3016–3021. doi:10.1021/j100212a041.
- [31] J.M. del Valle, J.M. Aguilera, An Improved Equation for Predicting the Solubility of Vegetable Oils in Supercritical CO₂, *Industrial & Engineering Chemistry Research*. 27 (1988) 1551–1553. doi:10.1021/ie00080a036.

- [32] S.K. Kumar, K.P. Johnston, Modelling the Solubility of Solids in Supercritical Fluids with Density as the Independent Variable, *The Journal of Supercritical Fluids*. 1 (1988) 15–22.
- [33] J. Méndez-Santiago, A.S. Teja, The Solubility of Solids in Supercritical Fluids, *Fluid Phase Equilibria*. 158-160 (1999) 501–510. doi:10.1016/S0378-3812(99)00154-5.
- [34] H. Cui, S. Qian, F. Qin, C. Wang, Solubility of 2,3,5,6 Tetrachloropyridine in Supercritical CO₂: Measurement and Correlation, *Journal of Chemical & Engineering Data*. 59 (2014) 269–274. <http://pubs.acs.org/doi/abs/10.1021/je400462d>.
- [35] D. Tuma, B. Wagner, G.M. Schneider, High-pressure Solubility Measurement of Solids in Near and Supercritical Fluids, in: G.Brunner (Ed.), *Supercritical Fluids as Solvents and Reaction Media*, Elsevier B.V, Amsterdam, San Diego, Oxford, London, 2004: pp. 121–146.
- [36] K.D. Bartle, A.A. Clifford, S.A. Jafar, G.. Shilstone, *Solubilities of Solids and Liquids With Low Volatility in CO₂*, (1990).
- [37] L.I. Cabezas, V. Fernández, R. Mazarro, I. Gracia, a. De Lucas, J.F. Rodríguez, Production of biodegradable porous scaffolds impregnated with indomethacin in supercritical CO₂, *Journal of Supercritical Fluids*. 63 (2012) 155–160. doi:10.1016/j.supflu.2011.12.002.
- [38] L.I. Cabezas, I. Gracia, M.T. García, A. De Lucas, J.F. Rodríguez, Production of Biodegradable Porous Scaffolds Impregnated with 5-fluorouracil in Supercritical CO₂, *Journal of Supercritical Fluids*. 80 (2013) 1–8. doi:10.1016/j.supflu.2013.03.030.
- [39] Z. Tian, N.C. Bing, Y. Zhang, L.L. Wang, W. Qiao, Supercritical Solvent Impregnation in Controlled-Release Drugs, *Advanced Materials Research*. 152-153 (2010) 1462–1465. doi:10.4028/www.scientific.net/AMR.152-153.1462.
- [40] O.S. Fleming, F. Stepanek, S.G. Kazarian, Dye Diffusion in Polymer Films Subjected to Supercritical CO₂: Confocal Raman Microscopy and Modelling, *Macromolecular Chemistry and Physics*. 206 (2005) 1077–1083. doi:10.1002/macp.200500075.
- [41] T.T. Ngo, C.L. Liotta, C. a. Eckert, S.G. Kazarian, Supercritical Fluid Impregnation of Different Azo-dyes into Polymer: In situ UV/Vis Spectroscopic Study, *Journal of Supercritical Fluids*. 27 (2003) 215–221. doi:10.1016/S0896-8446(02)00239-5.

- [42] D.L. Tomasko, X. Han, D. Liu, W. Gao, Supercritical Fluid Applications in Polymer Nanocomposites, *Current Opinion in Solid State and Materials Science*. 7 (2003) 407–412. doi:10.1016/j.cossms.2003.10.005.
- [43] I. Kikic, Polymer-Supercritical Fluid Interactions, *Journal of Supercritical Fluids*. 47 (2009) 458–465. doi:10.1016/j.supflu.2008.10.016.
- [44] J.J. Watkins, T.J. McCarthy, Polymerization in Supercritical Fluid-Swollen Polymers: A New Route to Polymer Blends, *Macromolecules*. 27 (1994) 4845–4847. doi:10.1021/ma00095a031.
- [45] A.R. Berens, G.S. Huvard, R.W. Korsmeyer, F.W. Kunig, Application of Compressed Carbon Dioxide in the Incorporation of Additives into Polymers, *Journal of Applied Polymer Science*. 46 (1992) 231–242. doi:10.1002/app.1992.070460204.
- [46] F. Baldi, F. Bignotti, A. Fina, D. Tabuani, T. Ricco, Mechanical Characterization of Polyhedral Oligomeric Silsesquioxane/Polypropylene Blends, *Journal of Applied Polymer Science*. 105 (2007) 935–943. doi:10.1002/app.
- [47] S.R. Jin, J.K. Lee, Isothermal Physical Aging of Poly(ethyl methacrylate)/Polyhedral Oligomeric Silsesquioxanes Nanocomposite Thin Films, *Advanced Materials Research*. 287-290 (2011) 2234–2239. doi:10.4028/www.scientific.net/AMR.287-290.2234.
- [48] M. Takala, M. Karttunen, P. Salovaara, S. Kortet, K. Kannus, T. Kalliohaka, Dielectric Properties of Nanostructured Polypropylene-Polyhedral Oligomeric Silsesquioxane Compounds, *IEEE Transactions on Dielectrics and Electrical Insulation*. 15 (2008) 40–50. doi:10.1109/T-DEI.2008.4446735.
- [49] F. Ciesielczyk, K. Szwarz-Rzepka, T. Jesionowski, Evaluation of physicochemical Properties of a New Group of SiO₂/silane/POSS Hybrid Materials, *Surface and Interface Analysis*. 45 (2013) 998–1007. doi:10.1002/sia.5199.
- [50] H. Mahfuz, F. Powell, R. Granata, M. Hosur, M. Khan, Coating of Carbon Fiber with Polyhedral Oligomeric Silsesquioxane (POSS) to Enhance Mechanical Properties and Durability of Carbon/Vinyl Ester Composites, *Materials*. 4 (2011) 1619–1631. doi:10.3390/ma4091619.
- [51] Y.H. La, R. Sooriyakumaran, B.D. McCloskey, R.D. Allen, B.D. Freeman, R. Al-Rasheed, Enhancing Water Permeability of Fouling-Resistant POSS-PEGM Hydrogels Using “Addition-Extraction” of Sacrificial Additives, *Journal of Membrane Science*. 401-402 (2012) 306–312. doi:10.1016/j.memsci.2012.02.021.

- [52] A. Fina, D. Tabuani, A. Frache, G. Camino, Polypropylene-Polyhedral Oligomeric Silsesquioxanes (POSS) Nanocomposites, *Polymer*. 46 (2005) 7855–7866. doi:10.1016/j.polymer.2005.06.121.
- [53] T. Hasell, Metal–Polymer Nanocomposites by Supercritical Fluid Processing, in: *Nanocomposites*, John Wiley & Sons, Inc, 2013: pp. 1–43. doi:10.1002/9781118742655.ch1.
- [54] D.L. Tomasko, H.B. Li, D.H. Liu, X.M. Han, M.J. Wingert, L.J. Lee, et al., A review of CO₂ Applications in the Processing of Polymers, *Industrial & Engineering Chemistry Research*. 42 (2003) 6431–6456. doi:10.1021/Ie030199z.
- [55] S. Kazarian, *Polymer Processing with Supercritical Fluids*, *Polymer Science, Ser. C*. 42 (2000) 78–101.
- [56] S. Yoda, K. Sato, H.T. Oyama, Impregnation of paclitaxel into poly(dl-lactic acid) Using High Pressure Mixture of Ethanol and Carbon Dioxide, *RSC Advances*. 1 (2011) 156. doi:10.1039/c1ra00070e.
- [57] G. Eris, D. Sanli, Z. Ulker, S.E. Bozbag, A. Jonás, A. Kiraz, et al., Three-dimensional Optofluidic Waveguides in Hydrophobic Silica Aerogels via Supercritical Fluid Processing, *Journal of Supercritical Fluids*. 73 (2013) 28–33. doi:10.1016/j.supflu.2012.11.001.
- [58] O. Muth, T. Hirth, H. Vogel, Polymer Modification by Supercritical Impregnation, *Journal of Supercritical Fluids*. 17 (2000) 65–72. doi:10.1016/S0896-8446(99)00042-X.
- [59] S.G. Kazarian, G.G. Martirosyan, Spectroscopy of Polymer/Drug Formulations Processed with Supercritical Fluids: In situ ATR-IR and Raman Study of Impregnation of Ibuprofen into PVP, *International Journal of Pharmaceutics*. 232 (2002) 81–90. doi:10.1016/S0378-5173(01)00905-X.
- [60] L. Manna, M. Banchemo, D. Sola, A. Ferri, S. Ronchetti, S. Sicardi, Impregnation of PVP microparticles with ketoprofen in the presence of supercritical CO₂, *Journal of Supercritical Fluids*. 42 (2007) 378–384. doi:10.1016/j.supflu.2006.12.002.
- [61] M. Banchemo, L. Manna, S. Ronchetti, P. Campanelli, A. Ferri, Supercritical Solvent Impregnation of Piroxicam on PVP at Various Polymer Molecular Weights, *Journal of Supercritical Fluids*. 49 (2009) 271–278. doi:10.1016/j.supflu.2009.01.008.
- [62] Y.A. Hussain, C.S. Grant, Ibuprofen Impregnation into Submicron Polymeric Films in Supercritical Carbon Dioxide, *Journal of Supercritical Fluids*. 71 (2012) 127–135. doi:10.1016/j.supflu.2012.07.014.

- [63] T. Hasell, L. Lagonigro, a. C. Peacock, S. Yoda, P.D. Brown, P.J. a Sazio, et al., Silver Nanoparticle Impregnated Polycarbonate Substrates for Surface Enhanced Raman Spectroscopy, *Advanced Functional Materials*. 18 (2008) 1265–1271. doi:10.1002/adfm.200701429.
- [64] S.G. Kazarian, N.H. Brantley, B.L. West, M.F. Vincent, C. a. Eckert, In situ Spectroscopy of Polymers Subjected to Supercritical CO₂: Plasticization and Dye Impregnation, *Applied Spectroscopy*. 51 (1997) 491–494. doi:10.1366/0003702971940765.
- [65] B.L. West, S.G. Kazarian, M.F. Vincent, N.H. Brantley, C. a Eckert, Supercritical Fluid Dyeing of PMMA Films with Azo-dyes, *Journal of Applied Polymer Science*. 69 (1998) 911–919. doi:10.1002/(SICI)1097-4628(19980801)69:5<911::AID-APP10>3.0.CO;2-R.
- [66] S. Üzer, U. Akman, Ö. Hortaçsu, Polymer Swelling and Impregnation Using Supercritical CO₂: A Model-Component Study Towards Producing Controlled-Release Drugs, *Journal of Supercritical Fluids*. 38 (2006) 119–128. doi:10.1016/j.supflu.2005.11.005.
- [67] J.M. Andanson, A. López-Periago, C. a. García-González, C. Domingo, S.G. Kazarian, Spectroscopic Analysis of Triflusal Impregnated into PMMA from Supercritical CO₂ Solution, *Vibrational Spectroscopy*. 49 (2009) 183–189. doi:10.1016/j.vibspec.2008.07.005.
- [68] S.G. Kazarian, N.H. Brantley, C.A. Eckert, Applications of Vibrational Spectroscopy to Characterize Poly(ethylene terephthalate) Processed with Supercritical CO₂, *Vibrational Spectroscopy*. 19 (1999) 277–283. doi:10.1016/S0924-2031(98)00073-3.
- [69] S. Sicardi, L. Manna, M. Banchemo, Diffusion of Disperse Dyes in PET Films During Impregnation with a Supercritical Fluid, *Journal of Supercritical Fluids*. 17 (2000) 187–194. doi:10.1016/S0896-8446(99)00055-8.
- [70] H. Liu, N. Finn, M.Z. Yates, Encapsulation and Sustained Release of a Model Drug, Indomethacin, Using CO₂-based Microencapsulation, *Langmuir*. 21 (2005) 379–385. doi:10.1021/la047934b.
- [71] O. Guney, A. Akgerman, Synthesis of Controlled-Release Products in Supercritical Medium, *AIChE Journal*. 48 (2002) 856–866. doi:10.1002/aic.690480419.
- [72] A.M. López-Periago, A. Vega, P. Subra, A. Argemí, J. Saurina, C. a. García-González, et al., Supercritical CO₂ Processing of Polymers for the Production of Materials with Applications in Tissue Engineering and Drug

Delivery, *Journal of Materials Science*. 43 (2008) 1939–1947.
doi:10.1007/s10853-008-2461-0.

- [73] K. Sugiura, S. Ogawa, I. Tabata, T. Hori, Impregnation of Tranilast to the Poly(lactic acid) Fiber with Supercritical Carbon Dioxide and the Release Behavior of Tranilast, *Fiber*. 61 (2005) 159–165. doi:10.2115/fiber.61.159.
- [74] O. Guney, A. Akgerman, Solubilities of 5-Fluorouracil and β -Estradiol in Supercritical Carbon Dioxide, (2000) 1049–1052.
- [75] C. Dilek, Supercritical Carbon Dioxide-Soluble Polyhedral Oligomeric Silsesquioxane (POSS) Nanocages and Polymer Surface Modification, *Journal of Supercritical Fluids*. 73 (2013) 171–177.
doi:10.1016/j.supflu.2012.10.012.
- [76] D.G.F. E.W. Lemmon, M.O., McLinden, Thermophysical properties of fluid systems, in: P.J. Linstrom, W.G. Mallard (Eds.), *NIST Chemistry WebBook*, NIST Standard Reference Database Number 69, June National Institute of Standards and Technology, Gaithersburg, MD, (n.d.).
- [77] A.M. Kartal, C. Erkey, Surface Modification of Silica Aerogels by Hexamethyldisilazane–Carbon Dioxide Mixtures and Their Phase Behavior, *The Journal of Supercritical Fluids*. 53 (2010) 115–120.
doi:10.1016/j.supflu.2009.11.004.
- [78] D. Sanli, C. Erkey, Bubble Point Pressures and Densities of Hexamethyldisiloxane–Carbon Dioxide Binary Mixture Using a Constant Volume View Cell, *The Journal of Supercritical Fluids*. 74 (2013) 52–60.
doi:10.1016/j.supflu.2012.11.017.
- [79] D. Sanli, C. Erkey, Demixing Pressures of Hydroxy-Terminated Poly(dimethylsiloxane)-Carbon Dioxide Binary Mixtures at 313.2 K, 323.2 K and 333.2 K, *Journal of Supercritical Fluids*. 92 (2014) 264–271.
doi:10.1016/j.supflu.2014.05.014.
- [80] S.G. Kazarian, M.F. Vincent, F. V Bright, C.L. Liotta, C.A. Eckert, R. V February, Specific Intermolecular Interaction of Carbon Dioxide with Polymers, *Journal of American Chemistry Society*. 118 (1996) 1729–1736.
doi:10.1021/JA950416Q.
- [81] M.R. Nelson, R.F. Borkman, Ab Initio Calculations on CO₂ Binding to Carbonyl Groups, *Journal of Physical Chemistry A*. 102 (1998) 7860–7863.
doi:10.1021/JP981824U.
- [82] P. Raveendran, S.L. Wallen, Sugar Acetates as Novel, Renewable CO₂ -philes, *Journal of American Chemical Society*. 124 (2002) 7274–7275.
doi:10.1021/ja025508b.

- [83] V.K. Potluri, J. Xu, R. Enick, E. Beckman, A.D. Hamilton, Peracetylated Sugar Derivatives Show High Solubility in Liquid and Supercritical Carbon Dioxide, *Organic Letters*. 4 (2002) 2333–2335. doi:10.1021/ol026007y.
- [84] V.K. Potluri, A.D. Hamilton, C.F. Karanikas, S.E. Bane, J. Xu, E.J. Beckman, et al., The high CO₂-Solubility of Per-acetylated α -, β -, and γ -cyclodextrin, *Fluid Phase Equilibria*. 211 (2003) 211–217. doi:10.1016/S0378-3812(03)00206-1.
- [85] L. Hong, M.C. Thies, R.M. Enick, Global Phase Behavior for CO₂-philic Solids: the CO₂+ β -d-Maltose Octaacetate System, *The Journal of Supercritical Fluids*. 34 (2005) 11–16. doi:10.1016/j.supflu.2004.10.003.
- [86] C. Dilek, C.W. Manke, E. Gulari, Phase Behavior of β -d Galactose Pentaacetate–Carbon Dioxide Binary System, *Fluid Phase Equilibria*. 239 (2006) 172–177. doi:10.1016/j.fluid.2005.11.013.
- [87] P. Raveendran, S.L. Wallen, Cooperative C-H...O Hydrogen Bonding in CO₂-Lewis Base Complexes: Implications for Solvation in Supercritical CO₂, *Journal of the American Chemical Society*. 124 (2002) 12590–9. doi:10.1021/ja0174635.
- [88] R. Fink, D. Hancu, R. Valentine, E.J. Beckman, Toward the Development of “CO₂-philic” Hydrocarbons. 1. Use of Side-Chain Functionalization to Lower the Miscibility Pressure of Polydimethylsiloxanes in CO₂, *Journal of Physical Chemistry B*. 103 (1999) 6441–6444. doi:10.1021/jp990333m.
- [89] F. Rindfleisch, T.P. DiNoia, M. a. McHugh, Solubility of Polymers and Copolymers in Supercritical CO₂, *The Journal of Physical Chemistry*. 100 (1996) 15581–15587. doi:10.1021/jp9615823.
- [90] G. ten Brinke, F.E. Karasz, Lower Critical Solution Temperature Behavior in Polymer Blends, *Macromolecules*. 17 (1984) 815–820. doi:10.1021/ma00134a049.
- [91] K. Szwarc-rzepka, T. Szatkowski, F. Ciesielczyk, T. Jesionowski, Preparation And Characterization Of SiO₂/Silane/POSS Functional Hybrids, 49 (2013). doi:10.5277/ppmp130226.
- [92] Y.R. Liu, Y.D. Huang, L. Liu, Thermal Stability of POSS/Methylsilicone Nanocomposites, *Composites Science and Technology*. 67 (2007) 2864–2876. doi:10.1016/j.compscitech.2007.01.023.
- [93] A. Fina, D. Tabuani, F. Carniato, A. Frache, E. Boccaleri, G. Camino, Polyhedral Oligomeric Silsesquioxanes (POSS) Thermal Degradation, *Thermochimica Acta*. 440 (2006) 36–42. doi:10.1016/j.tca.2005.10.006.

- [94] M. Voronkov, V. Lavrent'yev, Polyhedral Oligosilsesquioxanes and Their Homo Derivatives, *Topics in Current Chemistry*. 102 (1982) 199–236. http://link.springer.com/chapter/10.1007/3-540-11345-2_12.
- [95] C. Bolln, A. Tsuchida, H. Frey, R. Mu, Thermal Properties of the Homologous Series of 8-fold Alkyl-Substituted Octasilsesquioxanes, *Chemistry of Materials*. 9 (1997) 1475–1479. doi:10.1021/cm970090f.
- [96] L.J.M. Jacobs, M.F. Kemmere, J.T.F. Keurentjes, Sustainable Polymer Foaming Using High Pressure Carbon Dioxide: A Review on Fundamentals, Processes and Applications, *Green Chemistry*. 10 (2008) 731. doi:10.1039/b801895b.
- [97] E. Kiran, Polymer Miscibility, Phase Separation, Morphological Modifications and Polymorphic Transformations in Dense Fluids, *Journal of Supercritical Fluids*. 47 (2009) 466–483. doi:10.1016/j.supflu.2008.11.010.
- [98] R. Yoganathan, R. Mammucari, N.R. Foster, Impregnation of Ibuprofen into Polycaprolactone Using Supercritical Carbon Dioxide, *Journal of Physics: Conference Series*. 215 (2010) 012087. doi:10.1088/1742-6596/215/1/012087.
- [99] Z. Zhang, Y.P. Handa, CO₂- Assisted Melting of Semicrystalline Polymers, *Macromolecules*. 30 (1997) 8505–8507. doi:10.1021/ma9712211.

APPENDIX

DSC ANALYSIS RESULTS

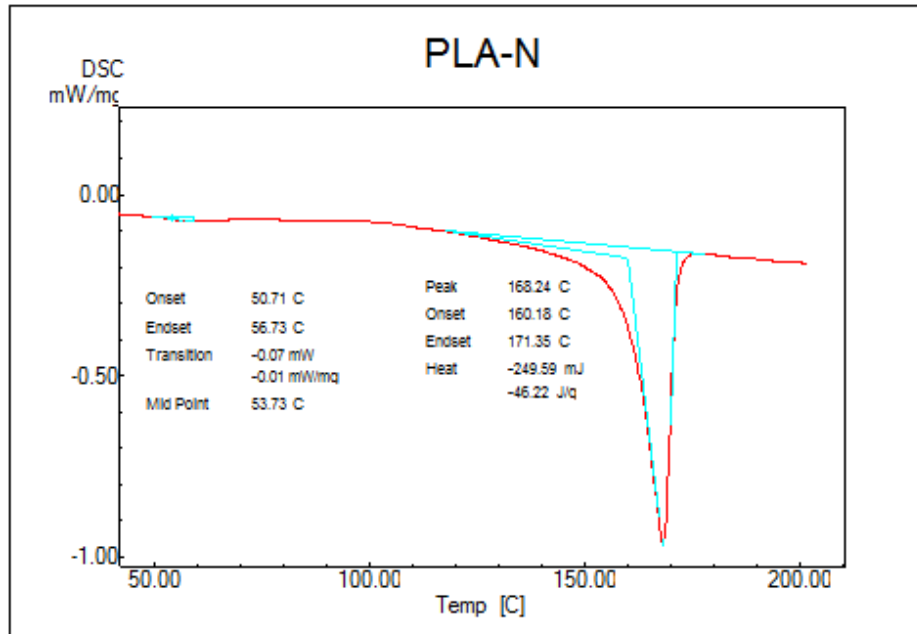


Figure A. 1 DSC plot of PLA-N Run 1.

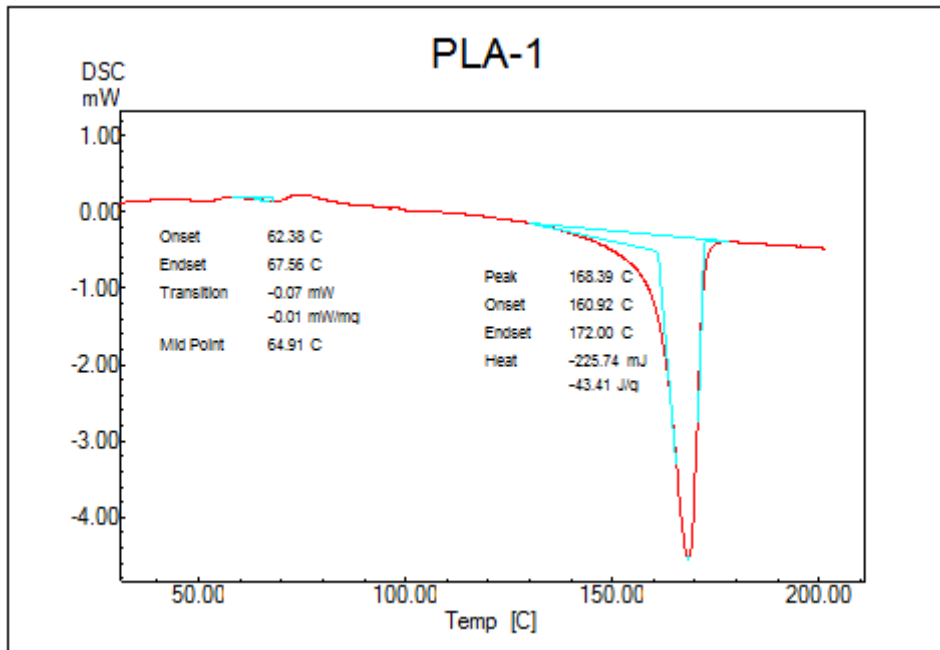


Figure A. 2 DSC plot of PLA-1 Run 1.

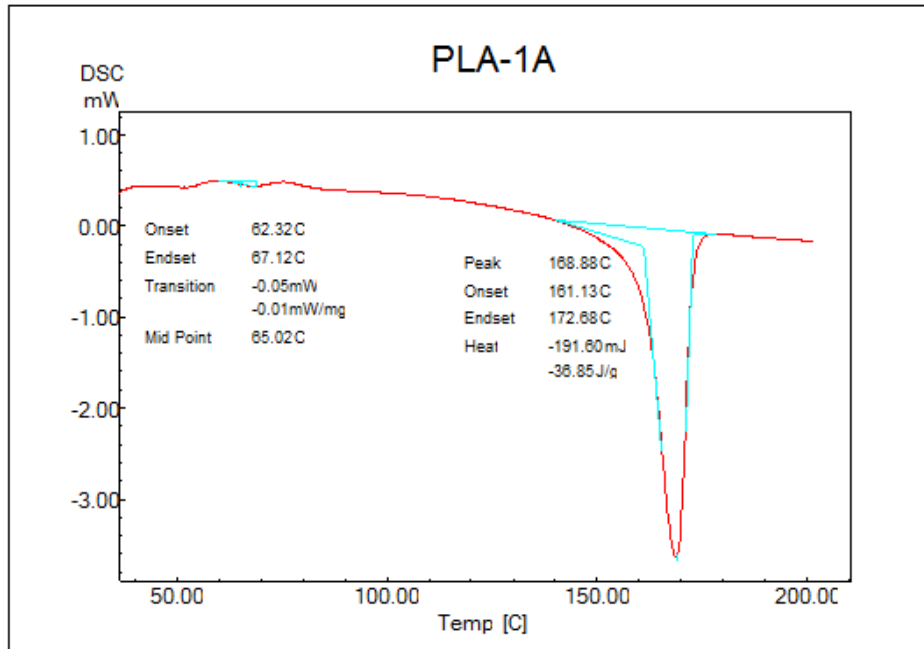


Figure A. 3 DSC plot of PLA-1A Run 1.

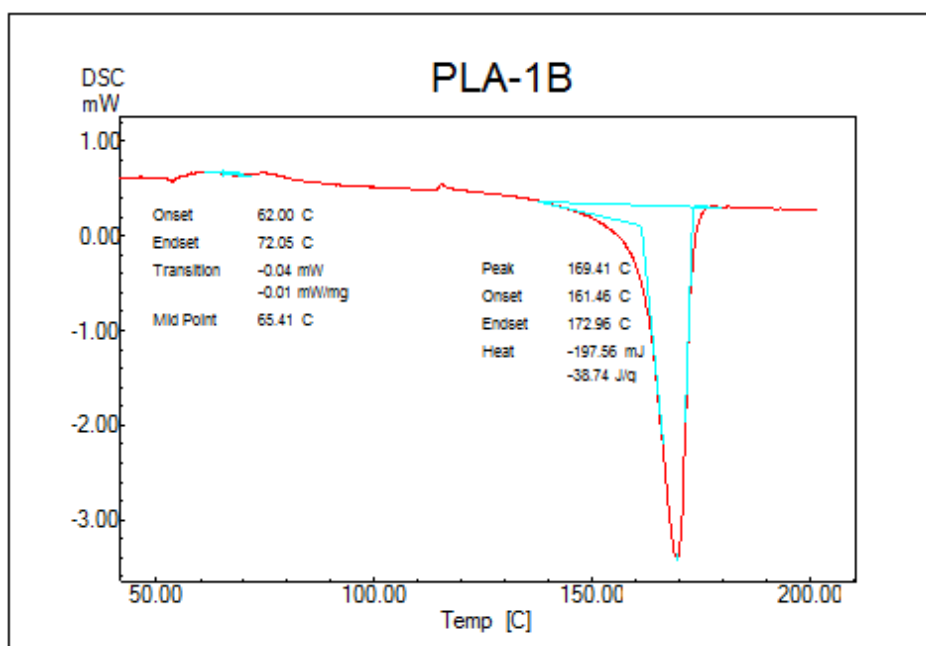


Figure A. 4 DSC plot of PLA-1B Run 1.

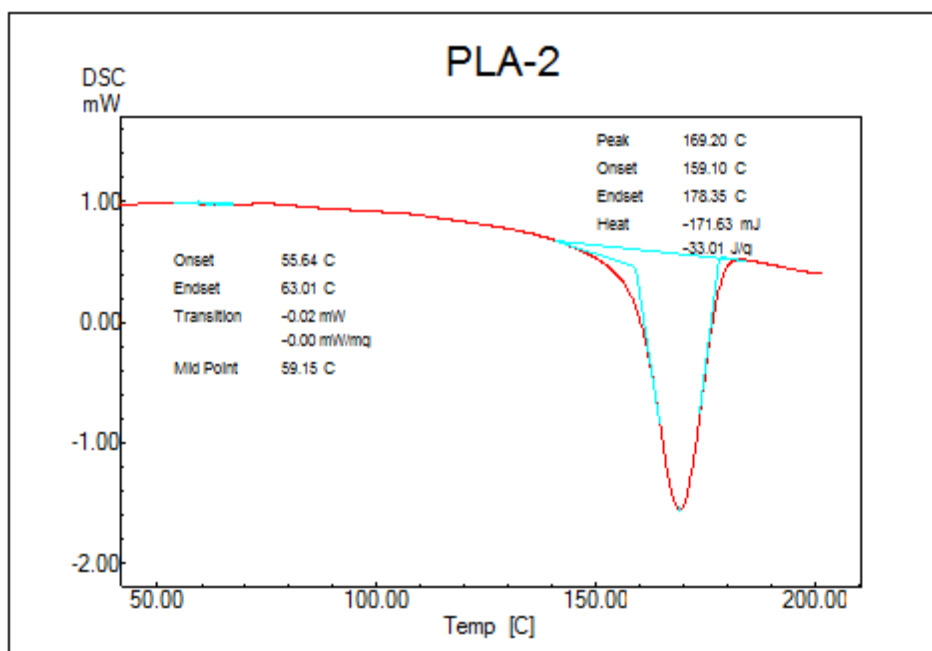


Figure A. 5 DSC plot of PLA-2 Run 1.

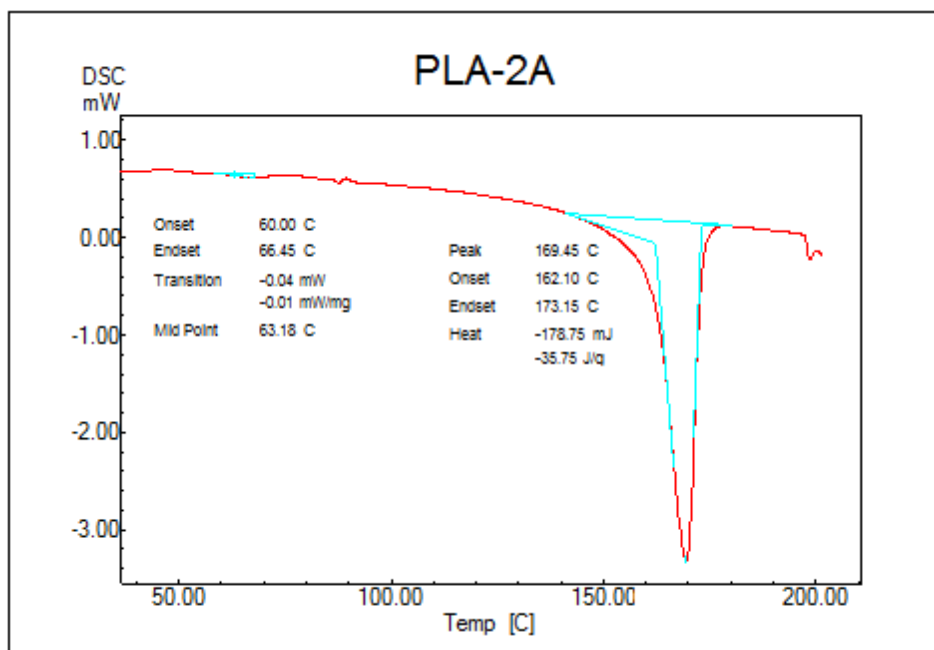


Figure A. 6 DSC plot of PLA-2A Run 1.

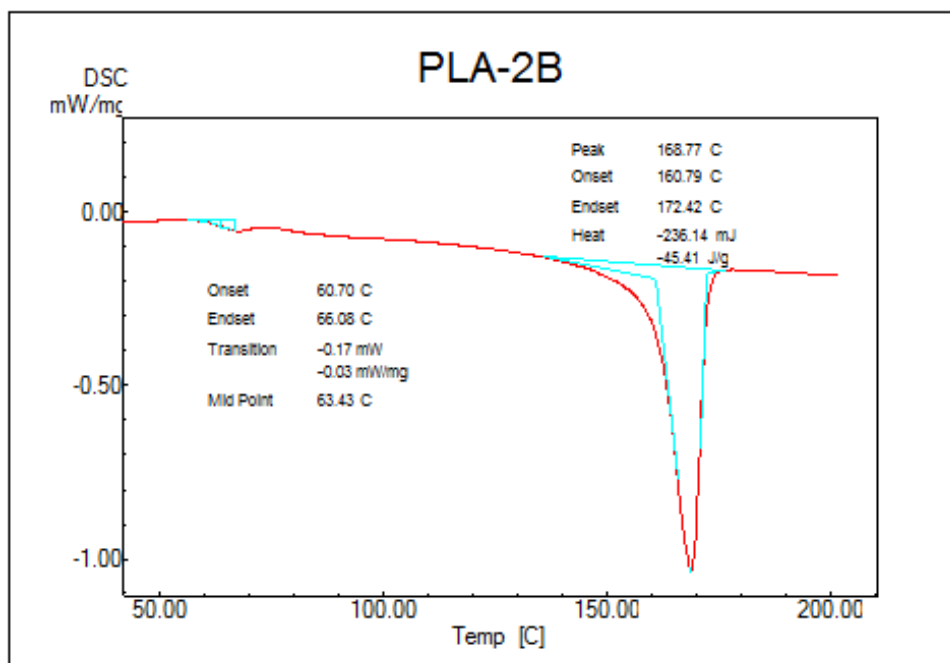


Figure A. 7 DSC plot of PLA-2B Run 1.

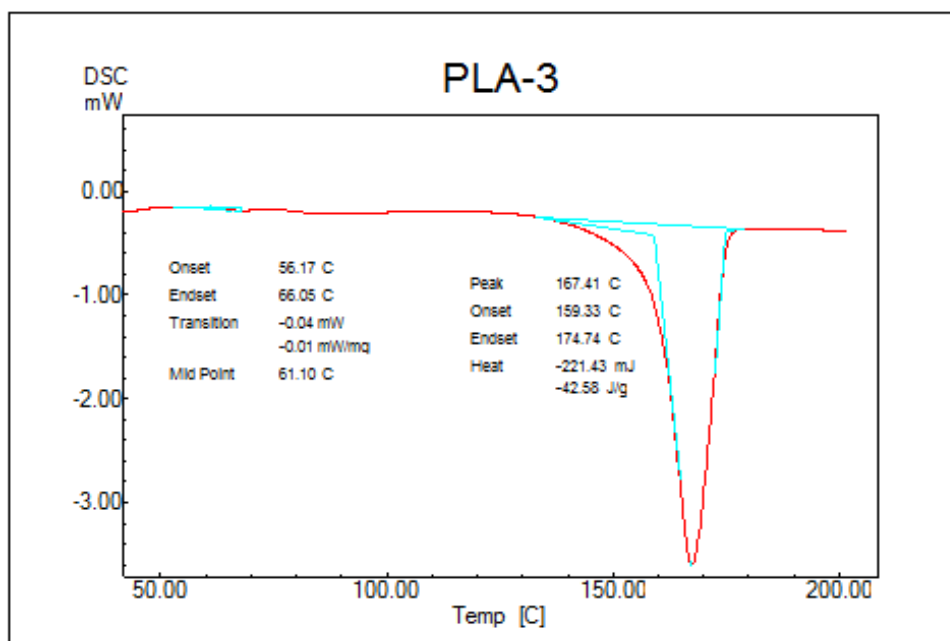


Figure A. 8 DSC plot of PLA-3 Run1.

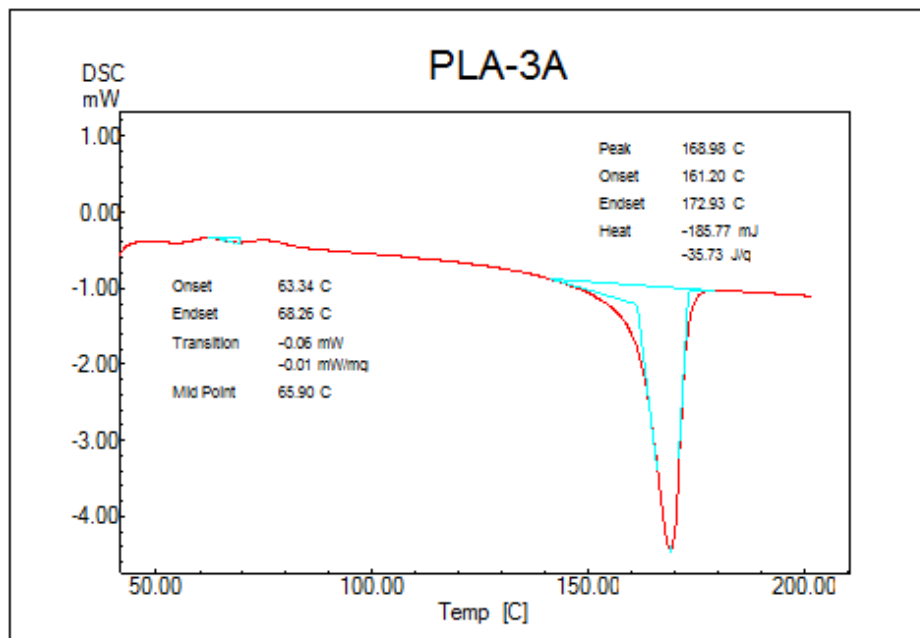


Figure A. 9 DSC plot of PLA-3A Run 1.

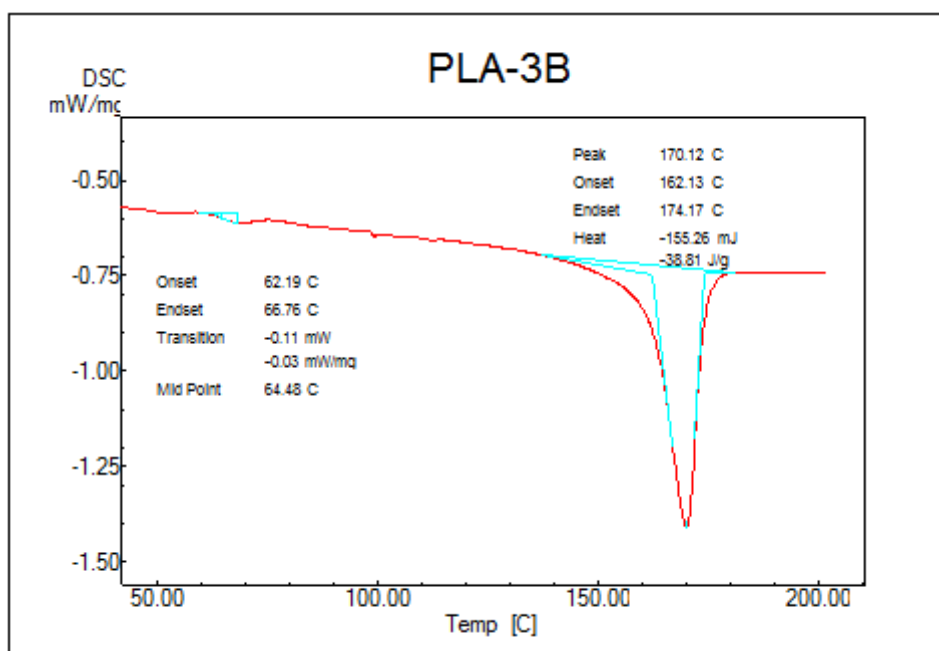


Figure A. 10 DSC plot of PLA-3B Run 1.